The Dissertation Committee for William Shane Walker certifies that this is the approved version of the following dissertation:

Improving Recovery in Reverse Osmosis Desalination of Inland Brackish Groundwaters via Electrodialysis

Committee:

Desmond F. Lawler, Supervisor

Benny D. Freeman

Lynn E. Katz

Kerry A. Kinney

Howard M. Liljestrand

Improving Recovery in Reverse Osmosis Desalination of Inland Brackish Groundwaters via Electrodialysis

by

William Shane Walker, B.S., M.S.E.

Dissertation

Presented to the Faculty of the Graduate School of

The University of Texas at Austin

in Partial Fulfillment

of the Requirements

for the Degree of

Doctor of Philosophy

The University of Texas at Austin

August 2010

Acknowledgements

In my opinion, the most fundamental challenge facing environmental engineers today is to develope feasible and sustainable means of providing clean water and sanitation to every person in the world. In the year 2000, the World Health Organization estimated that more than one billion people worldwide (nearly 15% of the world's population) lacked access to improved water supply, and over two billion people lacked access to improved sanitation (World Health Organization, 2000, §5.3). To address this tragedy, the United Nations defined Target 10 of the Millennium Development Goals to "Halve by 2015 the proportion of people without sustainable access to safe drinking-water and sanitation," and many of the other development goals are directly or indirectly related to water supply and sanitation (Varis, 2007). Considering that a large portion of the world's population lives in close proximity to the coast and that an untold measure of inland brackish groundwater lies untapped, perhaps desalination technology could be utilized to diminish world thirst. Thus, I am so grateful to have had the opportunity to study desalination technologies here in the Environmental and Water Resources Engineering program at The University of Texas at Austin.

I would first like to thank my dissertation committee for their investment of time, energy, and expertise into my studies. I am very thankful for their availability for discussion and helping me shape the experimental and mathematical methodology of this research. Special thanks to Dr. Liljestrand for many impromptu discussions about chemistry (both theoretical and practical). I am thankful for the discussions of thermodynamics with Dr. Freeman, which helped me better appreciate the philosophies

of science and engineering. I would also like to thank Dr. Freeman and Dr. Liljestrand for attending the Engineering Commencement, which was a meaningful occasion to me.

It is impossible to express the depth of my gratitude for the supervision and guidance of my advisor. Sincerely, Dr. Lawler has been a tremendous mentor, colleague, and friend. Indeed, he is a true academic. Granted, he is very particular regarding certain topics (*e.g.*, the use of the word "about", SI dimensions, units of Henry's constant, *etc.*), but more significantly, he is a devoted teacher, thoughtful scientist, and curious student. He has inspired me to be a professor who invests himself in effective teaching, valuable research, and service to his community.

Younggy Kim is the best colleague, office mate, and friend that a person could wish for. He is polite, genuine, kind, and sincere; he is a diligent scholar and a devoted husband and father. He has graciously and thoughtfully answered all of my questions (academic, hypothetical, and purely curious), even though most of them interrupted his own studies. I am also thankful for friendships with my other office mates, Chi Hoang and Abdalrahman Alsulaili.

My colleagues in the Lawler research group have been so helpful and friendly, and I have learned so much from them. Lauren Greenlee was instrumental in developing the Water Research Foundation project that funded much of my studies, and Jeff Nason helped me get started in the Lawler-PhD experience. Not only have my colleagues been helpful with coursework and research, but they are also great friends: Lee Blaney, Hector Garcia, Ari Herrera, Patrick McNamara, Scott Hekman, Mike Cobb, Mark Hughes, and Corin Marron. Thank you for all of the great conversations, struggles, and triumphs

shared among our research team. I am also grateful for the chance to work with students from École Centrale de Lille in France and for their contribution to the development of my research: François Chérel, Antoine Martin, Jeremy Durand, and Aurore Mercelat.

Thank you to those in the 9th floor "PhD Row" and the 7th floor "Quads" who were so friendly and obliging: Nate Johnson, Yongseok Hong, Brad Eck, Mara London, Shannon Stokes, and Tony Smith. I am also thankful for the great friendships with Cedric David and Eric Hersh (from Dr. Maidment's research group) and their contribution to my philosophical development. Support from Charlie Perego, Danny Quiroz, and Rebecca Christian was invaluable for research and academic progress. Throughout my time here in Austin, the EWRE program has been such a learning experience, and thanks are due to many others.

I am grateful for financial support from the Water Research Foundation and the Texas Water Development Board, which funded the majority of this research. I also appreciate financial support from The University of Texas at Austin, Cockrell School of Engineering, Thrust 2000 – Hagedorn Graduate Fellowship and the Membrane Research Fellowship sponsored by the National Water Research Instititute and the American Membrane Technology Association. I am also grateful for contributions from Black & Veatch, Carollo, CDM, HDR, and Malcolm Pirnie to the Foundation project.

Several mentors were especially influential in my decision to pursue graduate school, and I am thankful for their advice and encouragement: Mr. Tommy O'Brien at the City of Abilene and Dr. Ernst Kiesling and Dr. Ken Rainwater at Texas Tech University. Also, several of my fellow students at Texas Tech University encouraged me to consider

teaching, and I appreciate their continued friendship and support: Nick Meirsma, Greg Bolner, Jeremy Vernetti, Jeff Klement, Levi Hein, Seth Williamson, and Chris Rosckes.

Of course, I am especially thankful for the patient and loving support from my wife Brandi. She has been so understanding and supportive of me and my education, and I am forever indebted to her. She is such a wonderful person: kind, joyful, graceful, and beautiful. I am also thankful for prayerful support from my parents, brothers, and church family who have supported me throughout my life as a student and continue to support and encourage me in my transition to El Paso.

Finally, and most deeply, I am thankful to the Lord for breath, Life, vocation, and the opportunity to enjoy this education. To echo the words of King David:

> 1 Chronicles 29:13 *Now, our God, we give you thanks, and praise your glorious name.* 14 *... Everything comes from you, and we have given you only what comes from your hand.* (NIV)

The Lord has blessed me tremendously with family, friends, and a great education, and anything good that I am able to accomplish is only by His grace. I am excited about the opportunities that He will continue to give me to help people develop physical and spiritual water resources.

> John 7:37 *... Jesus stood and said in a loud voice, "If anyone is thirsty, let him come to me and drink.* 38 *Whoever believes in me, as the Scripture has said, streams of living water will flow from within him."* (NIV)

As the Lord leads me to the next chapter in my life, it is my goal to be a conduit of pure water. *Soli Deo Gloria*

Abstract

Improving Recovery in Reverse Osmosis Desalination of Inland Brackish Groundwaters via Electrodialysis

William Shane Walker, Ph.D.

The University of Texas at Austin, 2010

Supervisor: Desmond F. Lawler

As freshwater resources are limited and stressed, and as the cost of conventional drinking water treatment continues to increase, interest in the development of non-traditional water resources such as desalination and water reuse increases. Reverse osmosis (RO) is the predominant technology employed in inland brackish groundwater desalination in the United States, but the potential for membrane fouling and scaling generally limits the system recovery. The general hypothesis of this research is that electrodialysis (ED) technology can be employed to minimize the volume of concentrate waste from RO treatment of brackish water (BW) and thereby improve the environmental and economic feasibility of inland brackish water desalination. The objective of this research was to investigate the performance sensitivity and limitations of ED for treating BWRO concentrate waste through careful experimental and mathematical analysis of selected electrical, hydraulic, and chemical ED variables.

Experimental evaluation was performed using a laboratory-scale batch-recycle ED system in which the effects of electrical, hydraulic, and chemical variations were observed. The ED stack voltage showed the greatest control over the rate of ionic separation, and the specific energy invested in the separation was approximately proportional to the applied voltage and equivalent concentration separated. An increase in the superficial velocity showed marginal improvements in the rate of separation by decreasing the thickness of the membrane diffusion boundary layers. A small decrease in the nominal recovery was observed because of water transport by osmosis and electroosmosis. Successive concentration of the concentrate by multiple ED stages demonstrated that the recovery of BWRO concentrate could significantly improve the overall recovery of inland BWRO systems.

A mathematical model for the steady-state performance of an ED stack was developed to simulate the treatment of BWRO concentrates by accounting for variation of supersaturated multicomponent solution properties. A time-dependent model was developed that incorporated the steady-state ED model to simulate the batch-recycle experimentation. Comparison of the electrical losses revealed that the electrical resistance of the ion exchange membranes becomes more significant with increasing solution salinity. Also, a simple economic model demonstrated that ED could feasibly be employed, especially for zero-liquid discharge.

Table of Contents

List of Tables

List of Figures

List of Abbreviations

ADC	analog-to-digital converter
AEM	anion exchange membrane
AOP	advanced oxidation process
BWRO	brackish-water reverse osmosis
CEM	cation exchange membrane
CFD	computational fluid dynamics
CFSTR	continuous flow, stirred-tank reactor
CMC	carboxyl methyl cellulose
DAQ	data acquisition system
ED	electrodialysis
EDI	electrodeionization
EDR	electrodialysis reversal
GUI	graphical user interface
IC	ion chromatography
ICP-AES	inductively-coupled plasma – atomic emission spectroscopy
IEM	ion exchange membrane
MCL	maximum contaminant level
MEE	multi-effect evaporation
MF	micro-filtration
MGD	million gallons per day
MSF	multi-stage flash

NF	nano-filtration
NHE	normal hydrogen electrode
NOM	natural organic matter
PACl	poly-aluminum chloride
PFR	plug-flow reactor
RO	reverse osmosis
SCADA	supervisory control and data acquisition
SDS	sodium dodecyl sulfate
SEC	specific energy consumption
SWRO	sea-water reverse osmosis
TDS	total dissolved solids concentration (mass of salt per volume of solution)
UF	ultra-filtration
ZLD	zero-liquid discharge

List of Mathematical Symbols

Symbol		Units
a	ionic/molecular activity	[-]
$å$	Debye-Hückel ion-size parameter	[Å]
A	cross-sectional area	[m^2]
c	concentration	[mol L^{-1}]
CF	concentration factor	[-]
D	ionic/molecular diffusivity	[m^2 s^{-1}]
e	Euler's number	2.718…
E	energy	[J], [kWh]
F	Faraday constant	96485.3 C eq^{-1}
F	cumulative probability function	[-]
G	Gibb's free energy	[J], [kWh]
H	pressure head	[m]
i	current density (charge flux)	[A m^{-2}]
I	electrical current	[A], [C s^{-1}]
IAP	ion activity product	[-]
J	molar flux	[mol m^{-2} s^{-1}]
k	mass transport coefficient	[m/s]
k_B	Boltzmann constant	1.381×10^{-23} m^2 kg s^{-2} K^{-1}
K_{s0}	solubility product	[-]
L	length	[m]

m	mass	[kg]
MM	molar mass	[g/mol]
N_A	Avogadro's number	6.022×10^{23} mol^{-1}
N_{cp}	number of cell pairs	[-]
p	pressure	[Pa], [N m^{-2}], [kg m^{-1} s^{-2}]
P	power	[W]
Q	volumetric flow rate	[m^3 s^{-1}], [MGD]
q_e	electronic charge	1.602×10^{-19} C
r	recovery ratio	[-]
R	removal ratio	[-]
R	electrical resistance	[Ω]
$\tilde{R}$	areal electrical resistance	[Ω m^2]
Re	Reynolds number	[-]
R_g	molar gas constant	8.314 J mol^{-1} K^{-1}
S	saturation ratio	[-]
Sc	Schmidt number	[-]
Sh	Sherwood number	[-]
t	ionic transport number	[-]
T	temperature	[K]
u	ionic mobility	[m^2 V^{-1} s^{-1}]
v	velocity	[m s^{-1}]
V	volume	[m^3], [gal]

x	distance	[m]
z	ionic charge (including sign)	[-]
δ	diffusion boundary layer thickness	[m]
ε_0	electric constant (or permittivity of free space)	8.854×10^{-12} m^{-3} kg^{-1} s^4 A^2
ε_r	relative permittivity	[-]
θ	dimensionless hydraulic time	[-]
κ	conductivity (specific conductance)	[S m^{-1}]
Λ	equivalent conductivity	[S m^2 eq^{-1}]
λ	equivalent ionic conductivity	[S m^2 eq^{-1}]
μ	dynamic (absolute) viscosity	[kg m^{-1} s^{-1}], [Pa s]
ν	kinematic viscosity	[m^2 s^{-1}]
ν_d	stoichiometric salt-dissociation coefficient	[-]
ξ	current utilization	[-]
ρ	mass density	[kg m^{-3}]
τ	mean hydraulic residence time	[s]
ϕ	electric potential	[V]

Chapter 1 – Introduction

1.1 BACKGROUND

Clean water - this fascinating substance that quenches the thirst of land and people - is our planet's most precious resource. Unfortunately, this essential resource is becoming increasingly scarce as population growth and industrial development consume existing fresh water supplies. Even the United States is experiencing regional water shortages, particularly in arid regions such as the West and Southwest, as well as states such as Florida where a large percentage of water resources are brackish or sea waters. The production of drinking water in the United States mostly relies on freshwater sources, but as the demand increases and sources are depleted, other sources that require alternative technologies and treatment options must be explored (Hoffbuhr *et al.*, 2004).

One of the most promising methods of drinking water production from non-traditional sources is desalination, the process of turning brackish or sea water into fresh water. Salt water is almost ubiquitous around the world, and recent technological advancements suggest that wide-scale implementation of desalination can mitigate the impact of freshwater scarcity. The United States and the arid Middle Eastern countries have been leaders in developing desalination technologies in the last decade, and desalination production is expected to continue to grow rapidly (Fritzmann *et al.*, 2007). Global desalination production more than doubled from 17.3 million m^3/day (4570 MGD) in 1994 to 35.6 million m^3/day (9410 MGD) in 2004, as shown in Figure 1.1. A similar trend is observed for desalination capacity in the United States, totaling six million m^3/day (1600 MGD) in 2005 (Cooley *et al.*, 2006).

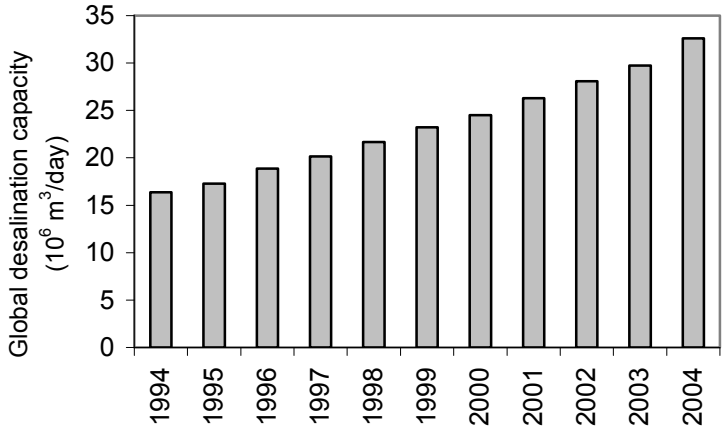

Figure 1.1 Recent global desalination production (Gleick *et al.*, 2006)

1.2 DESALINATION TECHNOLOGIES

Desalination technologies may be divided into two broad categories: thermal and membrane. Thermal technologies such as distillation, multi-stage flash (MSF), multi-effect evaporation (MEE), and vapor compression (VC) used for producing drinking water are generally more energy-intensive than membrane processes, and thus the thermal technologies are generally limited to the arid Middle East where source salinities are higher, thermal technologies are more familiar, and energy is less expensive (Fritzmann *et al.*, 2007). Most contemporary desalination technologies, especially outside of the Middle Easte, use membranes to separate salts from the product water, with the most common membrane processes being reverse osmosis (RO), nanofiltration (NF), and electrodialysis (ED). In 2002, the total worldwide desalination capacity was divided nearly equally between thermal and membrane technologies, although RO was the leading sector, as shown in Figure 1.2.

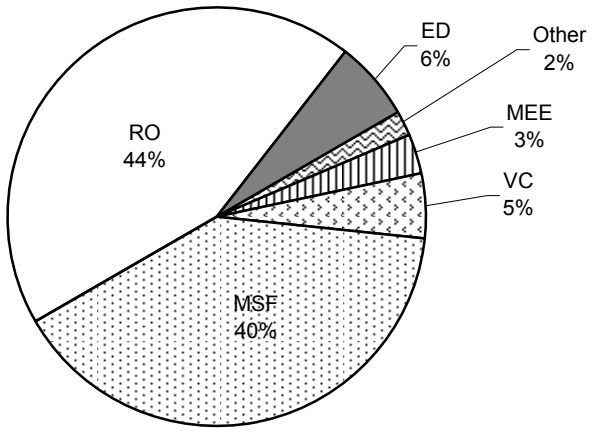

Figure 1.2 Global desalination capacity by technology (Zhou and Tol, 2005)

With recent improvements in structured RO membranes (consisting of a thin layer for the separation and a support layer for structural integrity), RO can operate at far lower pressures than earlier membranes and has become much less expensive; the average unit cost of RO has declined from \$5/m^3 (\$18.93/kgal) in 1970 to less than \$1/m^3 (\$3.79/kgal) (Zhou and Tol, 2005). A comparative cost analysis of producing 5000 m^3/day (1.32 MGD) from a 45 g/L TDS source was calculated thermo-economically at \$2.64/m^3 (\$9.99/kgal) for MSF and \$1.34/m^3 (\$5.07/kgal) for RO (Mabrouk *et al.*, 2007). In addition to the economical advantage of RO, increasing demand of desalination technology and brackish source availability have contributed to the popularity of RO technology. Thus, RO is currently the most popular desalination technology in the United States, comprising 69% of the total U.S. desalination capacity in 2005 (Gleick *et al.*, 2006).

1.3 RESEARCH CHALLENGE

A central problem in RO desalination is that the recovery ratio (the fraction of feed water that becomes product water) is limited. Brackish-water reverse osmosis (BWRO) systems are typically operated in a series arrangement with several stages, in which the concentrate from one stage is the influent to the next. The rejected ions magnify to high concentrations in the later stages, and the possibility of precipitation of various inorganic solids is the major limiting factor in recovery; scaling on a RO membrane must be avoided. Frequently, scaling is prevented by adding acid or anti-scalant compounds—complexing agents that allow the system to operate under conditions in which precipitates would otherwise be formed. Without such anti-scalants, recovery in BWRO systems is rarely greater than 75%, and even with them, recovery is rarely greater than 90% (Bonné *et al.*, 2000).

Low recovery rates prevent water-scarce inland regions from widely implementing RO to desalinate brackish groundwaters for new potable water resources, because the disposal of large volumes of waste is environmentally and financially impractical (Malmrose *et al.*, 2004; Nicot and Chowdhury, 2005). In many cases, permitting for disposal of residuals significantly inhibits desalination development by delaying the planning and design and adding financial costs. Consequently, for most inland brackish water reverse osmosis (BWRO) systems, the cost of concentrate disposal is the greatest single-cost of the entire desalination operation, sometimes greater than half of the entire desalination project cost (Reedy and Tadanier, 2008), and the cost of concentrate disposal can single-handedly control the feasibility of the project (Burbano *et al.*, 2007). Unless recovery is improved by more-efficient technologies for concentrate

waste treatment, RO use will have limited application to drought-susceptible inland regions (especially those requiring zero liquid discharge) and will be restricted to coastal areas (where disposal of the waste stream into the ocean is more environmentally and economically feasible). One more efficient technology that may improve recovery is electodialysis.

Electrodialysis[†] (ED) has been used for half a century to desalinate brackish and saline waters for potable use (Reahl, 2005). Rather than actively driving *water* through membranes with pressure (as in RO), ED drives *ions* through membranes with an electric field (which makes ED passive with respect to the bulk water flow). ED technology shows promise as a viable treatment process for BWRO concentrate for two primary reasons: it can achieve greater product recovery than RO (decreasing the total concentrate disposal), and it is more robust than RO with respect to feed turbidity, feed silica concentration, and biological growth (*i.e.*, ion-exchange membranes can tolerate a mild chlorine dose) (AWWA, 1995). While the symbiotic relationship of an RO-product with ED-concentrate treatment process has been successfully implemented in a few situations (Reahl, 1990), the scientific investigation of the use of ED as an RO concentrate treatment process is not well documented.

1.4 RESEARCH OBJECTIVES

The goal of this research was to investigate the utility of ED technology for increasing recovery in brackish water reverse osmosis (BWRO) systems by reducing the concentrate waste production, as shown in Figure 1.3.

[†] Within this document, the term "electrodialysis" or "ED" is primarily used as a category of technology and includes fixed-polarity electrodialysis as well as electrodialysis reversal (EDR).

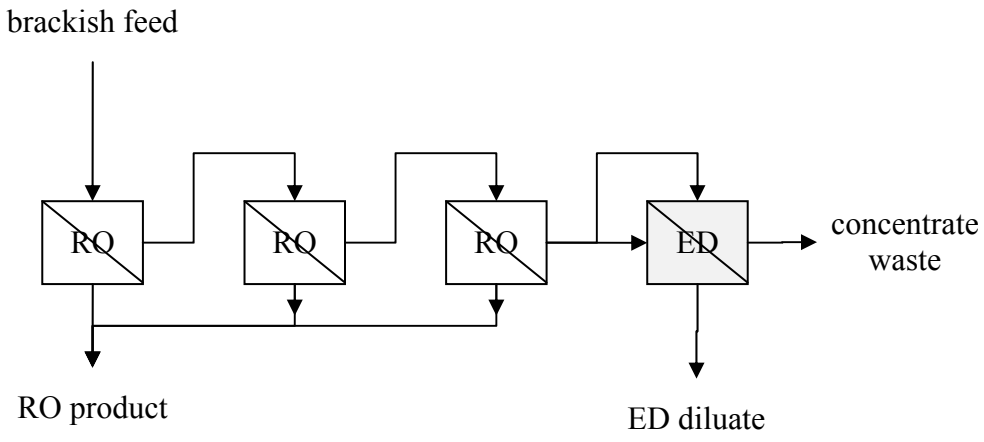

Figure 1.3 Conceptual schematic for improving BWRO recovery with ED

More specifically, the objectives of this research were to:

1. experimentally measure and quantify the efficacy and efficiency of electrodialysis separation of synthetic BWRO concentrates;
2. evaluate the performance sensitivities to electrical, hydraulic, and chemical design and operational variables;
3. develop a mathematical model to simulate batch-recycle electrodialysis performance on BWRO concentrates; and
4. perform a proof-of-concept economic cost-benefit analysis.

1.5 APPROACH

These objectives were accomplished with a research methodology utilizing laboratory experimentation and mathematical modeling (as shown in Figure 1.4) to systematically and quantitatively analyze the treatment performance of a laboratory-scale, batch-recycle ED apparatus on several synthetic BWRO concentrate wastes under various electrical, hydraulic, and chemical conditions.

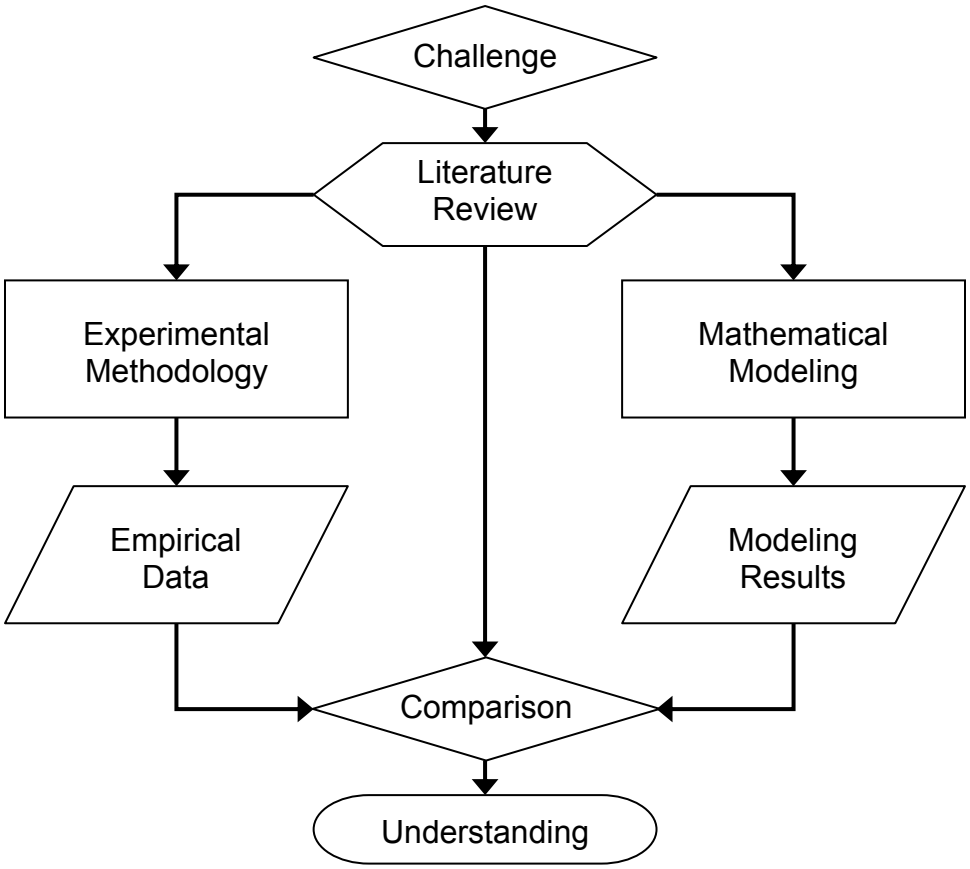

Figure 1.4 Research methodology flowchart

This dissertation communicates the details of each of the components of the research methodology shown in Figure 1.4. The introduction presented here is followed by a review of full-scale and laboratory-scale electrodialysis technology and operation in Chapter 2.

The experimental methodology (detailed in Chapter 3), which utilized continuous monitoring of the hydraulic flow rate and pressure-head loss, stack voltage and current density, and pH and electrical conductivity of each process stream, provided a detailed characterization of the process performance. Moreover, the specific ion composition of selected experimental samples was analyzed with ion chromatography and inductively

coupled plasma atomic emission spectroscopy. A discussion of experimental results is presented in Chapter 4, which responds to Objectives 1 and 2.

A combination of mathematical models (explained in Chapter 5) was developed to simulate the steady-state, single-pass operation of the laboratory-scale electrodialyzer (based on Nernst-Planck transport), as well as the batch-recycle experimental results. A preliminary cost-benefit model was developed based on the costs of electrodialysis treatment compared to the costs of alternative concentrate disposal methods. Results from these models and are presented in Chapter 6, which respond to Objectives 3 and 4. Finally, a summary of observations and conclusions drawn from this body of research are presented in Chapter 7.

Chapter 2 – Literature Review

Electrodialysis (ED) is a desalination process whereby ions are removed from the product stream using an electric field to drive them perpendicularly through ion-exchange membranes into the waste stream. The ED process was successfully demonstrated in 1940 (Tanaka, 2006), but it was not until 1953 that the first commercial ED process was installed by Ionics in Saudi Arabia (Tanaka, 2007). ED grew in application in the '50s, following the development of synthetic ion-exchange membranes (Mason and Kirkham, 1959; Mintz, 1963; Winger *et al.*, 1955). Subsequently, the world saw an increase in the use of electrodialysis technologies from 2 MGD in 1955 to greater than 200 MGD in 1992 (AWWA, 1995), and the global capacity in 2002 was approximately 500 MGD (Zhou and Tol, 2005).

After half a century of application, the ED process is well-documented. Several textbooks explain the fundamentals of electric, hydraulic, and chemical phenomena involved in the ED process (Bard and Faulkner, 2001; Bird *et al.*, 2007; Bockris and Reddy, 1998; Deen, 1998; Helfferich, 1962; Newman and Thomas-Alyea, 2004; Stumm and Morgan, 1995; Wright, 2007), and several other resources provide more practical details of industrial design and operation (AWWA, 1995; Meller, 1984; Noble and Stern, 1995; Prudich *et al.*, 2008; Strathmann, 2004; Tanaka, 2007). However, while ED has seen some applications to the treatment of BWRO concentrate waste (Reahl, 1990; Strathmann, 2004; Tanaka, 2007), little scientific investigation of its performance in this context has been documented. To appreciate the utility of ED, a review of the three inextricable aspects of the process (*i.e.*, electrical, hydraulic, and chemical) is helpful.

2.1 OVERVIEW OF ELECTRODIALYSIS (ED) PROCESS

2.1.1 Ion exchange membranes

The workhorses of the ED process are ion exchange membranes, which selectively permit or reject the transport of ions based on charge. Cation-exchange membranes (CEMs) permit cation transport but reject anion transport, and the reverse is true for anion-exchange membranes (AEMs). Ion exchange membranes are typically composed of hydrophobic polymers (such as polystyrene, polyethylene, or polysulfone) that have been modified to include "fixed" ions of one type of charge (Strathmann, 2004), making them "non-porous above the size of the interstitial spaces between the polymer chains in the cross-linked hydrated ion exchange resin" (Koprivnjak *et al.*, 2006). Most commercial CEMs have sulfonate ($-SO_3^-$) or carboxyl ($-COO^-$) fixed ions, and most commercial AEMs have quaternary ammonium ($-NR_3^+$) ions (Strathmann, 2004). The hydrated interstitial solution contains dissolved selected ions, as illustrated in Figure 2.1.

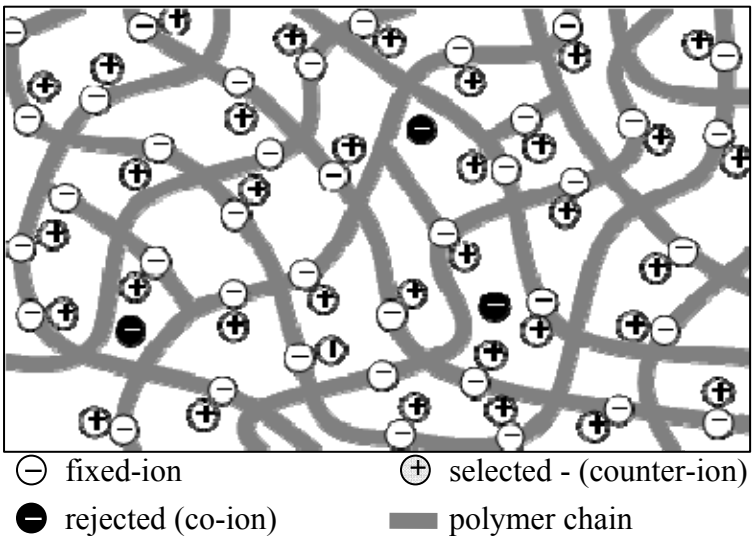

Figure 2.1 Cation exchange membrane schematic (adapted from Strathmann, 2004)

The type and concentration of functional groups chosen for the ion exchange membrane determine the ionic selectivity of the membrane. Some membranes have been tailored to achieve a strong selectivity of monovalent ions in sea water desalination (*e.g.*, Neosepta® membranes by Tokuyama used for isolating NaCl from sea water), while others have been created with balanced selectivities for "general desalination" (Strathmann, 2004). The ion exchange capacity is typically 0.5-2.0 equivalents per kilogram of dry polymer, and since the typical polymers have densities near that of water, the fixed charge density is approximately 0.5-2.0 equivalents per liter. Assuming a 1 mol/L concentration of monovalent fixed charges (c_{fixed}) and simple cubic packing arrangement, the average distance between charges (d_{avg}) can be approximated as:

$$d_{avg} = \left(c_{fixed}\ N_A\right)^{-\frac{1}{3}} = \left[\left(1000\,\frac{\text{mol}}{\text{m}^3}\right)\left(\frac{6.022\times10^{23}}{\text{mol}}\right)\right]^{-\frac{1}{3}} \approx 1.2\,\text{nm} \qquad (2.1)$$

which is quite close, considering that the H-O bond length of water is 96 pm, and the packing distance of water molecules in pure water is approximately 0.3 nm (Stumm and Morgan, 1995). Measured and modeled membrane pore diameters are in the range of 1.5-4 nm (Malewitz *et al.*, 2007).

2.1.2 Electrodialyzer stack

Commercial ED systems are composed of many pairs of alternating cation- and anion-exchange membranes (separated by plastic flow spacers) that all lie between an anode (positive) and a cathode (negative); a schematic diagram is shown in Figure 2.2. In the figure, the membranes are labeled with the sign of their fixed charge; *i.e.*, cation-exchange membranes (CEM) are shown with negative signs, and anion-exchange

membranes (AEM) with positive signs. The typical thickness of an ion exchange membrane ranges from 0.1-1.0 mm, and the typical thickness of a plastic spacer between membranes ranges from 0.3-2.0 mm. The space between adjacent ion-exchange membranes is called a *cell*, and the complete collection of membranes and spacers is referred to as a *stack*. The feed enters the cells at one edge of the stack (the bottom in the figure, ED stacks are typically operated in horizontal- or up-flow to sweep away gas bubbles), and as the water travels the pathway (in the *y*-dimension) between these membranes, cations are attracted toward the cathode (in the *x*-dimension) and anions to the anode under the influence of the applied electric field. (The *z*-dimension is unit-width.) The flux of these ions constitutes the electrical current through the electrodialyzer. As a result, some cells lose ions of both types of charge (creating the *diluate*) while the adjacent cells collect ions of both types (forming the *concentrate*).

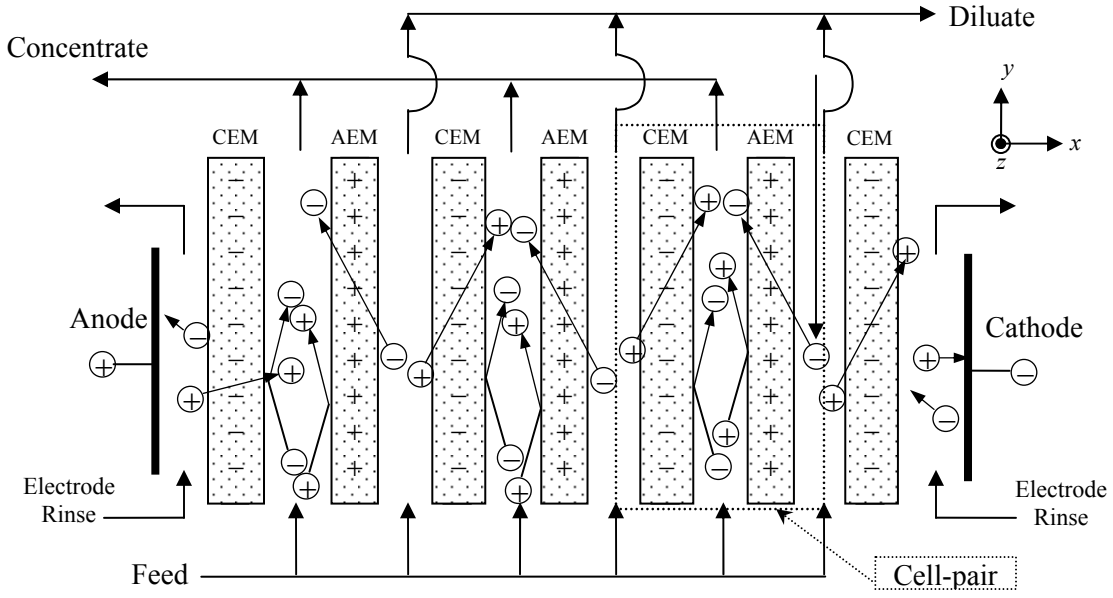

Figure 2.2 Electrodialysis Process Schematic - adapted from (Strathmann, 2004)

2.2 DESALINATION PROCESS PERFORMANCE METRICS

2.2.1 Chemical efficiency: removal ratio

The technical feasibility of a desalination process lies in the ability to remove salt from a feed stream and produce a product stream of lower salinity. The degree to which that technical goal is accomplished by a desalination process is quantified by the *removal ratio*, (*R*), which represents the "chemical efficiency" of the system and is defined as:

$$R = 1 - \frac{c_D}{c_F} \tag{2.2}$$

where c_D is the salt concentration of the effluent diluate (typically in units of mass of salt per volume of solution, following water quality regulations), and c_F is the salt concentration of the feed solution (Tanaka, 2007). (Removal ratios can also be calculated for individual ions). Typical removal ratios for a single-stage electrodialyzer range from 50% to 99% depending on source water quality (100-12,000 mg/L TDS), finished water quality (10-1000 mg/L), and system design (AWWA, 1995). It is important to note that the desired salt content of potable water is bounded; for aesthetic acceptability, the USEPA secondary standard for maximum TDS concentration in drinking water is 500 mg/L, while the TDS concentration should not be so low that the water exhibits reactive/corrosive tendencies within the distribution system (*e.g.*, TDS > 50 mg/L, for an order-of-magnitude comparison).

2.2.2 Hydraulic efficiency: recovery ratio

Another aspect of the efficiency of a desalination process is its hydraulic efficiency, or *recovery ratio*:

$$r = \frac{Q_D}{Q_F} = \frac{Q_D}{Q_C + Q_D} \tag{2.3}$$

where r is the recovery ratio, Q_C is the volumetric flow rate of the concentrate waste, Q_D is the volumetric flow rate of the product (diluate), and Q_F is the volumetric flow rate of the feed. In a single stage of ED, operated where the concentrate and diluate flow rates and feed concentrations are equal, the recovery (r) of a single stage is 50%.

As the removal ratio and recovery ratio increase, the concentration of salt in the concentrate waste stream increases. Consequently, the waste concentration factor (CF) can be calculated (for the entire system, independently of internal concentrate recycle) by material balance as:

$$CF = \frac{c_C}{c_F} = 1 + \frac{rR}{1 - r} \tag{2.4}$$

where c_C is the concentrate waste concentration, and c_F is the feed concentration. While the removal ratio does affect the magnitude of the concentration factor, the concentration factor is predominantly controlled by the recovery ratio (as shown in Figure 2.3), and the concentration factor increases dramatically with recovery ratios approaching zero liquid discharge (ZLD).[†]

[†] Note that while high recoveries are positively correlated with ZLD, a ZLD system does not necessarily achieve a high recovery, as sometimes it is necessary to waste some water (*e.g.*, solar evaporation) to achieve ZLD.

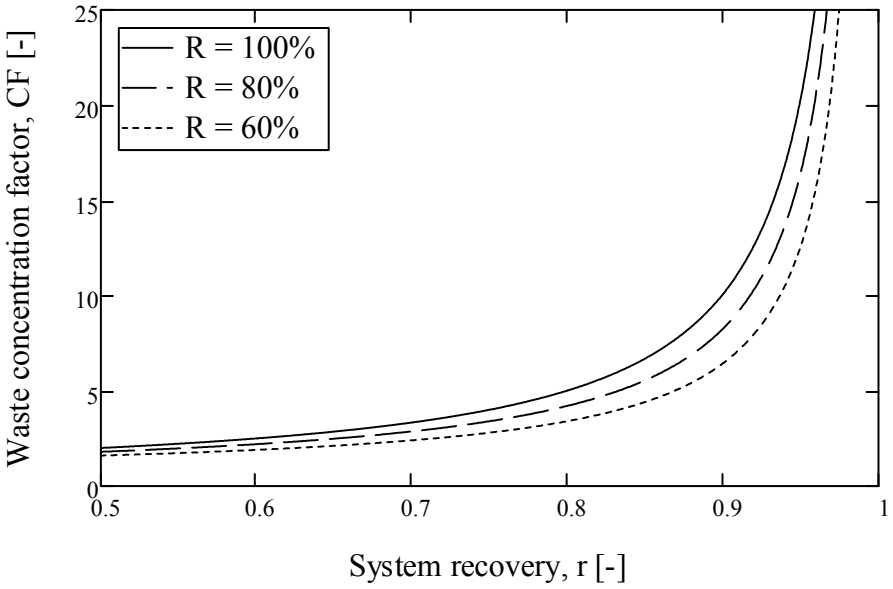

Figure 2.3 Influence of system recovery on waste concentration factor

2.2.3 Electrical efficiency: specific energy consumption

The other principal evaluation of process efficiency is specific energy consumption (SEC), which quantifies how much energy is consumed by the desalination process to produce a given volume of desalinated (product) water. The theoretical minimum SEC for desalinating water is the thermodynamically reversible change in Gibbs free energy required for the separation process (Strathmann, 2004):

$$\frac{\Delta G}{V_D} = \nu_d R_g T\left(c_F - c_D\right)\left(\frac{\ln\left(\frac{c_F}{c_C}\right)}{\frac{c_F}{c_C}-1} - \frac{\ln\left(\frac{c_F}{c_D}\right)}{\frac{c_F}{c_D}-1}\right) \tag{2.5}$$

where ΔG is the change in Gibbs free energy per volume of diluate (V_D), ν_d is the stoichiometric dissociation coefficient of the salt (*i.e.*, the summation of coefficients of ions in the salt dissociation equation; *e.g.*, $\nu_d = 2$ for NaCl), c is the concentration of salt

in the feed ($_F$), concentrate ($_C$), and diluate ($_D$). For example, desalinating a source water of 10,000 mg/L of NaCl to a potable 250 mg/L at 75% recovery would require a thermodynamic minimum of 0.20 kWh/m^3.

The thermodynamic second-law efficiency is the ratio of the reversible (minimum) energy invested to the irreversible (actual) energy invested. In practical desalination systems, the second-law efficiency can be much less than unity because of the irreversibility of operating at an appreciable desalination rate, in addition to the energy of pumping solutions through the system (Spiegler and El-Sayed, 2001). The actual SEC can be calculated for batch or continuous-flow desalination operations as:

$$SEC = \frac{E}{V_D} = \frac{P}{Q_D} \tag{2.6}$$

where *SEC* is the specific energy consumption (typically expressed in kWh/m^3), E is the total energy invested in a batch-desalination process to produce V_D volume of desalinated water, or P is the total power (energy per time) invested in a continuous-flow desalination process to produce Q_D volumetric flow of desalinated water. The SEC of a full-scale membrane desalination of brackish to sea water sources typically ranges from 1-10 kWh/m^3, depending on source water TDS, process technology, recovery ratio, and removal ratio (Adhikary *et al.*, 2004; Turek, 2003; Turek, 2004; Turek and Dydo, 2008). For comparison, the work equivalent of the SEC of a full-scale thermal process such as MED and MSF typically ranges from 20-40 kWh/m^3 (Semiat, 2008).

2.3 ELECTRODIALYSIS OPERATION

2.3.1 Chemical flux

Fundamentally, the driving force for the net migration of a particular species (*i*) is a gradient in its electrochemical potential (Bard and Faulkner, 2001; Bockris and Reddy, 1998; Newman and Thomas-Alyea, 2004; Strathmann, 2004). For dilute and moderate ionic concentrations, the transport of a particular ion within the electrodialyzer may be approximated by the Nernst-Planck Equation[†], which is the summation of diffusive and dispersive, electromigrative, and advective mechanisms (here shown for the *x*-dimension):

$$J_i = J_{i,D} + J_{i,\psi} + J_{i,adv} = -D_i \frac{dc_i}{dx} - \frac{F}{R_g T} D_i z_i c_i \frac{d\phi}{dx} + v_x c_i \tag{2.7}$$

where J is the molar flux of species i, D is the ionic diffusivity (or it may be a lumped parameter that includes both diffusion and dispersion), c is the molar concentration of species i, F is the Faraday constant (which is the product of Avogadro's number, N_A, and the elementary charge, q_e), R_g is the molar gas constant, T is the solution temperature, z is the sign and magnitude of the charge of the ion, ϕ is the electric potential, and v is the bulk solution velocity (Bard and Faulkner, 2001). The diffusivity of an ion is sometimes represented as ionic mobility, u_i, or equivalent ionic conductivity, λ_i, (sometimes "ionic equivalent conductance"), and these parameters are related by the following expression (Bard and Faulkner, 2001)[†]:

[†] A derivation of the Nernst-Planck Equation from the gradient in electrochemical potential is given in (Strathmann, 2004).

[†] Note that Newman and Thomas-Alyea (2004) define mobility differently: $u_i = \lambda_i / |z_i|F^2$ (*cf.* p. 284)

$$\frac{F}{R_g T} D_i |z_i| = u_i = \frac{\lambda_i}{F} \tag{2.8}$$

The electrical conductivity (κ) of an electrolyte solution (which is the reciprocal of the solution's electrical resistivity, ρ) is an aggregate of the ionic composition:

$$\kappa = \frac{1}{\rho} = \frac{F^2}{R_g T} \sum_{\mathrm{i}} D_{\mathrm{i}} z_i^{\,2} c_i = F \sum_{\mathrm{i}} u_{\mathrm{i}} |z_i| c_i = \sum_{\mathrm{i}} \lambda_{\mathrm{i}} |z_i| c_i \tag{2.9}$$

where the variables are the same as defined above (Strathmann, 2004). A discussion of the mathematical modeling of the electrical conductivity is presented in §2.7.2.

2.3.2 Electrical flux

The total electrical current density (charge flux), i_{tot}, passing through the ED stack is the summation of the fluxes of all charged species in solution,

$$i_{tot} = \sum_i i_i = F \sum_i z_i J_i \tag{2.10}$$

and the fraction of the current that a particular ion carries is called the transport number:

$$t_i = \frac{i_i}{i_{tot}} \tag{2.11}$$

where t is the transport number in the solution phase. (By definition, the summation of transport numbers equals unity.) For example, in a well-mixed NaCl solution, the transport numbers of Na^+ and Cl^- are approximately 0.4 and 0.6, respectively, because the diffusivity of Cl^- is approximately 50% greater than the diffusivity of Na^+. The transport number of a species in the membrane phase has the same definition but is usually distinguished by an overbar in literature, $\bar{t}_i$. The summation of transport numbers of

cations equals unity for an ideal CEM, and the summation of transport numbers of *anions* equals unity for an ideal AEM.

In an ideal ED system, the rate of separation of ions is proportional to the electrical current density through the electrodialyzer. In a real electrodialyzer, however, the number of salt ions separated is less than the electrical equivalent of the current density because of inefficiencies within real (non-ideal) ion exchange membranes and short circuiting of electrical current through influent and effluent hydraulic manifolds. Current utilization (or current efficiency), ξ, is the fraction of the electrodialyzer current density (*i.e.*, charge flux) that is ultimately effective at separating ions from the diluate to the concentrate stream, and it can be approximated as:

$$\xi = \frac{Q_d F\left(c_f - c_d\right)}{N_{cp} I} \tag{2.12}$$

where c_f and c_d are equivalent concentrations. Current utilization is typically greater than 90% (AWWA, 1995).

Considering the electrodialyzer as an electrically resistive device ("black box"), the electrical current density, i, passing through the electrodialyzer is given by:

$$i = \frac{\Delta\phi_{stack}}{\tilde{R}_{ed}} \tag{2.13}$$

where $\Delta\phi_{stack}$ [†] is the potential loss (or voltage drop, often reported in volts per cell-pair) across the stack, and $\tilde{R}_{ed}$ is the areal electrical resistance (Ω m^2) of the electrodialyzer (Landau, 1994).

[†] Note that the potential loss at the electrodes is quantified in §3.4.1, and detailed computations of the stack potential and resistance are explained in §5.4.

2.3.3 Hydraulic flow

The hydraulic conditions significantly influence the electrochemical performance of the ED system. Consider a concentrate and diluate cell-pair without inter-membrane spacers, from one CEM to the next CEM in an ED stack, as shown in Figure 2.4. If sufficient solution flow rate is delivered to achieve "moderate" turbulence, then the time-averaged velocity distribution between membranes includes: 1) a no-slip boundary condition at each membrane-fluid interface, 2) a steep linear velocity gradient in the fluid near the membrane surface known as the viscous sub-layer, 3) a transition from viscous-dominated fluid motion to inertial-dominated fluid motion, and 4) a "constant" velocity in the bulk flow where random inertial perturbations keep the bulk flow well-mixed (Bird *et al.*, 2002, §5.3), as illustrated by the velocity profile in the bottom of each cell in Figure 2.4. Theoretical treatments of the performance of ED with unobstructed laminar and completely mixed flow have been published (Solan and Winograd, 1969; Sonin and Probstein, 1968). However, most ED systems operate with inter-membrane spacers for structural support and to ensure moderate turbulence at lower bulk velocities.

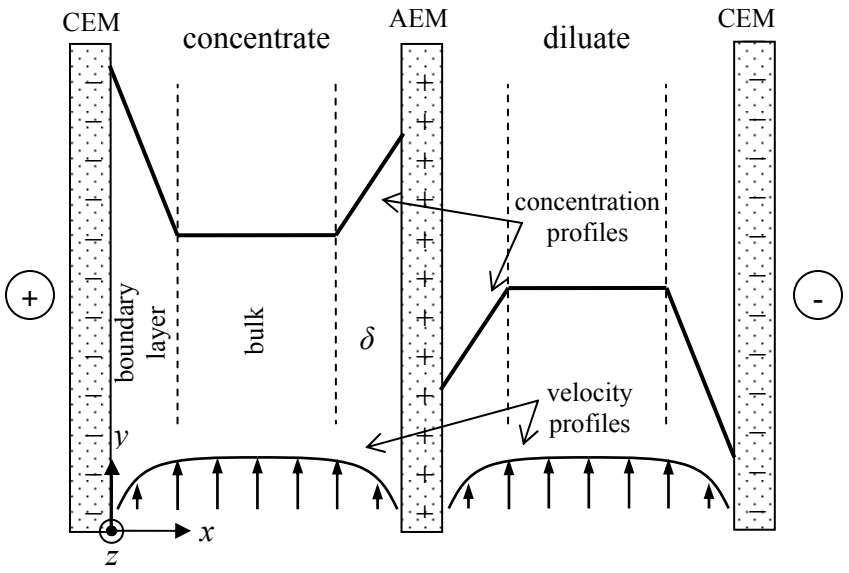

Figure 2.4 Simplified inter-membrane velocity and concentration profiles

While the complicated three-dimensional inter-membrane hydraulic behavior around spacers could be modeled with computational fluid dynamics (CFD) simulations, the hydraulic behavior is often approximated as one-dimensional with variations in the *x*-dimension and constant in the *y*- and *z*-dimensions. It is assumed that the spacers cause a well-mixed bulk flow and that the no-slip boundary condition at the membrane surface causes (symmetric) diffusion boundary layers, of thickness δ, with negligible mixing.

2.4 ELECTRODIALYSIS CHALLENGES

2.4.1 Concentration polarization

Under steady-state operation, as ions are removed from the diluate cell through the bounding membranes (in the *x*-dimension), the salt concentration decreases from the well-mixed bulk to the membrane surface (in the *x*-dimension), as shown in Figure 2.4. Conversely, as ions are supplied to the concentrate cell through the bounding membranes, the salt concentration decreases from the membrane surface to the bulk. Following the

hydraulic approximation above, the concentration profile (in the *x*-dimension) is approximated (idealized) as a constant concentration within the well-mixed bulk region, and linear concentration gradients in the diffusion boundary layers (Strathmann, 2004, §4.2).

The concentration difference between the two surfaces of each membranes is known as *concentration polarization* (Strathmann, 2004; Tanaka, 2007). Because the membranes reject one type of ion, the concentration gradient within the diffusion boundary layer reaches a magnitude such that the diffusive flux term (exactly) opposes the electromigration flux of the rejected ion within the diffusion boundary layer. That is, the concentration gradient in the diffusion boundary layer at a given point, *y*, along the flow path, is approximately proportional to the electrical current density flowing through the electrodialyzer (in the *x*-dimension) at *y*:

$$\frac{\Delta c_{dbl}}{\delta} \propto i \tag{2.14}$$

As illustrated in Figure 2.4, the magnitude of the concentration gradient adjacent to a CEM is generally greater than the concentration gradient adjacent to an AEM because the diffusivities of cations are generally less than anions. Also illustrated in Figure 2.4, the concentration of salts in the diluate diffusion boundary layer can be quite low, and the concentration of salts in the concentrate diffusion boundary layer can be high. Both cases are problematic, as shown subsequently.

2.4.2 Limiting current density: a diluate problem

As the current density through the electrodialyzer is increased from zero (by increasing the voltage at the electrodes), the concentration gradient in the diffusion

boundary layer becomes steeper. If the concentration gradient becomes too steep (or, if the diffusion boundary layer thickness is too large), then the salt concentration in the diluate diffusion boundary layer approaches zero at the membrane surface (as illustrated in Figure 2.4). The *limiting current density* (i_{lim}) occurs when the ions are "completely" depleted at the membrane surface, and the classic expression for the limiting current density of a binary salt (derived from the previous proportionality) is:

$$i_{\lim} = \frac{F|z|c_D}{\bar{t} - t}\frac{D}{\delta} = \frac{F|z|c_D}{\bar{t} - t}k \tag{2.15}$$

where δ is the diffusion boundary layer thickness, and the dilate molar concentration (c_D), ionic charge (z), membrane- and solution-phase transport numbers ($\bar{t}$ and t, respectively), and diffusivity (D) refer to the limiting ion (Lee *et al.*, 2002). For simplicity, and since the diffusion boundary layer thickness is an empirically determined parameter, the ratio of diffusivity to diffusion boundary layer thickness is often consolidated into a single mass-transfer coefficient, k. If the bulk diluate concentration is increased, or if the diffusion boundary layer thickness is decreased, then the limitation on electrical current is raised, which results in an increase in the maximum rate of desalination. Also, if the ion exchange membrane is less-restrictive (*i.e.*, the difference between the membrane- and solution-phase transport numbers is smaller), then the limiting current density will be higher.

2.4.3 Scaling and fouling: a concentrate problem

Brackish groundwater often has relatively high concentrations of calcium, magnesium, carbonate, and sulfate, which often leads to supersaturation of at least one of

their salts within the concentrate stream of a BWRO system. While the ED technology is more robust to precipitation than RO technology, the precipitation of salts is most likely to occur in the concentrate diffusion boundary layers (as illustrated in Figure 2.4), which can decrease the mass-transfer efficiency, increase electrical resistance, increase pumping head loss, and irreversibly damage the membranes (Strathmann, 2004; Yang *et al.*, 2005). Thus, scaling and fouling pose one of the greatest technical challenges of desalinating more concentrated solutions (Lee *et al.*, 2009).

The chemical expression for the dissociation of the general salt, $A_xB_{y\,(s)}$ is:

$$A_xB_{y\,(s)} \Leftrightarrow xA^{y+}_{(aq)} + yB^{x-}_{(aq)} \tag{2.16}$$

and the solubility constant of that expression, K_{s0}, is given by:

$$K_{s0} = \left\{A^{y+}_{(aq)}\right\}^x \left\{B^{x-}_{(aq)}\right\}^y \tag{2.17}$$

where the braces indicate activity of the aqueous species at equilibrium, and the activity of the solid is conventionally assigned the value of unity (Stumm and Morgan, 1995). A table of the negative logarithm of solubility constants (pK_{s0}) at 25°C for solid salts of common BWRO cations and anions is shown in Table 2.1. In addition, the pK_{s0} value for H_2SiO_3 is 25.7. For example, the aqueous concentration of calcium in equilibrium with calcite (c_{sat}), where calcium and carbonate are equimolar, is given by:

$$c_{sat,Ca^{2+}} = \left(K_{s0,calcite}\right)^{1/\nu_d} = \sqrt{10^{-8.35}} \approx 67\mu M \tag{2.18}$$

where ν_d is the summation of stoichiometric coefficients of the ions in the salt dissociation equation (*e.g.*, x+y).

Table 2.1 pK_{s0} values for common BWRO salts (Stumm and Morgan, 1995, App. 6.1)

Cation\Anion	Br^-	Cl^-	CO_3^{2-}	F^-	NO_3^-	OH^-	SO_4^{2-}
Ba^{2+}	-	-	8.3	5.8	-	-	10.0
Ca^{2+}	-	-	8.22 8.35	10.4	-	5.19	4.38 4.62
Cu^{2+}	-	-	9.6	-	-	19.3 20.4	-
Fe^{3+}	-	-	-	-	-	38.8 42.7	-
K^+	-	-	-	-	-	-	-
Mg^{2+}	-	-	4.54 7.45	8.2	-	11.16	-
Mn^{2+}	-	-	10.4	-	-	12.8	-
Na^+	-	-		-	-	-	-
Sr^{2+}	-	-	9.0	8.5	-	-	6.5
Zn^{2+}	-	-	10.0	-	-	15.5 16.8	-

The thermodynamic driving force for precipitation (*i.e.*, the magnitude of dis-equilibrium) of a particular compound can be characterized by the saturation ratio, *S*:

$$S = \left(\frac{IAP}{K_{s0}} \right)^{1/\nu_d} \tag{2.19}$$

where *IAP* is the ion activity product of the precipitating ions in the supersaturated solution. If *S* is less than unity, then the system will tend to dissolve any solid that may be present, and if *S* is greater than unity, then the system will tend to precipitate the solid salt. In addition to equilibrium, the kinetics of crystal growth has been shown to be positively correlated with the relative supersaturation, σ (Nielsen, 1984):

$$\sigma = S - 1 \tag{2.20}$$

Alternatively, the supersaturation of a solution with respect to a particular compound could be described by the saturation index (*SI*):

$$SI = \log\left(\frac{IAP}{K_{s0}}\right) \tag{2.21}$$

where the variables are the same as above. For example, the Langelier Saturation Index (*LSI*) is a quantification, in pH units, of a solution's solubility condition with respect to calcium carbonate. It is calculated as the difference between the actual pH (pH_{act}) of the solution and the pH under which precipitation of the given ion concentrations would occur (pH_{eq}):

$$LSI = pH_{act} - pH_{eq} \tag{2.22}$$

Thus, a negative *LSI* indicates that the solution is under-saturated, which will dissolve solid calcium carbonate. An *LSI* of zero means that the solution is poised at solubility, and a positive *LSI* indicates that the solution is super-saturated, which could result in solid calcium carbonate formation (Stumm and Morgan, 1995).

2.5 ELECTRODIALYSIS OPTIMIZATION

2.5.1 Hydraulic: improving the rate of mass-transfer

With respect to optimization, an inherent tradeoff exists in ED performance with respect to the inter-membrane velocity (the velocity of the solution flowing through a concentrate or diluate cell). Decreasing the inter-membrane velocity decreases the irreversible energy spent on fluid turbulence, which results in minimizing the cost of pumping solutions through the electrodialyzer (though the pumping cost is typically much less than the electrical separation cost). Decreasing the inter-membrane velocity

also requires a shorter flow distance for the same mean hydraulic residence time, which saves on the capital costs related to the size of the electrodialyzer. However, increasing the inter-membrane velocity in a *diluate* cell promotes mixing (and possibly, turbulence), which improves the rate-limiting mass-transport through the diluate diffusion boundary layer by decreasing the diffusion boundary layer thickness (*cf*. Figure 2.4).

Since the concentration gradient in the diffusion boundary layer is proportional to the current density, a decrease in the diffusion boundary layer thickness corresponds to a decrease in the change in concentration from the membrane surface to the interface between the diffusion boundary layer and the bulk. And since one of the larger contributions to electrical resistance in the solution phase occurs in the diluate diffusion boundary layers (because of a lack of charge carriers), a reduction in the diffusion boundary layer thicknesses results in a decrease in the electrical resistance of the stack (thus improving the electrical efficiency).

Dimensionless parameters commonly appearing in such rate of transport treatments are the Reynolds and Schmidt numbers. The Reynolds number (*Re*) characterizes the ratio of inertial and viscous forces of the fluid dynamics:

$$Re = \frac{\rho L_{char} \, \mathrm{v}}{\mu} = \frac{L_{char} \, v}{\nu} \tag{2.23}$$

where ρ is the solution mass-density, L_{char} is a characteristic length-scale of mixing (typically taken as the distance between the membranes), v is the solution velocity, μ is the absolute (dynamic) viscosity of the solution, and ν is the kinematic viscosity (Reynolds, 1883). Considering that the solution density and viscosity are near constant in

ED systems (across a wide range in salinity for a given operating temperature, as shown in Table 2.2), and since the mixing length scale is approximately constant for a given ED system, the Reynolds number is essentially a scalar of velocity in a particular ED system. Unfortunately, because of the variation in spacer structure and the complicated fluid dynamics, it is difficult to precisely characterize the turbulence of the boundary layers with the Reynolds number (as compared to flow through conduit). Moreover, it is nearly impossible to predict the laminar-turbulent transition of flow through an electrodialyzer. For simplicity and consistency for comparison among various ED systems, a representative Reynolds number is computed using the thickness of the spacer as the characteristic length-scale and the superficial velocity.

Table 2.2 Density and viscosities of seawater and fresh solutions

Solution[†]	Temperature T (°C)	Abs. Viscosity μ (10^{-6} kg m^{-1} s^{-1})	Density ρ (kg m^{-3})	Kin. Viscosity ν (10^{-6} m^2 s^{-1})
seawater	20	1070	1023	1.046
water	20	1002	998.2	1.003
	25	890	997.0	0.893
	30	798	995.7	0.800

[†] at standard sea-level atmospheric pressure (Franzini and Finnemore, 1997)

Similarly, the Schmidt number (*Sc*) represents the ratio of viscous and diffusive forces within the solution:

$$Sc = \frac{\mu}{\rho D} = \frac{\nu}{D} \tag{2.24}$$

where D is the diffusivity, which ranges from 0.2–2×10^{-9} m^2 s^{-1} for common ions, depending on concentration. Considering the range of the kinematic viscosity of an ED

process stream and the range of diffusivity of a common BWRO ion, the Schmidt number of these ions is in the range of 400-4000.

A non-dimensional mass-transfer coefficient can be created (*i.e.*, the Sherwood number, *Sh*), which has been shown to be related to the Reynolds and Schmidt numbers in the form:

$$Sh = \alpha_0 \, Re^{\alpha_1} \, Sc^{\alpha_2} \propto v^{\alpha_1} \tag{2.25}$$

where α_0, α_1, and α_2 are fitting parameters that may be theoretically approximated and empirically validated. α_0 is typically in the range of 0.6-1.2, and α_1 and α_2 are approximately 0.3-0.5, depending on geometry (Bird *et al.*, 2002, §22.2; Tanaka, 2007, §10.3.2). This functionality reiterates the coupling of the hydraulic and electrochemical behavior, and demonstrates that the limiting rate of mass-transport in an ED system (at a given electrical condition) is approximately proportional to the square root of velocity.

In addition, a decrease in the concentrate diffusion boundary layer thickness results in a lower concentration of salts at the membrane surfaces. This relationship could allow a system to operate at a greater current density either without reaching saturation or in supersaturated conditions where crystallization kinetics are tolerably slow. (Some work theorizes that while increased turbulence decreases the diffusion boundary layer thickness, it also increases the significance of limiting current depression in the presence of fouling anion-exchange films on CEMs and fouling cation-exchange films on AEMs (Grossman and Sonin, 1972; Grossman and Sonin, 1973), but their experimental results did not confirm that speculation.)

Naturally, researchers have sought to characterize the hydrodynamic flow conditions in ED systems with and without spacers (Belfort and Guter, 1972; Grigorchuk *et al.*, 2005; Shaposhnik *et al.*, 2006; Shaposhnik *et al.*, 1997; Shaposhnik *et al.*, 1995; Solan *et al.*, 1971; Sonin and Probstein, 1968; Tanaka, 2007) and to improve the mass-transport with novel spacer design (Balster *et al.*, 2006; Shahi *et al.*, 2001; von Gottberg, 1998). Spacers of various geometries and materials have been studied to simultaneously improve the electrochemical separation efficiency (increase the mass-transfer coefficient), increase the electrical efficiency (minimize the electrical resistance of the diluate diffusion boundary layer), and decrease the required pumping power. Furthermore, an increase in mixing in the concentrate cell can prevent scale formation in the stagnant regions that first show accumulation of precipitates (Berger and Lurie, 1962).

2.5.2 Hydraulic: improving recovery

Another strategy for improving the efficiency of ED is to increase the recovery of a single stage. This improvement can be accomplished by operating the concentrate stream at a lower flow rate than the diluate stream, but this operation results in a lower pressure in the concentrate cells than the diluate cells (trans-membrane pressure). (In full scale ED processes, the system is often intentionally operated such that the concentrate cells have slightly lower pressure than the diluate cells to prevent contamination of the diluate stream from leaks.) More commonly, the recovery of a single ED stage can be increased by recycling effluent concentrate to the influent concentrate, as illustrated in Figure 2.5.

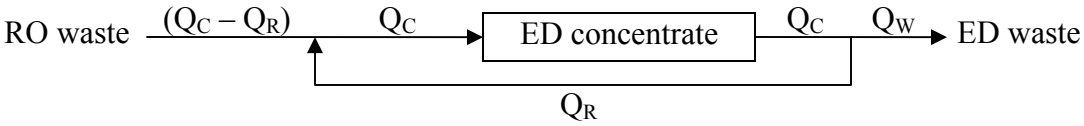

Figure 2.5 Schematic of concentrate recycling for increasing single-stage ED recovery

In such case, the single-stage recovery (r) is given by:

$$r = \frac{1}{2 - \frac{Q_R}{Q_C}} \tag{2.26}$$

where Q_C is the concentrate flow rate (which is typically equal to the diluate flow rate) through the stack, and Q_R is the flow rate that is recycled from the concentrate effluent to the concentrate influent. By material balance, the concentration of salt in the concentrate stream entering the stack ($c_{C,in}$) is:

$$c_{C,in} = c_F \left(1 + R \frac{2r - 1}{1 - r}\right) \tag{2.27}$$

where the parameters are the same as defined above. The first challenge in this type of operation is that, as the recovery ratio increases, precipitation in the concentrate stream is more likely to occur because of the elevated ionic concentrations. The ratio of the influent concentrate concentration ($c_{C,in}$) to the feed concentration (c_F), or the influent concentrate concentration factor (ICCF), is illustrated in Figure 2.6 for three removal ratios.

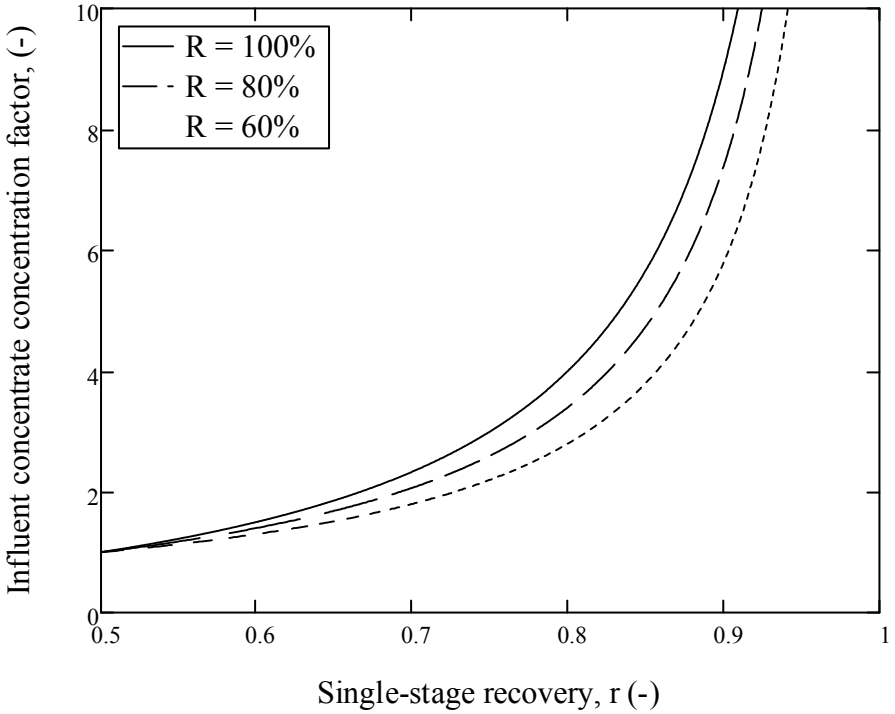

Figure 2.6 Influence of single-stage recovery on influent concentrate concentration factor for the system shown in Figure 2.5

For a single-stage electrodialyzer operating at 80% removal (which, in the context of this research, is producing a product concentration equal to the feed concentration of an RO system operating at 80% recovery and 100% removal), the influent concentrate concentration factor is approximately 2.1 and 4.2 (*i.e.*, approximately 10 or 20 times the concentration of the RO feed) for recoveries of 70% and 83%, respectively.

The second challenge in this type of operation is that, as the recovery ratio increases, precipitation in the concentrate stream is more likely to occur because a greater fraction of the concentrate effluent is recycled to the influent, which increases the total residence time of some of the flow and could allow time for seed crystals to form within the electrodialyzer. If the collection of concentrate cells within the electrodialyzer and

the recycle conveyance system are treated as ideal PFRs with mean hydraulic residence times, τ_C and τ_R, respectively, then the dimensionless time, θ, and cumulative probability function (F, or cumulative age distribution) of the system shown in Figure 2.5 are given parametrically in the following equations,

$$\theta = \frac{t}{\tau_C} = \begin{cases} 0 & if \quad n = 0 \\ 1 + (n-1)\left(1 + \dfrac{\tau_R}{\tau_C}\right) & if \quad n \geq 1 \end{cases} \tag{2.28}$$

$$F = \begin{cases} 0 & if \quad n = 0 \\ 1 - \left(\dfrac{Q_R}{Q_C}\right)^n & if \quad n \geq 1 \end{cases} \tag{2.29}$$

which are plotted in Figure 2.7 for two recoveries and recycle residence time ratios, τ_R/τ_C. Since the residence time of the concentrate is on the order of a minute, greater than 99% of the influent RO waste exits the ED concentrate recycling system within an hour.

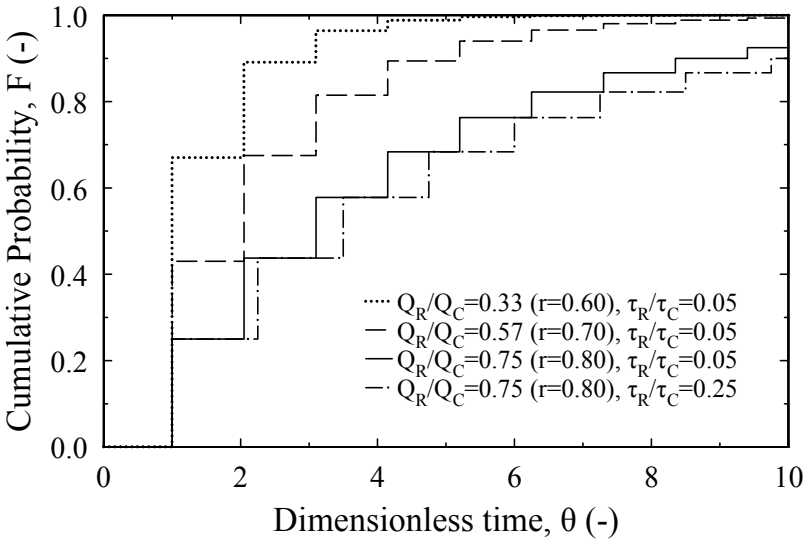

Figure 2.7 Cumulative probability (exit age) distribution of the concentrate recycle system shown in Figure 2.5

2.5.3 Electrical: decreasing the electrical resistance of the stack

The resistance of the stack varies along the flow path because it is a function of the current density and process stream salinities. The resistance of the stack is the summation of the resistances of the electrode rinse solutions and all cell pairs, and each cell pair is composed of eight electrically distinct regions (as illustrated in Figure 2.4): (1) the CEM, (2) the concentrate diffusion boundary layer adjacent to the CEM, (3) the concentrate bulk, (4) the concentrate diffusion boundary layer adjacent to the AEM, (5) the AEM, (6) the diluate boundary layer adjacent to the AEM, (7) the diluate bulk, and (8) the diluate boundary layer adjacent to the next CEM.

The areal resistances of many commercial AEMs and CEMs have been published (Strathmann, 2004; Tanaka, 2007), and typical values are in the range of 1-10 Ω-cm^2. The solution phase resistances are functions of chemical composition (Landolt and Börnstein, 1960b), and the areal electrical resistance of each of these regions, $\tilde{R}$, is given by:

$$\tilde{R} = \frac{w}{\kappa} \tag{2.30}$$

where w is the width (in the same direction as the electrical current) of the electrically resistive region, and κ is the electrical conductivity of that region. For example, a one millimeter thick bulk solution of 100 mM NaCl has an areal resistance of approximately 10 Ω-cm^2.

A gain in the efficiency of electrodialysis systems could be accomplished by developing ion exchange membranes with lower electrical resistance (by decreasing

width and increasing conductivity) while maintaining permselectivity. Also, the resistance of the bulk region decreases with increasing salinity, so the electrical resistance of the concentrate cell can be reduced by recycling concentrate. In addition, the electrical resistance of the diluate diffusion boundary layer can be reduced by reducing its thickness through enhancing mixing (*e.g.*, improved spacer design or increased velocity).

2.5.4 Chemical: preventing scaling and fouling

Because of the probability of supersaturation in the concentrate cells within ED, it is sometimes necessary to proactively prevent scaling and fouling. Some ED systems treating brackish sources can sufficiently prevent scaling and fouling by reversing the polarity of the voltage applied to the stack every 15-30 minutes, a process known as electrodialysis reversal (EDR).

Another technique for improving recovery and avoiding the complication of scaling in ED concentrate cells is to use standard CEMs and monovalent selective AEMs (such as Aciplex A 192, Neosepta ACS-3, or Selemion ASV) in the first stage and treat the diluate from the first stage with standard AEMs and monovalent selective CEMs (such as Aciplex K 192 or Neosepta CMS) (Strathmann, 2004). This arrangement avoids supersaturation of divalent salts in the concentrate cells of either stage, but upon mixing the concentrates from both stages, supersaturation and rapid precipitation could occur (AWWA, 1995).

In the treatment of very brackish sources, and especially BWRO concentrate wastes, electrical polarity reversal alone is insufficient to avoid precipitation, so chemicals are added to the concentrate process stream. Adding acid (*e.g.*, HCl or $CO_{2\,(g)}$)

to reduce the pH can be effective at preventing CO_3^{2-} and OH^- salt precipitation. However, with $CaSO_4$ and $BaSO_4$, saturation ratios greater than 2 and 10, respectively, generally require the use of antiscalants (Tanaka, 2007).

Antiscalants are organic compounds used to complex with supersaturated salts and delay precipitation. Depending on the saturation ratio and the concentration of antiscalant, precipitation may be delayed by minutes, hours, or even days. In traditional ED systems operating near or above saturation in the concentrate, condensed sodium phosphate, carboxyl methyl cellulose (CMC), or poly-acrylic acid is added to the concentrate stream to sufficiently delay precipitation, up to 225% saturation of sulfate salts (Berger and Lurie, 1962; Tanaka, 2007).

One of the most commonly used types of antiscalants in RO applications is based on phosphonate compounds. Amino tri-methylene phosphonic acid (ATMP, molecular weight 299.05 g/mol) and diethylene triamine pentamethylene phosphonic acid (DTPMP, molecular weight 573.2 g/mol) are effective antiscalants for calcium carbonate, calcium sulfate, and barium sulfate. The molecular structures of these antiscalant compounds are shown in Figure 2.8.

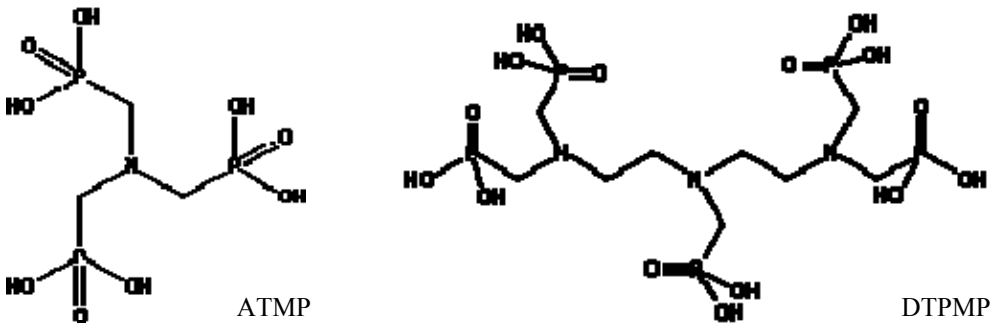

Figure 2.8 Molecular structure of ATMP and DTPMP antiscalants (WIC, 2007)

Most of the marketed antiscalants are proprietary mixtures of various organic compounds and polymers, and the product recommendations are site and application specific. Because of the risk of irreversible scaling on RO membranes, operators usually apply antiscalant with a safety factor. The mean hydraulic residence time of RO systems is on the order of minutes, so the concentrate waste stream contains "active" antiscalant, and may impact the performance of an ED concentrate treatment system.

One process for recovering this RO concentrate waste is to remove the principal scaling agents by precipitation and solid-liquid separation. One technique for facilitating precipitation is accomplished by raising the pH to precipitate calcium and magnesium salts, which can be achieved through standard softening treatment methods (Greenlee *et al.*, 2010a; Greenlee *et al.*, 2010b). Another technique is to inactivate the anti-scalant behavior of the antiscalant chemicals using an advanced oxidation process (AOP) such as ozone-peroxide (peroxone) treatment (Greenlee, 2009). A third technique is to induce precipitation by the addition of standard water treatment coagulant and surfactants such as poly-aluminum chloride (PACl) and sodium dodecyl sulfate (SDS) (Yang *et al.*, 2007).

2.6 BATCH-RECYCLE ELECTRODIALYSIS EXPERIMENTATION

The objective of the laboratory-scale batch-recycle reactor design experimentation is to observe the pseudo-steady-state operation of the electrodialysis system *as a function of time*, which is mathematically similar to the full-scale single-pass operation as a function of distance along the flow path, from inlet to outlet. The experimental apparatus is designed in such a way that the following batch-recycle and pseudo-steady-state criteria are (approximately) satisfied:

1. The chemical composition of the concentrate (C) or diluate (D) reservoir has no spatial gradients; that is, the reservoir is completely mixed and thus behaves as a continuous flow, stirred-tank reactor (CFSTR). This criterion is accomplished by vigorous continuous stirring.
2. At any point in time, the system is considered to be at pseudo-steady-state. This criterion is satisfied by minimizing the ratio of the mean hydraulic residence time of the electrodialyzer compared to the mean hydraulic residence time of the entire system; that is, the volume of the reservoir is significantly greater than the volume of solution in the electrodialyzer.

The experimentation is also designed in such a way that dynamic similitude is maintained between full-scale operation and batch-recycle experimentation for the following parameters:

1. Hydraulic - the velocity of the inter-membrane flow;
2. Electrical - the electric potential drop per cell-pair, and consequently, the current density
3. Chemical - the concentration of electrolytes, neutral compounds, and antiscalants in BWRO concentrate waste.

Thus, the batch-recycle experimentation transforms into the time domain what occurs as a function of distance along the flow path in a single-stage full-scale operation. That is, the current density and bulk concentration profiles of the concentrate and diluate streams are essentially the same in both systems, except that one is in time, and the other is in space. The major distinction between the transport phenomena in the full-scale

single-pass and laboratory-scale batch-recycle is the diffusional flux that occurs in the same direction as the bulk flow, which is essentially negligible in the batch-recycle experimentation.

Several experimental investigations of ED have been performed over the past decade, as documented in Table 2.3. While most researchers report the basic hydraulic, chemical, and electrical conditions of their experimentation, most work does not sufficiently characterize all three aspects for complete process performance understanding. Furthermore, while most research is performed with similar hydraulic and electrical conditions, most researchers have investigated simple salt mixtures with less complexity and lower concentration than RO concentrate wastes.

Table 2.3 Recent batch-recycle electrodialysis research

Research	IEM[A] Type cat/an	Pairs N_{cp} [-]	Area[B] A_{mem} [cm^2]	Flow[C] Q_D [L/hr]	Velocity[D] v_D [cm/s]	Solution	Temp. T [°C]	pH pH	Hardness [mEq/L]	Salinity[F] c [mEq/L]	Salinity TDS [g/L]	Voltage[G] ϕ_{nom} [V/cp]	Current i [A/m^2]	Electrical SEC [Whr/m^3]	Remarks
(Demircioglu *et al.*, 2001)	CMX/AMX	10	100	4-11	2-6[e]	NaCl	room	-	0	10	0.58	0.5, 1.0, 1.5	<300	-	ED is technically effective.
(Elmidaoui *et al.*, 2001)	CMX/ AFN, ACS, AMX, ADP, ADS	1	36	128	120[e]	Ain Sbit, Morocco	20	7.4	9.8	14	1.1	-	10	-	ACS was the most technically effective and efficient AEM for nitrate removal.
(Elmidaoui *et al.*, 2001)	CMX/ACS	10	200	18	7[e]	NaCl+ Na_2SO_4+ $NaNO_3$+ $NaHCO_3$	20	-	0	25	2.0	1.5	<600	-	Nitrate was separated more effectively than the other ions - especially divalents, and most especially sulfate.
(Elmidaoui *et al.*, 2001)	CMS/ACS	10	200	20	8[e]	Nzalaat Laadem, Morocco	-	8.0	6.8	12	0.83	0.5, 1.0	<600	44 107	Nitrate can be selectively removed from natural brackish waters with ED.
(El Midaoui *et al.*, 2002)	CMX/ACS	10	200	10-18	4-7[e]	Morocco	15 25 40	8.1	7.1	12	0.82	0.5, 1.0, 1.5	<600	-	Nitrate is most effectively removed at higher flowrates, higher voltages, and higher temperatures (15, 25, 40).
(Kabay *et al.*, 2002)	CMX/AMX	10	100	4-11	2-6[e]	NaCl KCl $MgCl_2$ $CaCl_2$	room	-	- - 20 20	10 10 20 20	0.58 0.75 0.95 1.1	0.3-1.5	-	290[†] 280 580 570	Separation rate is proportional to voltage; SEC is proportional to equivalent concentration and applied voltage, but insensitive to flow. [†] at 10 V
(Choi *et al.*, 2003)	CMX/AMX	5	200	-	5.7	NaCl	25	-	0	100	5.8	-	<800	1220	Cost optimization was performed as a function of current density (i_{opt}=58 A/m^2).
(Demircioglu *et al.*, 2003)	CMX/AMX	10	100	4-11	2-6[e]	KCl NaCl	room	-	0	10	0.75 0.58	0.3-1.5	<300	-	KCl is removed more efficiently than NaCl.
(Kabay *et al.*, 2003)	CMX/AMX	10	100	-	-	NaCl KCl $MgCl_2$ $CaCl_2$	room	2 4 6	- - 20 20	10 10 20 20	0.58 0.75 1.9 2.2	0.5, 1.0	-	290[†] 280 580 570	Minimum SEC occurred at pH 6. SEC is proportional to equivalent concentration of salt removed. [†] at pH 6, 10 V.
(Moon *et al.*, 2004)	CM-1/AM-1	10	200	-	-	KCl	-	-	0	400	30	-	300 500 700	-	Their mathematical model did not capture the curvature of separation *vs*. time.
(Van der Bruggen *et al.*, 2004)	CMV/AMV CMS/ACS	5	58	-	8-10	NaCl Na_2SO_4 $MgCl_2$ $MgSO_4$ $NaNO_3$	25	-	0 0 10 10 0	10	0.58 0.71 0.48 0.60 0.85	1.0, 2.0	-	-	The CMV/AMV configuration showed little cationic permselectivity between mono- and divalents, whereas the CMS/ACS configuration did show preferential selection of monovalent cations.
(Ortiz *et al.*, 2005)	CMXSb/AMX	80	550	6-9	2-3[e]	NaCl	room	-	0	34	2.0	0.5-1.0	-	-	Their mathematical model captured most of the curvature of separation *vs*. time.

[A] for general membrane properties and remarks, see (Strathmann, 2004, Appendix I); [B] the active area of a single membrane; [C] the flow through a single diluate cell
[D] the superficial velocity of a single diluate cell given by $v_D = Q_D / (h_{sp}\, w_{sp})$; [e] estimated with w_{sp} = 0.5 mm and/or $h_{sp} = (A_{mem})^{1/2}$; [F] $c_{eq} = \frac{1}{2} \Sigma\, c_i z_i$; [G] the nominal voltage $\phi_{nom} = \phi_{app} / N_{cp}$

(continued)

Table 2.3 Recent batch-recycle electrodialysis research (continued)

Research	IEM[A] Type cat/an	Pairs N_{cp} [-]	Area[B] A_{mem} [cm^2]	Flow[C] Q_D [L/hr]	Velocity[D] v_D [cm/s]	Solution	Temp. T [°C]	pH pH	Hardness [mEq/L]	Salinity[F] c [mEq/L]	Salinity TDS [g/L]	Voltage[G] ϕ_{nom} [V/cp]	Current i [A/m^2]	Electrical SEC [Whr/m^3]	Remarks
(Chandramowleeswaran and Palanivelu, 2006)	DVB QA/SA	0.5	120	20	0.4[e]	NaCl Na_2SO_4 textile CETP effluent	-	- - 8.6	0 0 9.5	128 57 119	7.5 5.0 6.7	<60	< 125	<200	ED is technically effective for treating CETP effluent, which is similar to RO concentrate.
(Kabay *et al.*, 2006a)	CMX/AMX	10	100	10	5[e]	NaCl Na_2SO_4 $NaNO_3$ KCl K_2SO_4 KNO_3 $CaCl_2$ $Ca(NO_3)_2$ $MgCl_2$ $Mg(NO_3)_2$	room	-	0 0 0 0 0 0 10 10 10 10	10	0.58 0.71 0.85 0.75 0.87 1.0 0.56 0.82 0.48 0.74	0.5, 1.0	-	-	Potassium salts were removed more efficiently than sodium salts, and the sulfate salts were removed less efficiently than others. Final cation removal ratios were similar for all salts at 10 V operation.
(Kabay *et al.*, 2006a)	CMX/AMX	10	100	10	5[e]	NaCl + $CaCl_2$ NaCl + $Ca(NO_3)_2$ $NaNO_3$ + $Ca(NO_3)_2$ Na_2SO_4 + $CaCl_2$ Na_2SO_4 + $Ca(NO_3)_2$ KCl + $MgCl_2$ KCl + $Mg(NO_3)_2$ KNO_3 + $Mg(NO_3)_2$ K_2SO_4 + $MgCl_2$ K_2SO_4 + $Mg(NO_3)_2$	room	-	5	10	0.57 0.70 0.84 0.63 0.77 0.61 0.74 0.88 0.67 0.81	0.5, 1.0	-	260[†] 320 300 300 310 300 320 310 330 320	SEC is essentially proportional to the equivalent concentration of salt removed. Ionic composition affects removal efficiency and mildly affects removal efficacy. [†] at 10 V.
(Kabay *et al.*, 2006b)	CMX/AMX	10	100	3-10	2-5[e]	NaCl NaCl + $CaCl_2$ NaCl + $CaCl_2$ NaCl + $CaCl_2$ $CaCl_2$ KCl KCl + $MgaCl_2$ KCl + $MgCl_2$ KCl + $MgCl_2$ $MgCl_2$	room	-	0 2.5 5 7.5 10 0 2.5 5 7.5 10	10	0.58 0.58 0.57 0.56 0.56 0.75 0.68 0.61 0.54 0.48	0.5, 1.0	< 40	~300[†]	Flow rate has negligible effect on SEC and removal efficacy. [†] at 10 V.
(Koprivnjak *et al.*, 2006)	CMX/AMX	-	-	-	-	CaCO3 + MgCO3 + SiO2 + NaOH + HCl + H2SO4 + NOM	-	4 - 8.8	0 - 30	8 - 80	0.33-3.5	-	-	-	92-95% of initial TOC concentrations (1-10 mM) were retained while simultaneously removing 50-90% of initial sulfate.
(Koprivnjak *et al.*, 2006)	CMX/AMX	-	-	-	-	Suwannee Riv. Withlacoochee Riv. Georgia, USA	-	6 9	0.2 4	1 4	0.18 0.39	-	-	-	88-102% of initial TOC concentrations (78 and 21 mM) were retained while simultaneously removing 40-80% of initial sulfate.

[A] for general membrane properties and remarks, see (Strathmann, 2004, Appendix I); [B] the active area of a single membrane; [C] the flow through a single diluate cell
[D] the superficial velocity of a single diluate cell given by $v_D = Q_D / (h_{sp}\, w_{sp})$; [e] estimated with $w_{sp} = 0.5$ mm and/or $h_{sp} = (A_{mem})^{1/2}$; [F] $c_{eq} = \frac{1}{2} \Sigma\, c_i z_i$; [G] the nominal voltage $\phi_{nom} = \phi_{app} / N_{cp}$

(continued)

Table 2.3 Recent batch-recycle electrodialysis research (continued)

Research	IEM[A] Type cat/an	Pairs N_{cp} [-]	Area[B] A_{mem} [cm^2]	Flow[C] Q_D [L/hr]	Velocity[D] v_D [cm/s]	Solution	Temp. T [°C]	pH pH	Hardness [mEq/L]	Salinity[F] c [mEq/L]	Salinity TDS [g/L]	Voltage[G] ϕ_{nom} [V/cp]	Current i [A/m^2]	Electrical SEC [Whr/m^3]	Remarks
(Banasiak *et al.*, 2007)		6	58	30	20	NaCl	-	-	0	17 - 598	1 - 35	1.3 - 3	< 1700	-	The separation rate is limited by the resistance of the membranes for salinities greater than approximately 0.2 Eq/L.
(Firdaous *et al.*, 2007)	CMX-S/ACS	20	69	10	7[e]	NaCl, $CaCl_2$, $MgCl_2$ binary combinations ternary combination	25	6.5 - 7.5	0 - 387	194 - 387	11 - 43	1.5	< 200	-	The concentration of other cations affect the transport selectivity of CEMs
(Ortiz *et al.*, 2007)	CMXSb/AMX	80	550	9	3[e]	NaCl	amb.	-	0	34	2.0	0.75-1.0	< 63	900[†]	ED desalination can be accomplished by direct connection to photovoltaic source. [†] estimated from I(t) and V(t) curves.
(Ortiz *et al.*, 2008)	CMX/AMX	70	500	11	3[e]	Alicante, Spain	amb.	8.1 8.2 8.0	14 27 40	33 70 77	2.3 4.5 5.0	0.5-1.0	< 90	920 1470 1690	ED desalination is effective for brackish groundwater sources. The experimental performance can be modeled mathematically. Production costs are estimated to be 0.17-0.32 €/m^3.
(Xu *et al.*, 2008)	CMS/AMS CMXSb/AMXSb	-	-	-	-	synthetic 1 synthetic 2 synthetic 3 Yuma CRW RO, AZ	-	-	9 129 110 50	96 159 140 73	6.4 9.6 9.0 4.9	-	-	-	Monovalent permselective membranes were not as effective on these supersaturated solutions as regular membranes were. RO concentrate treatment with precipitation and ED is theoretically cost effective.
(Zhang *et al.*, 2009)	PCSK/PCSA	5	64	30	4	NaHCO3 + NaCl + MgSO4 + Na2HPO4 + NaNO3 + organics	-	7-9	8.92	25.5	1.8	< 2	< 78	-	Acetate, methylammonium, aspartate, and protonated lysine were all separated effectively by electrodialysis, but glycine was not. This indicated that small organic ions can be separated, but zwitterionic compounds are not separated.
(Zhang *et al.*, 2009)	PCSK/PCSA	5	64	30	4	RO concentrate	-	-	-	>100	-	< 2	< 78	-	After 10 hours of batch-recycle, greater than 95% of the salinity was removed, but 85% of the initial TOC remained in the diluate, indicating very low transport of natural organic compounds.

[A] for general membrane properties and remarks, see (Strathmann, 2004, Appendix I); [B] the active area of a single membrane; [C] the flow through a single diluate cell
[D] the superficial velocity of a single diluate cell given by $v_D = Q_D / (h_{sp}\, w_{sp})$; [e] estimated with $w_{sp} = 0.5$ mm and/or $h_{sp} = (A_{mem})^{1/2}$; [F] $c_{eq} = \frac{1}{2} \Sigma\, c_i z_i$; [G] the nominal voltage $\phi_{nom} = \phi_{app} / N_{cp}$

2.7 MATHEMATICAL MODELING

2.7.1 Single-pass and batch-recycle

Several researchers have developed mathematical simulations of the performance of ED systems (Lee *et al.*, 2002; Moon *et al.*, 2004; Ortiz *et al.*, 2008; Ortiz *et al.*, 2005; Parulekar, 1998; Sadrzadeh *et al.*, 2007; Tsiakis and Papageorgiou, 2005). Unfortunately, many of them are limited to binary ionic solutions, or they omit one or more of the following phenomena which are not-insignificant in the treatment of BWRO concentrate:

- liquid-junction potentials
- diffusion potentials
- electrical resistance of the diffusion boundary layers
- variation in ionic diffusivities as a function of concentration
- osmotic transport of water across membranes
- electro-osmotic transport of water across membranes

While one mathematical model was found that treated multicomponent transport in electrodialysis (Senik *et al.*, 2006a), its applicability is limited to low concentrations (*e.g.*, up to 1000 mg/L TDS or 0.1 mol/L ionic strength). As of yet, no model has been found to describe the multicomponent transport of moderately-brackish solutions (e.g., 5000–15000 mg/L TDS).

2.7.2 Activity coefficients in brackish solutions

The activity coefficients of acid, base, and salt solutions, have been well studied and tabulated as functions of concentration and temperature (Landolt and Börnstein,

1960a; Lobo, 1981; Lobo and Quaresma, 1989; Pytkowicz, 1983; Robinson and Stokes, 1959). The mean ionic activity coefficient of a binary electrolyte is given by:

$$\gamma_{\pm} = \left[\left(\gamma_{A^{y+}} \right)^{x} \left(\gamma_{B^{x+}} \right)^{y} \right]^{\frac{1}{x+y}} \tag{2.31}$$

Many empirical and theoretical expressions have been developed to predict the activity coefficients of ions and neutral species in aqueous solution (Bockris and Reddy, 1998; Horvath, 1985; Kortum, 1965; Stumm and Morgan, 1995; Wright, 2007), but these are generally limited to low ionic strength. For example, the activity coefficient (γ_i) of an ion determined by the Extended Debye-Hückel Equation model is considered accurate within approximately two percent up to an ionic strength of 0.1 mol/L (Stumm and Morgan, 1995) and is given by:

$$\log(\gamma_i) = -A z_i^2 \frac{\sqrt{I}}{1 + B \, \mathring{a}_i \sqrt{I}} \tag{2.32}$$

Where z_i and $\mathring{a}_i$ are the charge and size parameter for species i (Stumm and Morgan, 1995), respectively and A and B are given by:

$$A = \frac{{q_e}^2 B}{8\pi \ln(10) \, \varepsilon_0 \varepsilon_r k_B T} \tag{2.33}$$

$$B = \sqrt{\frac{2{q_e}^2 N_A}{\varepsilon_0 \varepsilon_r k_B T}} \tag{2.34}$$

Table 2.4 Values of the Debye-Hückel parameter for select ions (Stumm and Morgan, 1995)

$å$ [Å]	Ion
9	H^+, Al^{3+}, Fe^{3+}
8	Mg^{2+}, Be^{2+}
6	Ca^{2+}, Cu^{2+}, Fe^{2+}, Mn^{2+}, Zn^{2+}
5	Ba^{2+}, Sr^{2+} CO_3^{2-}
4	Na^+, SO_4^{2-}
3	Ag_+, K^+, NH_4^+ Cl^-, ClO_4^-, I^-, NO_3^-,OH^-

Since A and B are approximately 0.51 $mol^{-1/2}$ $L^{3/2}$ and 0.33 $Å^{-1}$ $mol^{-1/2}$ $L^{3/2}$, respectively, and by assuming $å$ to be approximately equal to 3Å, Davies (1962) developed the following empirical expression to better model the activity coefficient behavior at higher ionic strengths, applicable up to ionic strengths of 0.5 mol/L (Stumm and Morgan, 1995):

$$\log(\gamma_i) = -0.5\, z_i^2 \left(\frac{\sqrt{I}}{1+\sqrt{I}} - 0.2I \right) \tag{2.35}$$

A comparison of the Debye-Hückel and Davies models to observed mean activity coefficients is shown in Figure 2.9; monovalent-monovalent salts are shown in part (a), and monovalent-divalent salts are shown in part (b). In this figure, it can be seen that the Debye-Hückel model has the advantage of distinguishing the behavior of ions of the same charge based on size, and for many salts, it is accurate within 10% up to ionic strengths near 1.0 M. The Debye-Hückel model is also much better than the Davies model at predicting the activity coefficients of carbonate and sulfate salts at higher ionic strengths. While the Davies model does attempt to capture the inflection at higher ionic

strengths, it poorly models some ions because all ions of a certain charge are treated identically, without regard to size.

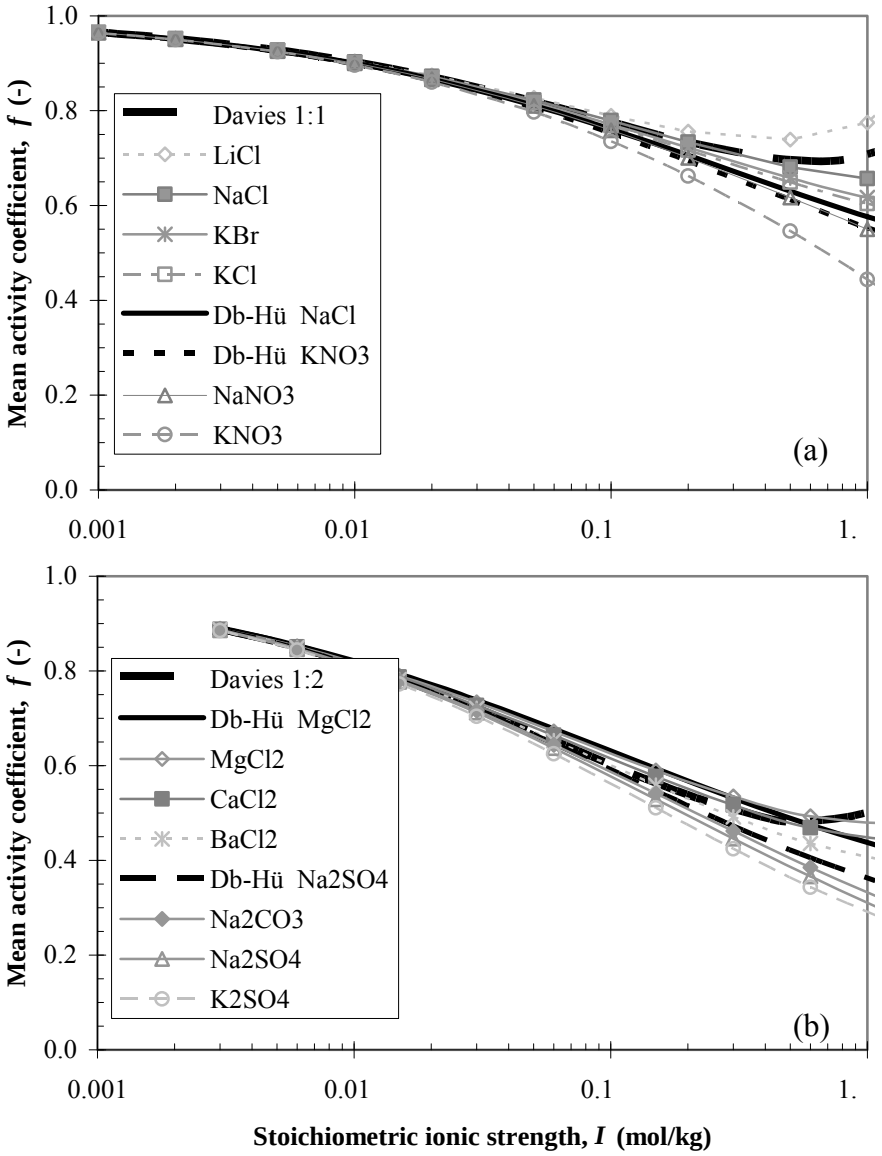

Figure 2.9 Comparison of activity coefficient models to literature data (CRC, 2005b)

Another model modifies the Extended Debye-Hückel expression to account for the increasing activity at higher ionic strengths (Gustafsson, 2010; Wright, 2007),

$$\log(\gamma_i) = -Az_i^2 \frac{\sqrt{I}}{1 + B\,\mathring{a}_i \sqrt{I}} + b_i I \tag{2.36}$$

but the empirical parameter, b_i, must be determined for each ion. More complicated models have been developed that are applicable at higher ionic strengths, such as the empirical Specific ionic Interaction Theory (SIT) (Guggenheim and Turgeon, 1954) or the more rigorous, thermodynamically-based Pitzer model (Pitzer, 1991). However, these models are more computationally demanding than the Debye-Hückel and Davies.

2.7.3 Electrical conductivity of brackish solutions

One of the essential relationships in modeling the performance of an electrodialysis system is the precise calculation of the electrical conductivity of the process solutions as a function of the ionic concentrations. The equivalent conductivity (sometimes "molar conductivity" or "equivalent conductance") of a binary solution, Λ, is calculated as the conductivity (κ) normalized by equivalent concentration (c),

$$\Lambda = \frac{\kappa}{c} \tag{2.37}$$

and has been well studied and tabulated as functions of binary electrolyte concentration and temperature (Landolt and Börnstein, 1960b; Lobo, 1981; Lobo and Quaresma, 1989; Noyes, 1907; Robinson and Stokes, 1959). The equivalent conductivity at infinite dilution, Λ_0, can be calculated by (Bard and Faulkner, 2001; Bockris and Reddy, 1998):

$$\Lambda_0 = \lambda_+ + \lambda_- \tag{2.38}$$

where λ_+ and λ_- are the equivalent ionic conductivities at infinite dilution of the cation and anion, respectively (CRC, 2005a), which have been deduced from binary equivalent conductivity data.

Binary models

For concentrations less than 1 mmol/L, a simple empirical relationship was observed to describe the equivalent conductivity (Λ) as a function of the concentration of the solution, known as Kohlrausch's law (Horvath, 1985; Landolt and Börnstein, 1960b),

$$\Lambda = \Lambda_0 - A\sqrt{c} \tag{2.39}$$

where A is an empirical constant. A theoretical expression, known as the Debye-Hückel-Onsager theory (Atkins and De Paula, 2006; Wright, 2007) is able to precisely predict the equivalent conductivity of a binary electrolyte up to concentrations of 3 mEq/L (Bockris and Reddy, 1998),

$$\Lambda = \Lambda_0 - \left(A + B\,\Lambda_0\right)\sqrt{c} \tag{2.40}$$

where A and B are derived constants of physical parameters. A better fitting expression due to Falkenhagen (Kortum, 1965) is,

$$\Lambda = \Lambda_0 - \left(B_1\Lambda_0 + B_2\right)\frac{\sqrt{c}}{1 + B\,\mathring{a}_i\,\sqrt{c}} \tag{2.41}$$

where B_1, B_2, and B are derived constants of physical parameters, and c is the concentration of the dissolved electrolyte. Many other empirical and theoretical expressions have been proposed describing the equivalent conductivity as functions of concentration to various powers (Cussler, 1997; Landolt and Börnstein, 1960b), but these are limited to binary solutions.

Multicomponent models

For *multicomponent* solutions at infinite dilution, the electrical conductivity (κ) of an aqueous solution can be calculated as:

$$\kappa_0 = \sum_i \lambda_{i,0}\, c_i \left| z_i \right| \tag{2.42}$$

where $\lambda_{i,0}$ is the equivalent ionic conductivity at infinite dilution, c_i is the molar ionic concentration, and $|z_i|$ is the magnitude of charge of species i (Bard and Faulkner, 2001).

The method detailed in *Standard Methods* (Eaton *et al.*, 2005) begins with the infinite dilution equivalent conductivity calculation (above) and then modifies it by multiplying by the square of the monovalent Davies activity coefficient:

$$\kappa_{calc} = \kappa_0 \gamma^2_{Davies,mono} \tag{2.43}$$

This model is reportedly limited to solutions with less than 2500 mg/L TDS, and as one might suspect, it performs poorly for solutions with relatively high concentrations of divalent species.

Similarly, the model proposed by Senic *et al.* (2006b) can be used to calculate the conductivity of a multicomponent solution up to 50 mmol/L, but again, this limiting concentration is far less than the concentrations in the present research. Another model (Kurup *et al.*, 2009) describes the multicomponent transport within electrodeionization (EDI), but because of the significant differences between EDI and ED (and, therefore, certain approximations regarding cell electrical conductance in the model), the model is not applicable to ED systems.

For more concentrated and multi-component solutions, more sophisticated simulations such as the Mean Spherical Approximation and its semi-empirical extensions (Anderko and Lencka, 1997; Aseyev, 1998; Bernard *et al.*, 1992; Bockris and Reddy, 1998; Pawlowicz, 2008; Pawlowicz, 2010) involve many mathematical terms specific to certain ions and combinations of ions. However, a model of this type would not be practical to implement into the mathematical model in this research. Thus, the construction of a mathematical model is necessary that incorporates a simple, but relatively accurate calculation of activity coefficients and equivalent ionic conductivities in multicomponent solutions at high ionic strengths, in order to precisely model the performance of the electrodialyitic treatment of BWRO concentrate waste.

2.8 SUMMARY

The fundamentals of hydraulic, electrical, and chemical phenomena employed in ED systems are integrally connected to the overall performance. The rate of separation is proportional to the (electrical) current density, which is limited by the (chemical) diffusion boundary layer, the thickness of which is controlled by the (hydraulic) inter-membrane velocity. The electrical behavior of an ED system is dominated by the resistance of the stack, but the contributions of other electrical losses (which many researchers neglect) are not insignificant in precisely describing the performance of the system. The operation of ED systems is limited by a lack of ions in the diluate diffusion boundary layer and a supersaturation of ions in the concentrate diffusion boundary layer, so the diffusion boundary layer thickness must be sufficiently thin and the applied voltage sufficiently low to avoid both cases.

The chemical composition of experimental ED solutions has mostly been simple binary salts at mild brackish concentrations, not representative of RO concentrate waste. While experimental and full-scale ED treatments of brackish waters have been proven technically and economically feasible (AWWA, 1995; Reahl, 2005; Strathmann, 2004; Tanaka, 2007; Xu *et al.*, 2008), the application of ED to treat RO concentrate waste has not been systematically evaluated and reported in the scientific literature. Specifically, a fundamental quantification of the multi-component transport of supersaturated brackish solutions has not been performed. Hence, a thorough and systematic experimentation and documentation of the performance of ED is required for understanding the beneficial use of ED in RO concentrate waste treatment.

Chapter 3 – Experimental Methodology

The objective of the experimental work was to quantitatively observe the hydraulic, electrical, and chemical behavior of electrodialytic treatment of BWRO waste. The effects of process variables on the desalination efficacy and efficiency were evaluated through precise electrodialysis experimentation. The experimental plan and descriptions of the experimental design, experimental apparatus, analytical techniques, and data analysis are presented here.

3.1 Experimental plan and variables

Based on the research goal and objectives presented in Chapter 1 and the fundamental concepts outlined in Chapter 2, the scope of experimentation investigated the performance sensitivities and limitations with respect to the following variables:

1. Electrical: ion-exchange membrane types and applied voltage;
2. Hydraulic: inter-membrane velocity; and
3. Chemical: feed water and antiscalant composition.

The experimental plan was designed to isolate the impact of each variable without performing complete factorial experimentation. A set of discrete values were selected for each variable – chosen strategically to span the spectrum of ED treatment. A "standard value" was selected from that range for defining a standard set of experimental variables, which allows the methodical isolated variation of each variable. These standard values and variable ranges are shown in Table 3.1.

Table 3.1 Experimental variables, standard values, and discrete value ranges

Variable	Standard Value	Range
Membrane type	CMV/AMV	CMV/AMV, PCSK/PCSA
Stack voltage	1.0 V/CP	0.5, 1.0, 1.5 V/CP
Superficial velocity	2 cm/s	1, 2, 4 cm/s
Feed water	AZ, TX	AZ, TX, FL
Antiscalant type	ATMP	ATMP, DTPMP
Antiscalant dose	2 mg/L	1, 2, 8 mg/L (raw)
Removal ratio	98%	20%, 40%, 60%, 80%, 98%
Concentrate recovery	50%	50%, 75%, 85%

The membranes used in this experimentation are general desalination ion exchange membranes, and the electrical and hydraulic conditions simulate typical full-scale ED systems. The feed water and antiscalant compositions are representative BWRO concentrate wastes, and the range of the concentrate recovery by ED simulates multiple hydraulic stages. More specific details regarding the experimental parameters are provided in the following sections.

3.2 EXPERIMENTAL DESIGN

3.2.1 Experimental apparatus

A batch-recycle electrodialysis experimental apparatus similar to other works (Choi *et al.*, 2003; Moon *et al.*, 2004; Ortiz *et al.*, 2005) was assembled with accoutrements for precisely monitoring hydraulic, electrical, and chemical behavior; a process schematic is shown in Figure 3.1. Laboratory-scale gear pumps were used to circulate each of the three process streams: diluate (D), concentrate (C), and electrode rinse (E); the flow rate (Q) through each stream was monitored continuously. The flow rates of the concentrate and diluate streams were controlled by electronic liquid flow-

controllers. The electrode rinse stream combined the anode and cathode in parallel because the reactions at the anode and cathode produce equivalent amounts of protons and hydroxides, respectively, and the stack loses the equivalent amount of cations to the catholyte that it gains from the anolyte. The reservoirs were one-liter Erlenmeyer flasks that were stirred by non-heating magnetic stirrers (VELP Scientifica, model F203A0160) and were approximately ideal continuous-flow, stirred-tank reactors (CFSTRs); they were monitored continuously for pH, conductivity (κ), and temperature (T). The mass of the diluate reservoir was monitored continuously to gravimetrically quantify water and electrolyte transfer. Pressure (P) was monitored at the inlet and outlet of the electrodialyzer for each of the process streams to characterize the head loss through each stream and the average trans-membrane pressures. A passive heating bath and active cooling coil system controlled the experimental temperature (not shown in Figure 3.1) within one-degree Celsius change; without this feature, the temperature of the process streams would increase during an experiment because of electrical resistance and hydraulic turbulence dissipated as heat. Details of the hydraulic, electrical, and chemical controls are discussed subsequently.

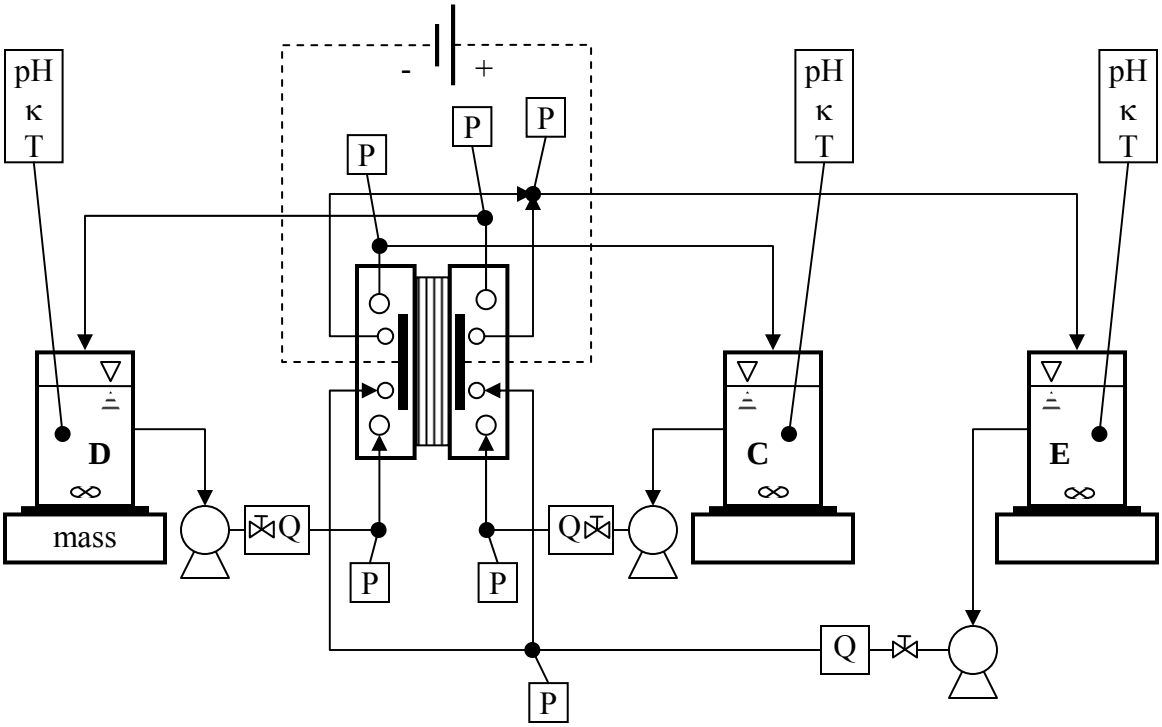

Figure 3.1 Batch-recycle experimental ED apparatus schematic

3.2.2 Experimental procedure

The general experimental procedure was as follows:

1. prepare experimental and pre-rinse solutions for system equilibration
2. engage recycling and small voltage application on a pre-rinse solutions to approach dynamic equilibration of the membranes with the solution
3. evacuate pre-rinse solution and load apparatus with the experimental solutions
4. run experimental solutions with full data acquisition and periodic sampling
5. analyze samples by IC, ICP, alkalinity, *etc.*

More detailed procedures for solution preparation, experimentation, and analysis are presented in the following sections.

3.2.3 Experimental electrodialyzer

A PCCell ED 64002 electrodialyzer (shown in Figure 3.2) was acquired from PCCell/PCA, GmbH (Germany). The anode was expanded titanium metal with platinum/iridium coating, and the cathode was expanded stainless steel. The end-plates surrounding the electrodes and compressing the stack were machined polypropylene. The manufacturer recommended a maximum voltage application of 2 V per cell-pair and a maximum flow rate of 8 L/hr per cell. The active cross-sectional area subjected to the applied electric field was 64 cm^2. Plastic woven screen/mesh spacers (shown in Figure 3.3) of thickness 0.41 mm physically separated the anion- and cation-exchange membranes, providing a superficial (empty) volume of 2.6 cm^3 per cell and an actual volume-porosity of 0.78.

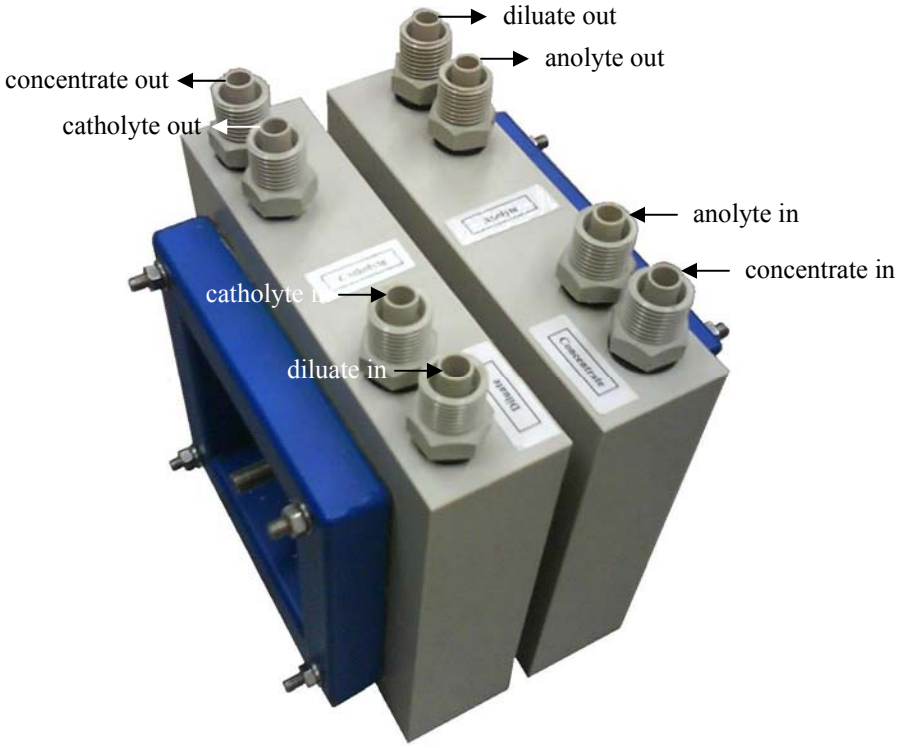

Figure 3.2 PCCell ED 64002 electrodialyzer (PCCell/PCA, GmbH, Germany, 2007)

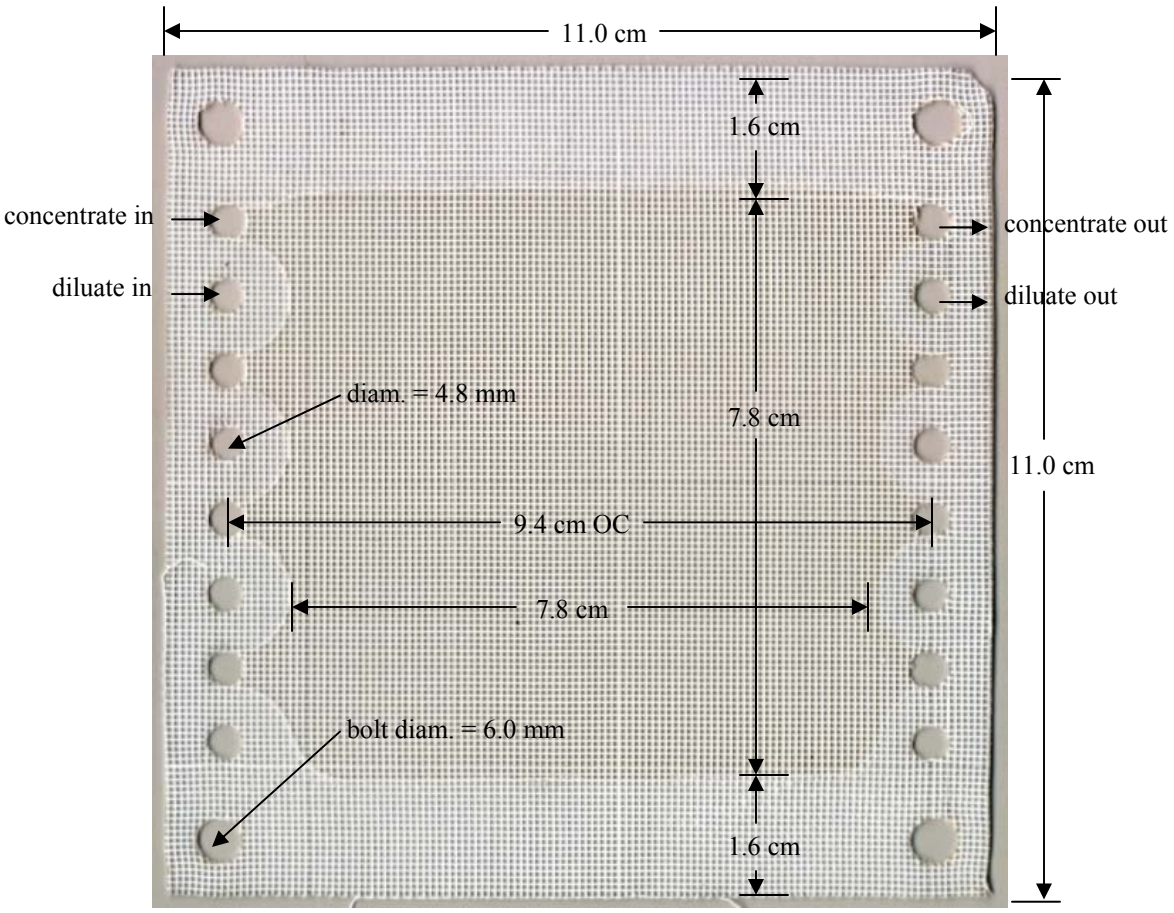

Figure 3.3 PCCell ED 64002 mesh spacer (concentrate cell)

Two combinations of membranes were used in this experimentation: CMV-AMV and PCSK-PCSA. CMV and AMV are low resistance Selemion (Asahi Glass) membranes for general desalination (Strathmann, 2004), and have ion exchange capacities of 1.95 mEq/g (Tuan *et al.*, 2006) and 1.98 mEq/g (Malewitz *et al.*, 2007), respectively. Similarly, PCSK and PCSA are also general desalination membranes (PCA, 2005), with ion exchange capacities of approximately 1.0 and 1.5 mEq/g (Zhang *et al.*, 2009), respectively. Cation exchange membranes are commonly made of sulfonated polystyrene on a PVC fabric (Tuan *et al.*, 2006), and the anion exchange membranes are

usually made with tertiary and quaternary ammonium functional groups (PCA, 2005; Strathmann, 2004).

3.2.4 Data acquisition software and hardware

Three principal LabVIEW™ supervisory control and data acquisition (SCADA) software programs were developed for controlling and monitoring the electrodialysis experimentation. Subroutines were developed to query data from each of the RS232 instruments and analog-to-digital converters (ADC), and these subroutines were integrated in a time looping structure to query data, visualize those data to the graphical user interface (GUI), and record the data to a comma delimited text file (.csv) for post-processing data analysis. National Instruments LabVIEW 8.5 was installed on a Dell Precision 340 desktop computer (dual 2.2 GHz Pentium 4 processors, 1 GB RAM, two serial ports) running Windows XP Professional Service Pack 2, and the computer was fitted with an SIIG CyberSerial 4S RS232 PCI card to provide four additional serial ports.

A National Instruments multi-function ADC (NI USB-6008) was used to monitor the pressure transducers and the electrode rinse flow meter. Another National Instruments multi-function ADC (NI USB-6009) was used to control and monitor the concentrate and diluate liquid flow-controllers. At each data collection iteration during an experiment (every three seconds), the analog voltage output signal (0-6 V) from each of the flow meters and pressure transducers was recorded for one second at a rate of 1 kS/s (*i.e.*, 1000 data points), and the recorded analog data was converted to digital signal (11 bit resolution for the USB-6008 and 13 bit resolution for the USB-6009) and

transmitted to the SCADA via USB. The arithmetic mean of each one-second data set for each signal was computed within the LabVIEW routine and recorded in a text file for each three-second data collection iteration. Mass, voltage, electrical current, conductivity, pH, and temperature measurements were transmitted digitally through RS232 serial connections (typically 9600 bits/s).

With one of the custom LabVIEW programs (Calibration – Pressure Transducers.vi), the user inputs the hydrostatic pressure applied to the pressure transducers by a measured height of water in a wall manometer, and the user is able to query and record the analog voltage output (as described above) from the pressure transducers that corresponds to that hydrostatic pressure. After several pressure measurements spanning the range of experimental pressures, the LabVIEW program performs linear regression on the calibration data and records the regression coefficients in a file to be used by the other experimental LabVIEW programs.

Another of the LabVIEW programs (Instrument Observation.vi) queries each measurement device and visualizes the data for the user to monitor during experimental setup (especially the pre-rinse exercise before the experiment). This program automatically loops every three seconds, until the user exits the program.

The custom LabVIEW program that was used during experimentation (ED Experiment SCADA.vi), is an extended version of the Instrument Observation.vi which allows the user to record chemical experimental conditions and specify electrical conditions for automated control. The program loops every three seconds, querying the instruments, displaying the experimental data to the GUI, and writing those data to an

output comma delimited text file. The output file includes the parameters listed in Table 3.2 for each sample (every three seconds) during the experiment.

Table 3.2 ED experimental output file data

Metadata	Hydraulic	Electrical	Chemical
Date	Mass change (g) †	Stack Voltage (V)	pH
Time (s)	Flow (L/min)	Current (A)	pH electrode mV
	$Head_{in}$ (cm)	Power (W)	Temp (°C)
	$Head_{out}$ (cm)	Stack Resistance (Ω)	Conductance (mS)
	Head loss (cm)		Cell constant (/cm)
	Trans-membrane head (cm)		Conductivity (mS/cm)

† diluate only

3.3 HYDRAULIC CHARACTERIZATION AND CONTROL

3.3.1 Electrodialyzer stack assembly

The ordering of ion exchange membranes within the stack has little consequence when the number of cell pairs is great, but it has significant hydraulic and chemical implications for laboratory scale systems. Four stack combinations are possible, as shown in Figure 3.4. With *n+1* CEMs and *n* AEMs, as shown in part (a), the stack has *n* concentrate cells and *n* diluate cells; the bounding concentrate and diluate cells exchange only cations with the adjacent anolyte and catholyte rinse, respectively. If the stack has *n* CEMs and *n+1* AEMs, as shown in part (b), then the stack again has *n* concentrate cells and *n* diluate cells, but the bounding diluate and concentrate cells exchange anions with the anolyte and catholyte rinse, respectively. However, if the stack is constructed with *n* CEMs and *n* AEMs with the bounding CEM adjacent to the anolyte, as shown in part (c), then the stack has *n* concentrate cells and *n-1* diluate cells, and one of the bounding concentrate cells gains cations from the anolyte while the other bounding concentrate cell

gains anions from the catholyte. Finally, if the stack has *n* AEMs and *n* CEMs with the bounding AEM adjacent to the anolyte, then the stack has *n-1* concentrate cells and *n* diluate cells (one of which loses cations to the catholyte, and another loses anions to the anolyte.

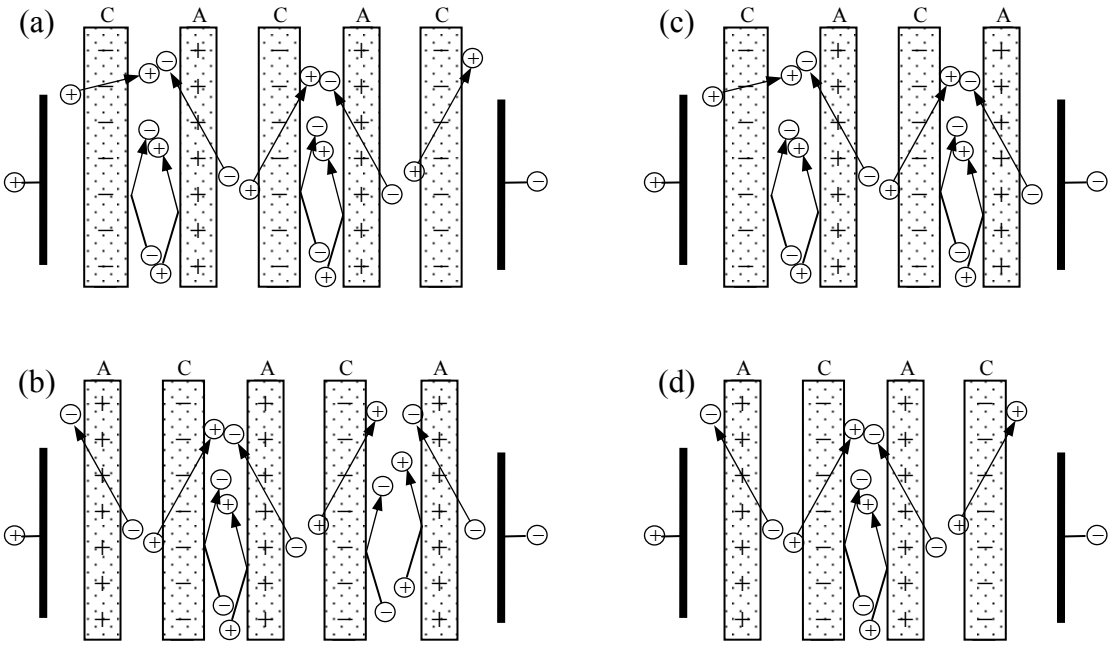

Figure 3.4 Electrodialyzer stack construction: ion exchange membrane combinations

The stack assembly described in part (a) was selected for the following reasons. First, the hydraulic behaviors of the concentrate and diluate streams are theoretically identical; that is, equal concentrate and diluate stream flow rates would produce approximately equivalent bulk velocities, and hence equivalent head loss (an operational nicety). Also, since the electrode rinse (anolyte and catholyte) is operated in hydraulic parallel (as shown in Figure 3.1), the average pressure in the electrode rinse chambers can be controlled to match the average pressure in the concentrate and diluate cells. Second,

because the anolyte theoretically loses cations to the concentrate at the same rate that the catholyte gains cations from the diluate, the pH and electrical conductivity in the electrode rinse stream should remain stable over the course of the experiment. This stack arrangement also allows the use of an electrode rinse solution with the same initial cation concentration as the concentrate and diluate streams but with anion composition lacking chloride (to avoid chlorine production at the anode).

3.3.2 Inter-membrane cell volume

The "empty bed" volume of experimental solution in either a concentrate cell, V_C, or a diluate cell, V_D, was calculated to be 2.62 mL per cell according to the following:

$$V_C = V_D = w_s A \tag{3.1}$$

where w_s is the width of the spacer (*i.e.*, the distance between the membranes, 0.41 mm) and A is the cross-sectional area of the spacer (64 cm^2). The actual total stack volume in the concentrate or diluate cells can then be calculated as:

$$V_{stack,C} = V_{stack,D} = V_C N_{cp} \varepsilon \tag{3.2}$$

where N_{cp} is the number of cell-pairs in the stack (*e.g.*, 10) and ε is the volume porosity of the mesh spacer (0.78), which can be approximated by:

$$\varepsilon = 1 - \frac{\pi d_f{}^2 s}{2 L^2 w_s} \tag{3.3}$$

where d_f is the spacer filament diameter (0.22 mm), s is the arc-length (0.899 mm) of the repeating filament unit-length (L, 0.865 mm), and w_s is the width of the spacer. It was assumed (based on the minor temperature changes in the electrodialyzer and the minor

swelling potential of the ion-exchange membranes) that the inter-membrane volume was constant throughout the experimentation.

3.3.3 Flow rate

The laboratory scale gear pumps (manufacturer: Greylor Co., model PQM-1/115, supplier: Cole-Parmer, K-07012-00, 2007/2008 catalog) used to supply the flow rate of each of the three process streams were 115 VAC, 3500 rpm, 1600 mL/min gear pumps, and the supplier's pump curve is shown in Figure 3.5. These gear pumps were used instead of peristaltic pumps to minimize pressure oscillation within the electrodialyzer.

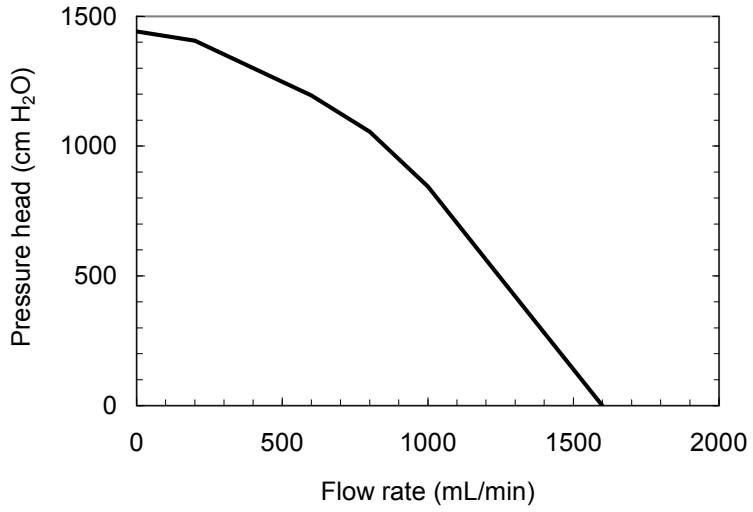

Figure 3.5 ED Experimental gear pump curve (Cole-Parmer, 2007)

Volumetric flow rate through the concentrate and diluate streams was controlled and monitored with two McMillan Co. analog Liquid FLO-CONTROLLERs® (model 401-6-A4), and the electrode rinse stream was operated at maximum capacity (*ca.* 1.25 L/min) through a McMillan Co. FLO-SENSOR® (model 101-6-D-AB) analog flow meter. Each flow controller and meter was calibrated according to the procedure in

Appendix A. The flow controllers and meter were powered by a 12 VDC signal from a BK Precision® 1696A switching-mode, direct current (DC), programmable power supply.

3.3.4 Residence time, superficial velocity, and Reynolds number

The mean hydraulic residence time of the concentrate and diluate streams was computed according to the following formula:

$$\tau_C = \frac{V_C}{Q_C},\ \tau_D = \frac{V_D}{Q_D} \tag{3.4}$$

where τ is the mean hydraulic residence time of the concentrate or diluate stream, V is the ED cell volume of the particular stream (calculated according to §3.3.2), and Q is the flow rate of the particular stream through a single cell.

The superficial velocity in the concentrate and diluate streams was computed according to the following formula:

$$v_C = \frac{L_{flowpath}}{\tau_C},\ v_D = \frac{L_{flowpath}}{\tau_D} \tag{3.5}$$

where v is the superficial velocity of the concentrate or diluate stream, and L is the flow path length of the electrodialyzer stack (approximately 9.4 cm for this experimental apparatus).

The Reynolds number (useful for indicating laminar or turbulent flow characteristics) of the concentrate and diluate streams was computed according to the following formula (Balster *et al.*, 2006):

$$Re_C = \frac{\rho\, w_s\, v_C}{\mu},\ Re_D = \frac{\rho\, w_s\, v_D}{\mu} \tag{3.6}$$

where *Re* is the average Reynolds number of the inter-membrane solution of the concentrate or diluate stream, ρ is the mass density of the solution, w_s is the thickness of the spacer (*i.e.*, the characteristic length scale is defined as the distance between the membranes), v is the superficial velocity of the stream, μ is the dynamic (absolute) viscosity of the solution.

3.3.5 Pressure-head

Pressure-head of the concentrate and diluate streams was monitored at the electrodialyzer inlets with OMEGA® PX481A-015G5V analog pressure transducers (linear range of 0–15 psi) and at the electrodialyzer outlets with ICSensor® 114-005G analog pressure transducers (linear range of 0-5 psi). Pressure-head of the electrode rinse stream was monitored at the anolyte and catholyte inlets and outlets (which are in hydraulic parallel) with ICSensor® 114-005G analog pressure transducers. All six pressure transducers were calibrated simultaneously, once per week, according to the procedure in Appendix B. The pressure transducers are also powered by same 12 VDC signal from the BK Precision® 1696A power supply that also powers the flow meters.

Pressure-head loss in the concentrate or diluate stream was calculated as:

$$\Delta H = H_{inlet} - H_{outlet} \tag{3.7}$$

where ΔH is the pressure-head loss in the particular stream, H_{inlet} is the pressure-head of the particular stream at the inlet to the ED endplate, and H_{outlet} is the pressure-head at the outlet of the endplate.

The trans-membrane pressure-head is the average difference in pressure between the concentrate and diluate cells within the stack and is a driving force for the flux of

water across the membranes by pressure-driven permeation. The trans-membrane pressure-head is calculated as:

$$\Delta H_{trans} = \left(\frac{H_{inlet} + H_{outlet}}{2} \right)_{concentrate} - \left(\frac{H_{inlet} + H_{outlet}}{2} \right)_{diluate} \quad (3.8)$$

where ΔH_{trans} is the trans-membrane pressure-head, which is the difference in average inter-membrane pressures within the concentrate stream and diluate stream. Experiments were performed by setting the diluate flow rate and controlling the concentrate flow rate to provide zero trans-membrane pressure-head. This ensured that 1) negligible pressure-driven permeation occurred between the concentrate and diluate cells, 2) that the volumes (and thus, mean hydraulic residence times) of the concentrate and diluate cells were approximately equal, and most importantly, 3) that the diluate diffusion boundary layers were reproducible between experiments.

In assembling the ED stack, the end-plates compressing the stack were tightened until no leaks were observed, and a diluate flow rate of 80 mL/min of 0.1 mol/L NaCl per diluate cell produced a diluate hydraulic head loss gradient of approximately 15±1 cm/cm for each electrodialyzer-stack assembly.

3.3.6 Diluate mass

The mass of the diluate reservoir was monitored continuously to the nearest 0.1 g with a Mettler Toledo® XS6001S digital mass balance, which quantified the mass of water and salt transported across the membranes. The mass of water transported by electro-osmosis and osmosis were calculated by subtracting the mass of salt removed (determined by concentration analysis).

3.4 ELECTRICAL CHARACTERIZATION AND CONTROL

The electrical voltage and current applied to the electrodialyzer were controlled and monitored by a BK Precision® 9123A switching mode, direct current (DC), regulated, programmable power supply (1–30 V ± 0.1 mV, 0.1–5 A ± 0.05 mA). The accuracy of the applied voltage and current was verified by a handheld digital multimeter.

3.4.1 Voltage loss at the electrodes

In most full-scale operations with hundreds of cell pairs, the electrical voltage losses at the electrodes are not significant compared to the resistive potential loss of the stack. In laboratory-scale ED systems, however, the voltage loss at the electrodes is a significant fraction of the total applied.

The voltage drop across the stack ($\Delta\phi_{stack}$, often reported in volts per cell-pair) is less than the voltage applied to the electrodes, $\Delta\phi_{app}$, because of thermodynamic and kinetic losses at the electrodes:

$$\Delta\phi_{stack} = \Delta\phi_{app} - \Delta\phi_{electrodes} \tag{3.9}$$

The voltage loss at the electrodes, $\Delta\phi_{electrodes}$, is given by:

$$\Delta\phi_{electrodes} = \Delta\phi_{equ} + \Delta\phi_{kin} + \Delta\phi_{rinse} \tag{3.10}$$

where $\Delta\phi_{equ}$ is the voltage drop from gas equilibrium at the electrodes, $\Delta\phi_{kin}$ is the electrode overpotential corresponding to the kinetics of gas production at the electrodes, and $\Delta\phi_{rinse}$ is the voltage drop from the electrical resistance of the electrode rinse solutions.

Since the electrodialyzer is operated as an electrolytic cell (as opposed to a galvanic cell), electrons are supplied to the cathode from an external power supply, and oxidation-reduction (redox) reactions occur at the surface of the electrodes to exchange electrons for ions at the electrode-solution interface. At the anode, oxygen (from water) is oxidized, producing oxygen gas, protons, and electrons according to the reaction (written as reduction):

$$O_2 + 4H^+ + 4e^- \Leftrightarrow 2H_2O \qquad (E^0 = 1.229 \text{ V } vs. \text{ NHE}) \tag{3.11}$$

where E^0 is the standard reduction potential of the reaction. The reduction potential of the anode in equilibrium with the reaction, E_{anode}, is given by:

$$E_{anode} = E^0 - \frac{R_g T}{4F} \ln\left(\frac{\{H_2O\}^2}{p_{O_2} 10^{-4\,pH}} \right) \tag{3.12}$$

where braces indicate activity, p is pressure in atmospheres, and pH is the negative logarithm of the activity of hydrogen (hydronium) ions in solution. At the cathode, hydrogen (from water) is reduced, producing hydrogen gas and hydroxide ions according to the reaction (written as reduction),

$$2H_2O + 2e^- \Leftrightarrow H_2 + 2OH^- \qquad (E^0 = -0.828 \text{ V } vs. \text{ NHE}) \tag{3.13}$$

and the reduction potential (*vs.* NHE) of the cathode, $E_{cathode}$, is given by:

$$E_{cathode} = E^0 - \frac{R_g T}{2F} \ln\left(\frac{p_{H_2} 10^{-2(pK_w - pH)}}{\{H_2O\}^2} \right) \tag{3.14}$$

where pK_w is the negative logarithm of the ion-product of water, which is dependent on temperature and concentration (Stumm and Morgan, 1995). Summing the voltage drop at both electrodes gives the voltage drop to maintain gas equilibrium at the electrodes:

$$\Delta\phi_{equ} = E_{anode} - E_{cathode} \tag{3.15}$$

which is approximately 1.23 V for most ED electrode rinse solutions.

In addition to the electrical potential that is thermodynamically required to maintain equilibrium of the gas-production equations just mentioned, the surface *overpotential* is the "excess" electric potential supplied to drive the heterogeneous reaction at a certain rate. The overpotential, η, of the ED electrodes can be modeled by the Butler-Volmer expression and the Tafel approximation:

$$\eta = \frac{R_g T}{\alpha F} \ln\left(\frac{i}{i_0}\right) \tag{3.16}$$

where α is a modified transfer coefficient, i_0 is the exchange current density, and i is the current density through the electrodialyzer (Bard and Faulkner, 2001). This expression is a semi-empirical treatment[†] of the charge-transfer limitations associated with the reaction mechanisms at the electrode. The kinetic electrical potential loss at the electrodes, $\Delta\phi_{kin}$, is the summation of the two overpotentials:

$$\Delta\phi_{kin} = \eta_{an} + \eta_{cat} \tag{3.17}$$

Finally, the resistive potential loss in the rinse solution can be calculated by:

$$\Delta\phi_{rinse} = i\frac{w}{\kappa_{rinse}} \tag{3.18}$$

where i is the current density, w is the distance between the electrodes and the stack, and κ_{rinse} is the conductivity of the rinse solution.

[†] The Butler-Volmer model of electrode kinetics is theoretically developed for one-step, one-electron, outer-sphere reactions, and while the production of H_2 and O_2 are multi-step, multi-electron, and inner-sphere reactions, the theoretical treatment of these reactions is mathematically similar. The Tafel approximation neglects the contribution of current from the "reverse" equilibrium reaction at each electrode (*e.g.*, there is negligible anodic current at the cathode, and *visa versa*).

The voltage loss from the electrodes was determined experimentally by measuring the voltage and current density relationship of the electrodes and electrode rinse solution of the electrodialyzer, constructed without membranes or spacers (*i.e.*, no concentrate or diluate cells). Experimental and model data for the overpotential (*i.e.*, the summation of the overpotentials of both electrodes was modeled as a single overpotential) and total electrode voltage loss for each of the three electrode rinse solutions are shown in Figure 3.6. Each component of the total electrode voltage loss (equilibrium voltage, overpotential, and resistive loss) was modeled according to the aforementioned equations, and the modified transfer coefficient, exchange current density, and resistive width model parameters were determined to be $\alpha = 0.1074$, $i_0 = 0.4599 \frac{\text{A}}{\text{m}^2}$, and $w = 5.15\,\text{mm}$, respectively. These model parameters were practically insensitive to the electrode rinse composition, as shown in part (a) of Figure 3.6.

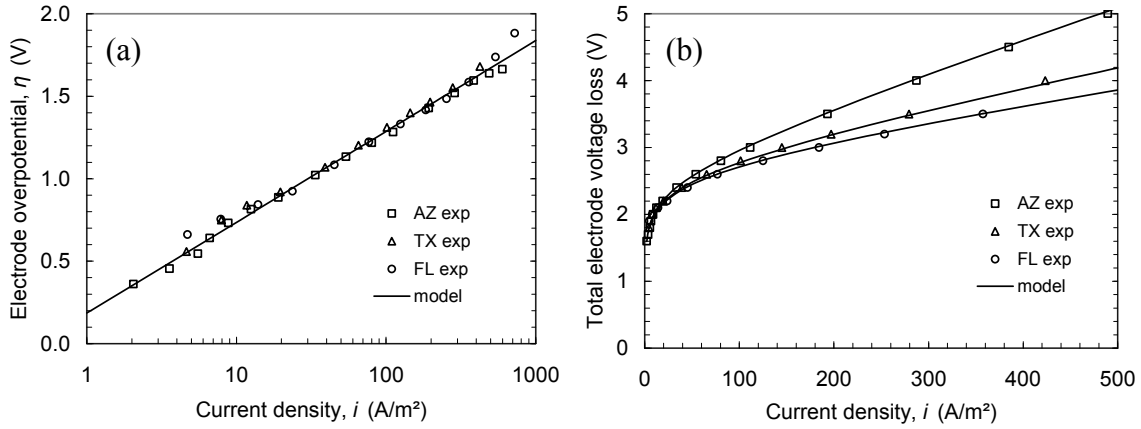

Figure 3.6 ED experimental electrode (a) overpotential and (b) total voltage loss

The total electrode voltage loss (shown in part (b) of Figure 3.6) is a function of the conductivity of the electrode rinse solution, which was approximately 11.8 mS/cm,

20.1 mS/cm, and 26.9 mS/cm for the Arizona, Texas, and Florida electrode rinse solutions, respectively.

3.4.2 Stack voltage application

For a desired stack voltage (*e.g.*, 1.0 Volts per cell-pair), the actual voltage applied to the electrodes was calculated by the experimental LabView SCADA according to the methods in the previous section. Every three seconds, the applied voltage was recalculated and corrected to maintain the desired stack voltage, accounting for the voltage loss at the electrodes based on the instantaneous current density and electrode rinse conductivity.

3.4.3 Power and specific energy

The electrical power (P_{elec}) consumed by the electrodialyzer was calculated by:

$$P_{elec} = \Delta\phi_{stack} I \tag{3.19}$$

where $\Delta\phi_{stack}$ is the voltage across the electrodialyzer stack, and I is the electrical current through the electrodialyzer. The hydraulic power (P_{hyd}) required to pump the concentrate or diluate solution through the stack was computed by:

$$P_{hyd} = \rho g Q \Delta H \tag{3.20}$$

where ρ is the solution density, g is the gravitational constant, Q is the volumetric flow rate, and ΔH is the head loss through the stack. The specific energy consumption (SEC) of the electrodialyzer was calculated by summing the electrical and hydraulic powers, integrating over the duration of the experiment, and normalizing by the volume of diluate produced:

$$SEC = \frac{1}{V_{dil}} \int \left(P_{elec} + P_{hyd} \right) dt \tag{3.21}$$

3.5 CHEMICAL CHARACTERIZATION AND CONTROL

3.5.1 Experimental BWRO solutions

Three representative brackish groundwaters were selected to provide a variety in the following characteristics: total dissolved solids (TDS) concentration, hardness, alkalinity, boron concentration, and silica concentration. Generally, more energy is required to desalinate waters of greater salinity, and the scaling potential of the water is correlated with hardness, as the salts of multivalent ions are generally much less soluble than those of monovalents. Almost all of the alkalinity in natural waters is from the carbonate system, which contributes to scaling potential. Boron is a difficult species to remove with RO, so the design and operation of some RO systems is controlled by satisfying the provisional drinking water guideline of 0.5 mg/L (World Health Organization, 2006). Silica is also problematic at low concentration because of its low solubility and abrasive crystalline geometry. Hence, source waters were selected from Arizona, Texas, and Florida with raw water quality and synthetic BWRO concentrate waste characteristics shown in Table 3.3. The salinity of the wastes ranged from approximately 8 to 19 g/L, and these waters also varied in relative hardness, alkalinity, and problematic sparingly-soluble species. Procedures for solution preparation, experimentation, and sampling are presented in Appendix C, Appendix D, and Appendix E, respectively.

Table 3.3 Selected brackish groundwater and RO concentrate waste characteristics

Characteristic	Maricopa Co., AZ	Cameron Co., TX	Martin Co., FL
TDS (mg/L)	1585[A]	3730[B]	3775[B]
pH	7.5	7.8	7.7
Ion balance (mEq/L)	-1.8	-0.5	-2.8
Simulated recovery	80%	75%	80%
Concentration factor	5	4	5
Synthetic TDS (mg/L)	7886	14778	18626
Ionic strength (mM/L) [C]	159	242	324
Na + Cl (% of TDS)	52%	56%	76%
Hardness (mEq/L)	94	58	102
Alkalinity (mEq/L)	16	22	12
Silica (mg/L as SiO_2)	-	50	71
Boron (mg/L as B)	-	43	-

[A] average of several water analyses, [B] SM 2540 C, 20th Ed., [C] calculated by Visual MINTEQ (v. 2.61)

Typical ED systems only tolerate low iron and manganese concentrations – 0.3 mg/L and 0.1 mg/L, respectively (AWWA, 1995). Pre-treatment removal of iron and manganese typically employs aeration or chemical oxidation followed by filtration (AWWA, 1995). Recent pretreatment (hypochlorite addition to produce 2 mg/L free-chlorine, one minute of static mixing, and Filtronics FV-03 Electromedia granular media filtration) for pilot-scale brackish groundwater desalination by tandem RO-ED demonstrated effective removal to less than 5 μg/L of iron and manganese (Wiesner *et al.*, 2009). Thus, in this research, iron and manganese were not included in the synthetic solutions prepared for ED experimentation.

A brackish groundwater treatment study in Maricopa County, Arizona by the US Bureau of Reclamation (Jurenka and Chapman-Wilbert, 1996) detailed the composition of Well S5 in Avandale (southwest of Phoenix). The mass- and mole-concentrations of

the predominant ion composition of the raw Maricopa groundwater are summarized in Table 3.4 (sorted by descending mass concentration for cations, anions, and neutral species). A synthetic water was formulated to simulate the concentrate waste from a theoretical BWRO system treating water from Well S5 (with recovery ratio, r = 80% and removal ratio, R = 100%, which gives a concentration factor of five), and the ion concentrations of that synthetic formula are also shown in Table 3.4. Because of the ion imbalance of -1.8 mEq/L in the raw water composition analysis, it was necessary in the formulation of the synthetic mixture to exceed the reported sodium concentration by 30%; all other constituents were supplied in proportion to the raw water analysis. The total carbonate in the raw water was calculated from measured alkalinity and pH, and all carbonate in the synthetic concentrate was added as bicarbonate. Zinc and copper were not included in the synthetic because of their relatively low concentrations. To avoid the oxidation of chloride to chlorine gas at the anode (which can destroy the ion exchange membranes), the electrode rinse solution was identical to the synthetic concentrate composition listed in Table 3.4 except that 94.36 mM of the chloride (99.9% of the 94.39 mM, all but 0.03 mM) was replaced by nitrate, and 20 mM of the resulting nitrate concentration was replaced by acetate for buffering at pH 5. (Replacing chloride with sulfate or carbonate would promote precipitation in the electrode rinse chamber.)

Table 3.4 Raw and concentrate compositions for Maricopa County, AZ

Constituent	C_{raw} [mg/L]	C_{raw} [mM]	$C_{simulated}$ [mg/L]	$C_{simulated}$ [mM]	$\Delta C/C_{conc}$ [%]
Ca^{2+}	206	5.14	1030	25.7	0.0%
Na^{+}	132	5.77	879	39.2	32.5%
Mg^{2+}	103	4.24	515	21.2	0.0%
Ba^{2+}	0.40	0.003	2.0	0.015	0.0%
Fe^{3+}	0.45	0.008	-	-	-
Zn^{2+}	0.44	0.007	-	-	-
Cu^{2+}	0.06	0.001	-	-	-
Mn^{2+}	0.06	0.001	-	-	-
Cl^{-}	669	18.9	3346	94.4	0.0%
HCO_3^{-}	203	3.32	1013	16.6	0.0%
SO_4^{2-}	198	2.06	991	10.3	0.0%
NO_3^{-}	17.4	0.281	87.2	1.41	0.0%
F^{-}	0.230	0.012	-	-	-
Σ	1531	39.7	7887	209	

Similarly, a water composition analysis of groundwater that supplies the North Cameron RO facility in Cameron County, TX was performed by Ana-Lab Corp. (Kilgore, TX) in mid 2007. The mass- and mole-concentrations of the predominant ion composition of the raw groundwater results are summarized in Table 3.5. The electrode rinse solution was identical to the synthetic concentrate composition except that all of the chloride was replaced by nitrate, and 20 mM of the resulting nitrate concentration was replaced by acetate for buffering at pH 5.

Table 3.5 Raw and concentrate compositions for Cameron County, Texas

Constituent	C_{raw} [mg/L]	C_{raw} [mM]	$C_{simulated}$ [mg/L]	$C_{simulated}$ [mM]	$\Delta C/C_{conc}$ [%]
Na^+	931	40.5	3922	171	5.3%
Ca^{2+}	153	3.82	612	15.3	0.0%
Mg^{2+}	81.4	3.35	326	13.4	0.0%
K^+	15.6	0.399	62.4	1.60	0.0%
Sr^{2+}	7.42	0.085	29.7	0.339	0.0%
Mn^{2+}	0.045	0.001	-	-	-
Ba^{2+}	0.015	0.000	-	-	-
Cl^-	1110	31.3	4439	125	0.0%
SO_4^{2-}	991	10.3	3964	41.3	0.0%
HCO_3^-	338	5.55	1354	22.2	0.0%
Br^-	4.88	0.061	19.5	0.244	0.0%
$B(OH)_3$	61.2	0.990	245	3.96	0.0%
SiO_2	12.4	0.206	49.6	0.826	0.0%
Σ	3645	96	14,877	393	

Water quality data of groundwater in Florida was gathered from the South Florida Water Management District's DBHYDRO database (SFWMD, 2008), and Sample P9750-2 from Station MF-37 at a depth of 2049 ft on 26 OCT 2001 was selected as the representative water for this study. The mass- and mole-concentrations of the predominant ion composition of the raw groundwater results are summarized in Table 3.6. The electrode rinse solution was identical to the synthetic concentrate composition except that all of the chloride was replaced by nitrate, and 20 mM of the resulting nitrate concentration was replaced by acetate for buffering at pH 5.

Table 3.6 Raw and concentrate compositions for Martin County, Florida

Constituent	C_{raw} [mg/L]	C_{raw} [mM]	$C_{simulated}$ [mg/L]	$C_{simulated}$ [mM]	$\Delta C/C_{conc}$ [%]
Na^+	905	39.35	4828	210	6.7%
Ca^{2+}	179	4.47	895	22.3	0.0%
Mg^{2+}	132	5.43	660	27.2	0.0%
Sr^{2+}	26.4	0.301	132	1.51	0.0%
K^+	25.0	0.639	125	3.20	0.0%
Fe^{3+}	0.353	0.006	-	-	-
Ba^{2+}	0.060	0.000	-	-	-
Mn^{2+}	0.013	0.000	-	-	-
Cl^-	1866	52.7	9333	263	0.0%
SO_4^{2-}	384	4.00	1920	20.0	0.0%
HCO_3^-	146	2.40	732	12.0	0.0%
F^-	0.55	0.029	-	-	-
SiO_2	14.2	0.236	71.0	1.18	0.0%
Σ	3685	110	18,626	559	-

3.5.2 Antiscalants

Two phosphonate antiscalants manufactured by Thermphos Trading GmbH were selected: Dequest® 2006 and 2066. Dequest® 2006 is an amino tri-methylene phosphonic acid (ATMP, molecular weight 299.05 g/mol), which acts as a general scale inhibitor. Dequest® 2066 is marketed as another general scale inhibitor (and especially against barium sulfate), and is composed of diethylene triamine pentamethylene phosphonic acid (DTPMP, molecular weight 573.2 g/mol). The molecular structures of these antiscalant compounds are shown in Figure 2.8, and recommended doses from the manufacturer are "less than 20 mg/L", but research on the delay of precipitation by these compounds indicates that a raw dose of approximately 1.5 mg/L is sufficient (Cobb, 2009; Hekman,

2009). The concentration of antiscalants in experimental samples was determined by measuring phosphorous by ICP.

3.5.3 Temperature control and monitoring

A passive, continuously circulating, heating water bath system (shown in Figure 3.7) was used to maintain a constant temperature of the experimental electrodialysis solutions (25.2°C ± 0.5°C), each of which was monitored with a Thermo Orion 4-Star pH and conductivity meter fitted with an Orion® 013005 conductivity/temperature cell. Approximately thirty liters of tap water were heated to 24.3°C ± 0.2°C with a Lab-Line Magnestir Bath™ (monitored and controlled by the custom LabVIEW SCADA via a thermistor and solid-state relay), and this heat buffer was circulated through two, four-liter baths – one each for the concentrate reservoir and the electrode rinse reservoir.

A separate reservoir contained ice and water (also shown in Figure 3.7), and the chilled water was circulated through tubing coiled around the submerged concentrate beaker, through tubing coiled around the submerged electrode-rinse beaker, and then through a coaxial-jacketed tubing around the diluate electrodialyzer effluent. The chilled-water was pumped by a miniature gear-pump that was actively controlled by the custom LabVIEW SCADA via the Orion 4-star temperature readings and a solid-state relay (not shown). The chilled-water circulation was engaged when the experimental concentrate solution temperature exceeded 25 °C.

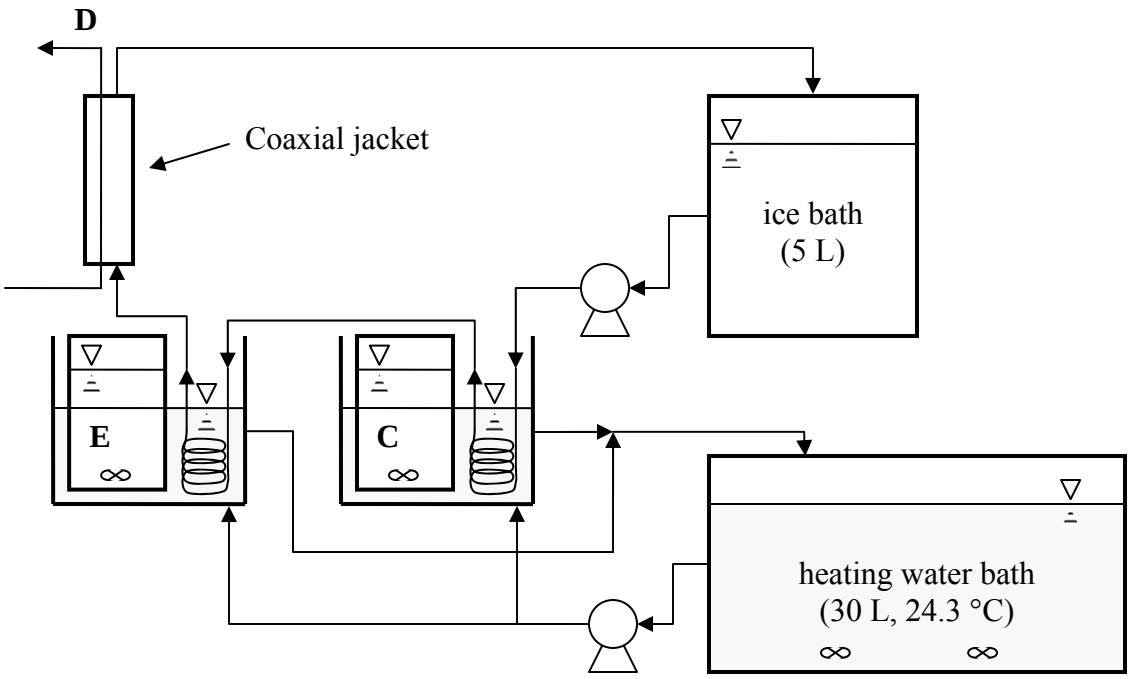

Figure 3.7 Temperature control schematic

3.5.4 pH

The pH of each experimental reservoir was monitored with a Thermo Orion 4-Star pH and conductivity meter fitted with an Orion® 9157 pH probe. Each pH probe was calibrated with pH 4, 7, and 10 buffer solutions according to Standard Methods (Eaton *et al.*, 2005, §4500-H+).

3.5.5 Conductivity

The conductivity of each experimental reservoir was monitored with a Thermo Orion 4-Star pH and conductivity meter fitted with an Orion® 013005 conductivity and temperature cell. Each conductivity cell was calibrated using standard solutions: 0.0067 M KCl (100 mS/cm), 0.01 M KCl (1.412 mS/cm), 0.1 M KCl (12.89 mS/cm), and 1.0 M KCl (111.9 mS/cm), according to Standard Methods (Eaton *et al.*, 2005, §2510).

Conductivity cells were periodically cleaned by soaking in 1 M hydrochloric acid, followed by soaking in distilled water. (For reference, the conductivity of the distilled water in the laboratory was consistently 0.5–0.7 mS/cm, which would rise to approximately 1.4 mS/cm after equilibration with the atmosphere.)

3.5.6 Alkalinity

The alkalinity of samples from select experiments was determined by titration with hydrochloric acid according to Standard Methods (Eaton *et al.*, 2005, §2320). Sample volumes of 100 mL were titrated under simultaneous observation of pH and conductivity to determine the precise titration end-point. The titrant was standardized with a basic solution prepared with 0.1 M Certified ACS NaOH.

3.5.7 Ion chromatography (IC)

During experimentation, 50-100 μL samples (depending on concentration) were periodically withdrawn by pipette from the experimental reservoirs and diluted to 10 mL (1/200-1/100 dilutions); 8 mL were retained for ICP analysis, and the remaining 2 mL were used for IC analysis. The retained 2 mL dilution was subsequently diluted by the addition of 2 mL of distilled water, creating final dilutions of 1/400-1/200. Standard concentrations were prepared from mixtures of Certified ACS stocks of NaCl, $NaNO_3$, and Na_2SO_4. Example calibration standard curves for chloride, nitrate, and sulfate by ion chromatography are shown in Figure 3.8.

The concentrations of chloride, nitrate, and sulfate ions in experimental samples were determined according to Standard Methods (Eaton *et al.*, 2005, §4110) using an ion chromatography (IC) system composed of Metrohm® hardware (838 Advanced Sample

Processor, 762 IC Interface, 752 IC Pump Unit, 733 IC Separation Center, 732 IC Detector, and 709 IC Pump) fitted with a 150 mm Metrosep A supp 5 IC column (PN 6.1006.520, SN 7704583). Metrohm software *IC Net® v. 2.3 SR3* was used to perform the IC analyses. Wash and rinse solutions of 0.1 M H_2SO_4 and distilled water were used to regenerate the internal carbonate suppressor. The eluent was composed of 3.2 mM Na_2CO_3 and 1.0 mM $NaHCO_3$ in distilled water. A stepwise procedure for the IC analysis is listed in Appendix F.

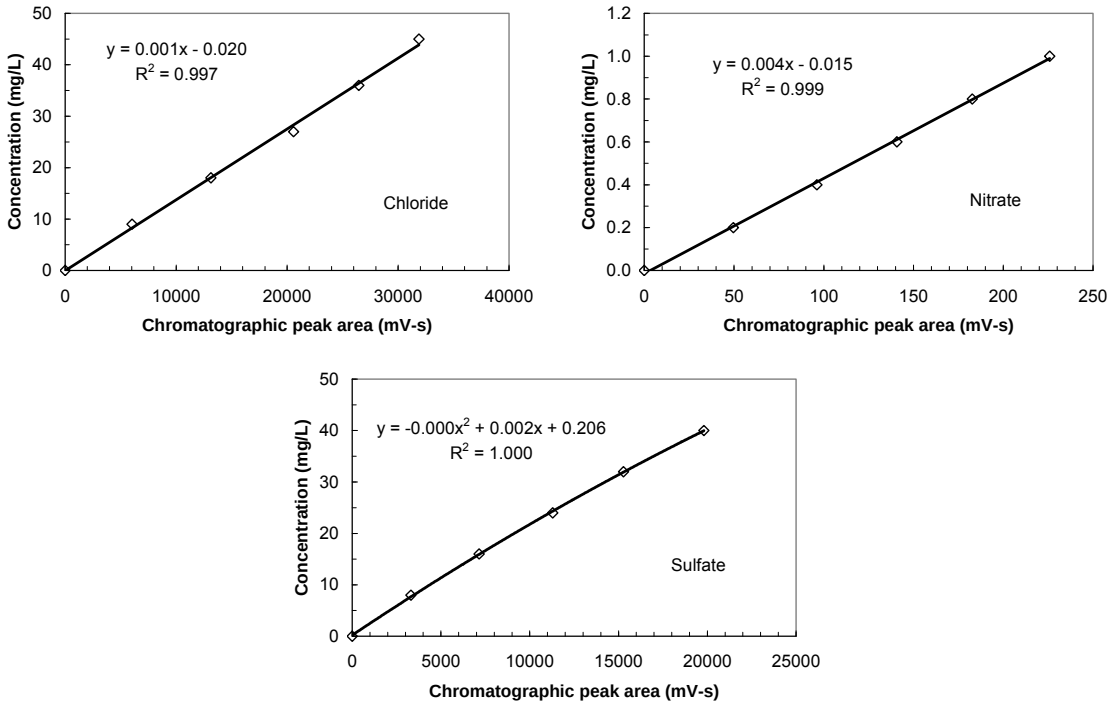

Figure 3.8 Example IC calibration standard curves for chloride, nitrate, and sulfate

3.5.8 Inductively coupled plasma - optical emission spectroscopy (ICP-OES)

The remaining 8 mL dilutions retained from above for ICP analysis were acidified (2% by volume) with the addition of 160 µL of concentrated (70%) nitric acid. The concentrations of cations in solution were determined using a Varian 710-ES ® ICP

Optical Emission Spectrometer (OES) with a SPS 3 Autosampler and *ICP Expert II*® software (v. 1.1), according to Standard Methods (Eaton *et al.*, 2005, §3125). Argon was used as the nebulizer propellant, and wavelengths analyzed in the OES for each cation are presented in Table 3.7. Example calibration standard curves for calcium, magnesium, and sodium (reproduced from the *ICP Expert II*® software) are shown in Figure 3.9[†], and a stepwise procedure is listed in Appendix G.

Table 3.7 Elements and wavelengths analyzed with ICP

Element	Wavelengths (nm)		
B	249.678	249.773	
Ba	233.527	455.404	493.408
Ca	315.887	317.933	
K	766.490	769.897	
Mg	280.270	285.213	
Na	588.995	589.592	
P	177.434	213.618	
Si	250.690	251.611	288.158
Sr	407.771	421.552	460.733

[†] An internal reference of 5 mg/L Sc was tested in an attempt to linearize the calibration curves, but it only improved a few of the curves. In fact, the application of the Sc internal reference actually exacerbated the nonlinearity of some of the curves. Furthermore, the relative standard deviations (RSD) of many analytes alone were better than the Sc measurements. Hence, an internal reference was not used, and quadratic regressions were employed for some standard curves. Multiple wavelengths were analyzed for each element, because some wavelengths are more precise under various conditions. In each analysis, the wavelength with the highest correlation coefficient (and/or lowest RSD) for each element was selected for concentration calculations.

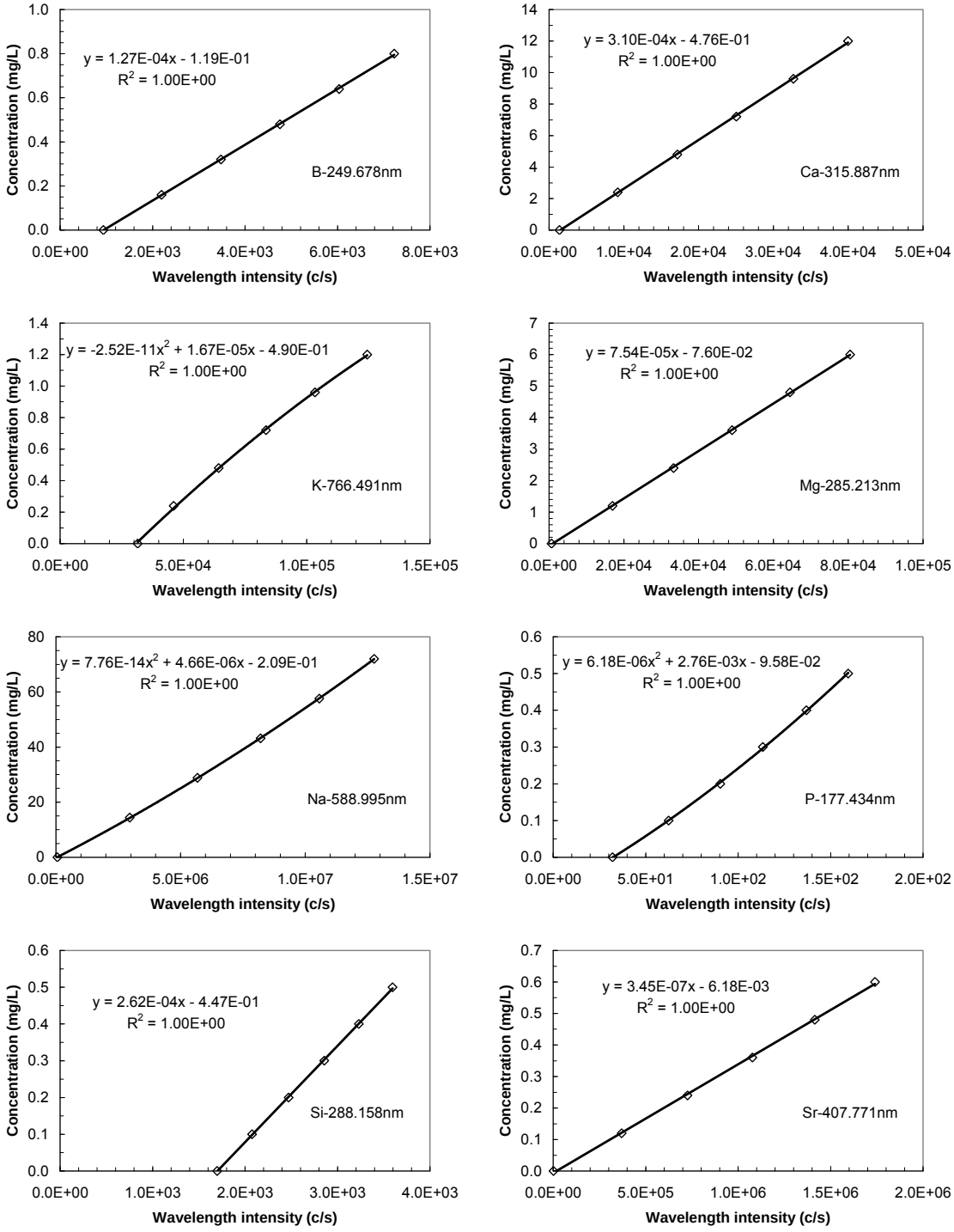

Figure 3.9 Example ICP calibration standard curves for B, Ca, K, Mg, Na, P, Si, and Sr

3.6 DATA ANALYSIS

Output files from the custom LabVIEW SCADA were analyzed with National Instruments DIAdem software. A custom Visual Basic Script within the DIAdem software was used to calculate current density, removal ratio, electrical power, hydraulic power, and specific energy consumption. The current density (i) was calculated according to the following formula:

$$i = \frac{I}{A} \tag{3.22}$$

where I is the electrical current through the electrodialyzer, and A is the perpendicular cross-sectional area through which the current is flowing (*i.e.*, 64 cm^2 in the laboratory system).

Because of the variation in types and concentrations of certain ions, the removal ratio based on conductivity was selected as an approximate "universal" metric of comparison of treatment efficacy (though conductivity is only approximately proportional to total dissolved solids concentration). The conductivity removal ratio (R_κ) at any time during the experiment was calculated as:

$$R_\kappa = 1 - \frac{\kappa_D}{\kappa_{D,0}} \tag{3.23}$$

where κ_D is the conductivity of the diluate reservoir during the experiment at time t, and $\kappa_{D,0}$ is the conductivity of the diluate reservoir at the beginning of the experiment.

Electrical power, hydraulic power, and specific energy consumption were calculated according to the formulas presented in §3.4.2.

Chapter 4 – Experimental Results

Experimental evaluation of the utility of electrodialysis in treating brackish groundwater reverse osmosis (BWRO) concentrate was performed according to the methods detailed in Chapter 3. The effects of electrical, hydraulic, and chemical variables are presented here.

4.1 ELECTRICAL: EFFECTS OF STACK VOLTAGE

4.1.1 Experimental conditions

An applied electric potential (voltage) is the driving force for ionic separation in electrodialysis, and it is the principal controlling factor for the rate of separation. Experiments were performed at three different voltage applications (0.5, 1.0, and 1.5 Volts per cell-pair) for treating the synthetic Arizona concentrate, and the experimental solutions contained 5 mg/L of DQ2006 antiscalant.

The initial concentrate and diluate solution volumes were each one liter, which simulated a 50% single-stage electrodialysis recovery. The electrodialyzer was fitted with 11 CMV membranes and 10 AMV membranes to create ten cell-pairs (ten concentrate cells and ten diluate cells). The diluate superficial velocity was held constant at approximately 2.4 cm/s, which produced a head loss of approximately 60 kPa/m (2.7 psi/ft).

4.1.2 Chemical efficiency

Bulk separation

The ionic separation of each experiment is shown in Figure 4.1. As the ions were continuously separated from the diluate and transported to the concentrate, the

conductivity of the diluate (which is approximately proportional to the bulk concentration of ions) decreased from its initial value of 11.5 mS/cm, as shown in part (a), and the removal ratio (based on diluate conductivity) increased, as shown in part (b) of Figure 4.1. The conductivity of the concentrate increased to slightly less than double the initial value, and the curvature of the separation rate was similar to those reported by Ortiz *et al.* (2005) The experiment simulated 50% single-stage recovery, which would result in a doubling of the concentrate concentration at complete removal, but approximately 5% of the initial water mass of the batch diluate solution was transported to the concentrate solution over the course of the experiment by osmosis and the electromigration of solvated cations. Most significantly, no precipitation occurred in the concentrate solution *during* an experiment (except one in which the pH was raised by the addition of 0.1 M NaOH), which demonstrates that the concentration polarization of electrodialysis was sufficiently small that the concentration of ions in the concentrate diffusion boundary layers does not overcome the ability of the antiscalant to prevent precipitation.

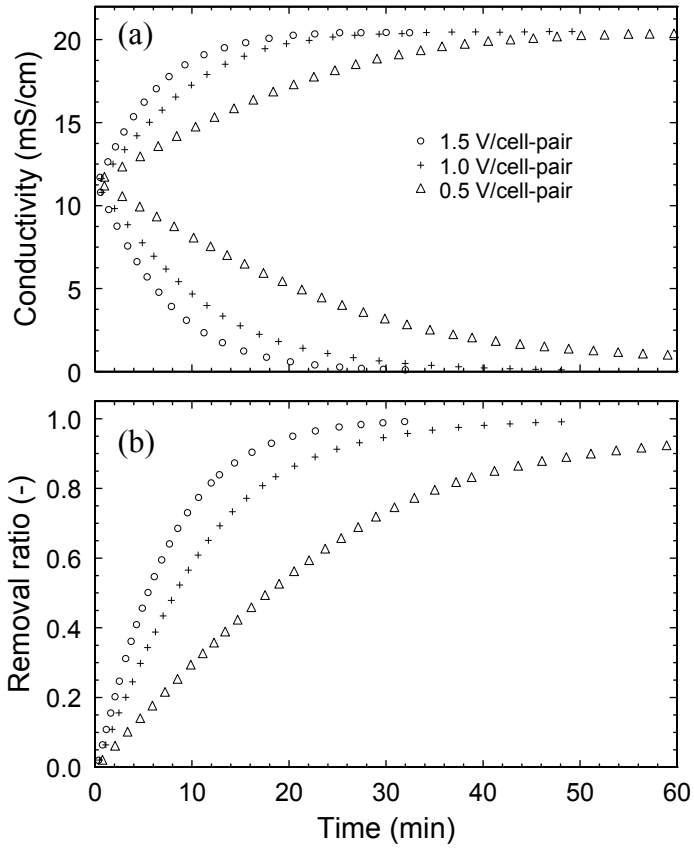

Figure 4.1 Effect of stack voltage on separation efficiency

As expected, the separation rate increased with increasing voltage, because the increased electric field strength increases the rate of electromigration, as shown by the Nernst-Planck Equation (Eq. 2.7), as well as the results of Elmidaoui *et al.* (2002; 2001) and Kabay (2002). Hence, the concentration of the diluate decreases more rapidly with greater applied voltages. Furthermore, the rate of removal was approximately proportional to the applied stack voltage for removal ratios less than approximately 40%, and the rate of removal deviated significantly from linearity above 80% removal. In the context of a BWRO system operating at 80% recovery, an electrodialysis system operating at 50% recovery and 80% removal ratio produces a diluate product that has the

same concentration as the RO feed and a concentrate that is nine times as concentrated. In such case, the ED diluate could possibly be recycled to the RO influent stream. Greater or lesser removal could be achieved for optimal cost efficiency in the electrodialytic treatment of BWRO concentrate.

Ionic separation

During experimentation, samples were drawn from the experimental concentrate and diluate solutions at nominal conductivity removal ratios of 0, 0.2, 0.4, 0.6, 0.8, and 0.99 and subsequently analyzed by IC and ICP methods for anion and cation concentrations, respectively. In all of the experiments, the initial pH was 8.0, and the diluate pH rose steadily to approximately 9.0 at a removal ratio of 90% while the concentrate pH decreased to approximately 7.8, as shown in Figure 4.2. The increase in pH of the diluate and decrease in pH of the concentrate is consistent with other research (Grossman and Sonin, 1972; Rajan *et al.*, 1968). The cause of these pH changes is a combination of several phenomena. The increase in pH of the diluate and decrease in pH of the concentrate is complicated by the changing ionic strength of each solution, which not only affects the mixed acidity constants in equilibrium calculations (Stumm and Morgan, 1995), but also affects concentrations of pH controlling species such as HCO_3^- and CO_3^{2-}. Furthermore, variation in ionic strength changes the electrical liquid-junction potential of the glass pH probe (Bard and Faulkner, 2001; Wiesner *et al.*, 2006), which can shift pH readings by a few tenths of a pH. Considering the mild focus of pH in this research, separation of these phenomena was not pursued.

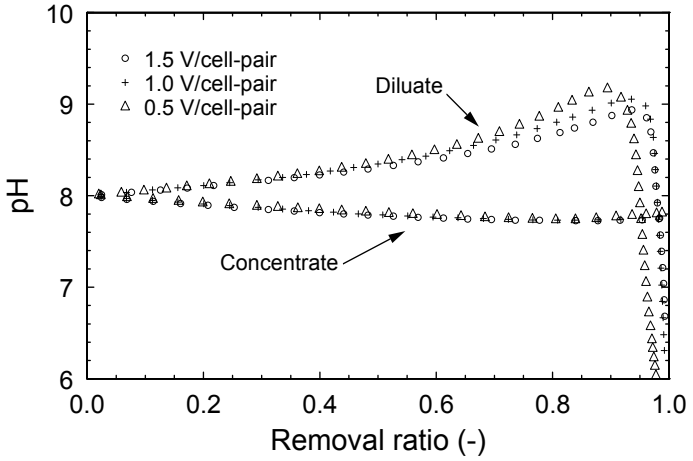

Figure 4.2 Effect of stack voltage on pH

In general, most salt ions were separated at approximately the same rate as conductivity, though the rate of separation of some ions was sensitive to voltage application. The effect of voltage application on the removal of four of the predominant ions in the Arizona concentrate (calcium, sodium, chloride, and sulfate) is shown in Figure 4.3.

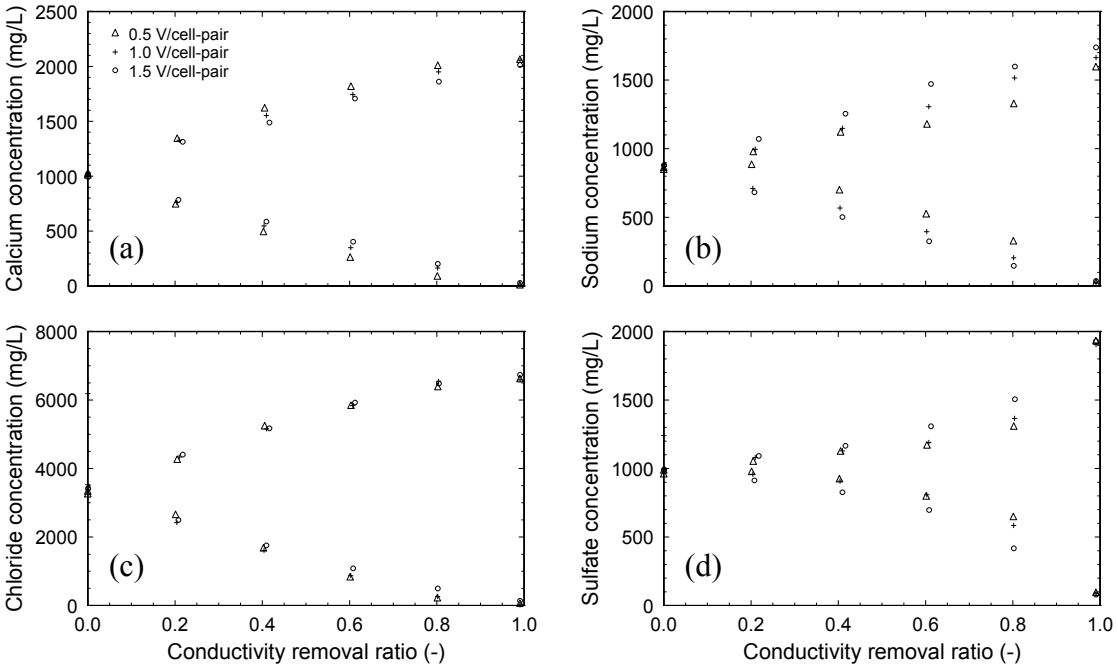

Figure 4.3 Effect of stack voltage on removal of select ions

The distinct concavity of the sulfate concentration versus conductivity removal is consistent with the results of Kabay *et al.* (2006a) and a consequence of the large fraction of sulfate that is complexed with calcium, magnesium, and sodium (creating neutral and single-charge compounds), leaving only approximately 54% of the total sulfate as free sulfate. The distribution of chemical species in each of the BWRO concentrates used in this study was calculated using Visual MINTEQ and is recorded in Appendix H.

At higher voltage applications, sodium and sulfate were separated more rapidly relative to the bulk conductivity removal. Several related factors affect the variation in separation rate as a function of voltage. Considering the simplified concentration profiles in Figure 2.4, an application of higher voltage (and consequently, a higher current density) would result in a steeper concentration gradient for each ion in the diffusion boundary layers. As the current density increases, an ion with a lower diffusivity

approaches limiting current density (*i.e.*, the current density at which the concentration is zero at the membrane surface) before an ion with a higher diffusivity. As one ion nears limiting current density, an increase in voltage causes an increase in the transport numbers of other ions of the same charge to make up the increase in current density. Also, as the concentrations decrease through the boundary layer, the concentrations of ion complexes decrease, and different gradients in certain ions cause different concentrations of complexes, which also affects the transport numbers of ions.

4.1.3 Electrical efficiency

The initially steady rate of separation (*i.e.*, the approximate linearity in the rate of separation for removal ratios less than approximately 40%, shown of Figure 4.1 (b)) can be attributed to the relatively stable voltage losses within the stack. The diluate resistive loss increases as the diluate conductivity decreases, and conversely, the concentrate resistive loss decreases as the concentrate conductivity increases. In ED treatment systems that produce potable water directly from brackish sources, the resistance of the diluate solution is the predominant culprit of voltage loss. However, the electrical resistance of the ion exchange membranes has a more significant influence in the treatment of solutions of greater conductivity (*e.g.*, BWRO concentrate). While the membrane resistance was practically constant throughout the experiments, the total resistance of the stack increased as the diluate solution decreased in conductivity, which caused the current density to decrease throughout the experiment, as shown in Figure 4.4.

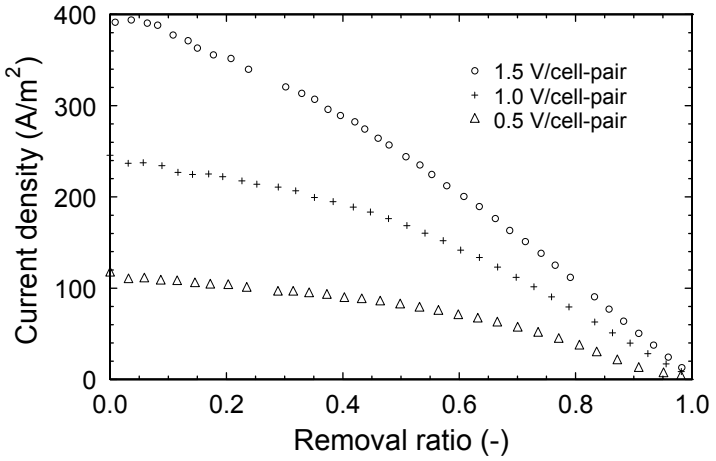

Figure 4.4 Effect of stack voltage on current density

With greater voltage application, the current density (and hence, the separation rate) is greater for a given removal ratio. This correlation between current density and applied voltage is approximately proportional, though voltage losses attributable to liquid junction and diffusion potentials reduce the current density from linearity at greater voltage applications.

However, the cumulative electrical charge (*i.e.*, the integration of electrical current with time) that is required to achieve a given removal ratio is practically independent of voltage application. A thermodynamic minimum charge of approximately 12836 Coulombs (*i.e.*, the product of Faraday's constant and the total number of equivalents of charge in the experimental solution) is required for complete separation of the Arizona BWRO concentrate. Normalizing the experimental cumulative charge by this thermodynamic minimum (shown in Figure 4.5) reveals that these experiments were executed with current efficiencies greater than 90% (*i.e.*, the reciprocal of the ordinate value at 100% removal). That is, approximately 90% or more of the

electrical current is effectively utilized for separating ions. The linearity of the data in Figure 4.5 demonstrates the stable current efficiency of this process and the approximate linearity between conductivity and concentration.

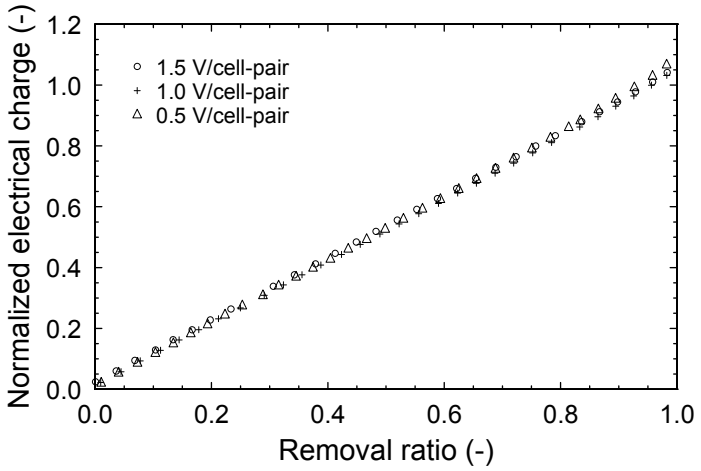

Figure 4.5 Effect of stack voltage on charge efficiency

While the total charge investment is practically insensitive to the voltage application, the specific energy (*i.e.*, the amount of invested energy per unit volume of diluate, frequently reported in kWh/m^3) of the process is approximately linearly proportional to the stack voltage, as shown in Figure 4.6. This behavior was also observed by Kabay *et al.* (2002; 2006a). As previously mentioned, the magnitudes of the concentration gradients in the diffusion boundary layers are approximately proportional to the current density (and applied voltage). Since diffusion is an irreversible process, an increase in the applied voltage causes the separation process to operate more irreversibly, which increases the specific energy investment. (This phenomenon is a practical illustration of the Second Law of Thermodynamics.)

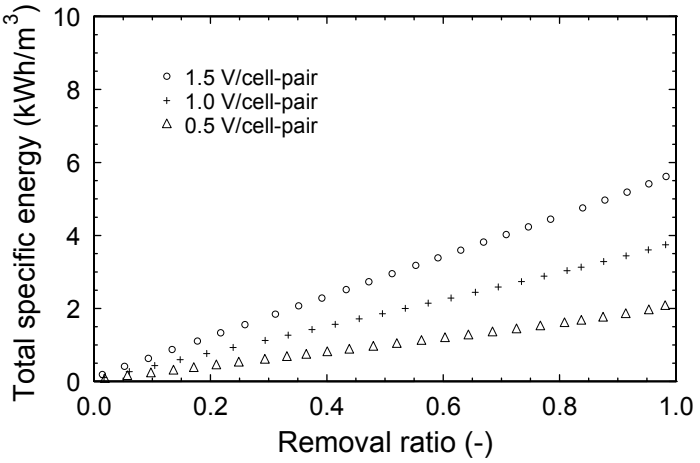

Figure 4.6 Effect of stack voltage on specific energy

The specific energy reported in Figure 4.6 includes the electrical energy applied to the stack, as well as the hydraulic energy invested to pump the solution through the electrodialyzer. At 99% removal, the hydraulic energy accounted for 0.7%, 1.7%, and 8.2% of the total specific energy for the 1.5, 1.0, and 0.5 V per cell-pair experiments, respectively. The nonlinearity of the specific energy at very high removal ratios (especially for lower voltage applications) is a reflection of the fact that the hydraulic pumping power is constant with time.

4.1.4 Hydraulic efficiency

The mass of the diluate reservoir was measured continuously during the experiment to quantify the flux of water through the membranes by electroosmosis and osmosis, and the change in mass is shown in Figure 4.7 as a function of (a) conductivity removal ratio and (b) time. For all voltage applications, the mass change was predominantly influenced by electroosmotic flux, which is demonstrated by the linearity with removal ratio (up to approximately 90% for the higher voltage applications). Due to

the significantly slower rate of separation at the lowest voltage application, the difference in concentration between the concentrate and diluate cells drives an osmotic flux of water and is noticeable in the downward curvature of the 0.5 V/CP at removal ratios greater than 80%. Together, electroosmosis and osmosis reduced the single-stage BWRO concentrate recovery from a nominal 50% to an actual 48%.

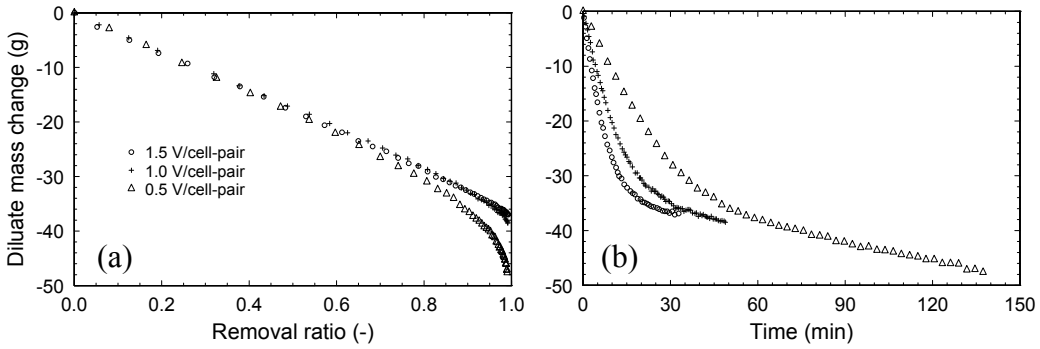

Figure 4.7 Effect of stack voltage on mass transport by (a) removal ratio and (b) time

The diluate mass change data for the 1.5 V/cell-pair and 0.5 V/cell pair were analyzed to quantify the flux rates by electroosmosis and osmosis, respectively, as shown in Figure 4.8. For the 1.5 V/CP data shown in Figure 4.8 (a), linear regression of the mass change versus removal ratio from zero to 80% reveals that approximately 3.5 g of water were transferred per gram of salt by electroosmosis. That is, approximately 11.4 moles of water were transferred per equivalent of salt separated, which is slightly higher than Strathmann's (2004) estimate of 2-10 moles per equivalent. In the Arizona BWRO concentrate, a large fraction of the cation equivalent concentration comes from divalent species, which have higher primary solvation numbers than monovalent cations

(Bockris and Reddy, 1998). Moreover, Larchet *et al* (2004) demonstrated that the water-to-salt ratio in electroosmosis is practically constant in concentrations up to 1 mol/L.

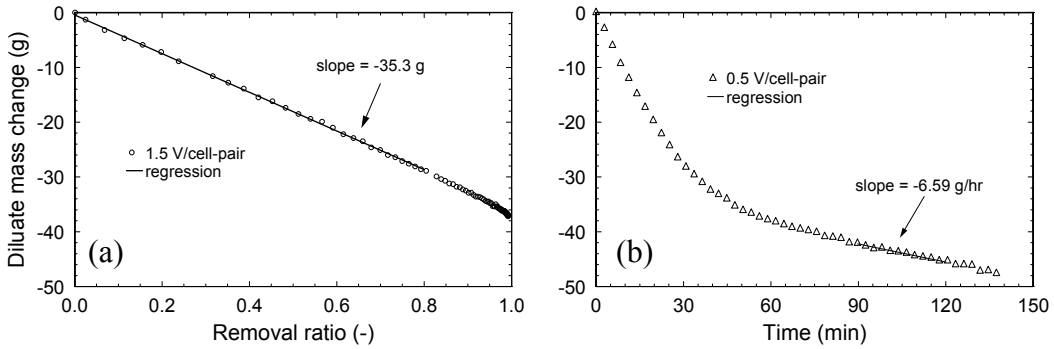

Figure 4.8 Rates of water flux by (a) electroosmosis at 1.5 V/cell-pair and (b) osmosis at 0.5 V/cell-pair

For the 0.5 V/CP data shown in part (b), linear regression of the mass change versus experimental time from 90 to 120 minutes (corresponding to conductivity removal ratios of approximately 0.968 and 0.985, respectively, and thus involving approximately 0.134 g of salt transfer and 0.466 g of water transfer by electroosmosis), reveals an average flux of approximately 42.3 g/ m^2-hr (*i.e.*, approximately 1.2×10^{-8} m/s) of water by osmosis. By approximating that the concentrations at the membrane surfaces were equal to the bulk concentrations (because at high removal ratios, the current density, and therefore the magnitudes of the concentration gradients in the diffusion boundary layer, were small), the difference in concentration between the concentrate and diluate was approximately 193 mol/m^3 and 250 mol/m^3 at 90 and 120 minutes, respectively. The osmotic pressure (Π) of each solutions was calculated for both conditions with the Carnahan and Starling corrected van't Hoff approximation:

$$\Pi = \frac{RT}{\overline{V}_w}\ln\left(a_w\right) \approx RT\left(\frac{1+\phi+\phi^2-\phi^3}{\left(1-\phi\right)^3}\right)\sum_i c_i \qquad (4.1)$$

where c_i is the molar concentration and □ is the volume fraction of the solute in solution. Over the 30 minute period, the average trans-membrane osmotic pressure difference was approximately 5.8 atm (85 psi). The average osmotic permeability (P) of the AMV and CMV membranes was calculated to be 1.2×10^{-10} kg·m/m^2·s·atm with the following expression:

$$P = \frac{J_{osmosis}\, h_{mem}}{\Delta\Pi} \tag{4.2}$$

where $J_{osmosis}$ is the flux of water, h_{mem} is the thickness of the membrane, and $\Delta\Pi$ is the average trans-membrane osmotic pressure.

4.2 ELECTRICAL: EFFECTS OF MEMBRANE TYPE

4.2.1 Experimental conditions

Two sets of experimentation were performed similarly to the experimentation described above in which the effects of the membrane type were investigated. One set of experimentation was conducted with a 10 cell-pair stack of 11 CMV and 10 AMV membranes, and the other was conducted with a 9 cell-pair stack of 10 PCSK and 9 PCSA membranes. With each stack, experiments were performed with applied voltages of 0.5, 1.0, and 1.5 Volts/cell-pair, and all experiments were conducted with synthetic Texas RO concentrate, an antiscalant dose of 9-12 mg/L of ATMP, superficial velocity of 4.8 cm/s, and a nominal single-stage ED recovery of 50%.

4.2.2 Chemical efficiency

Bulk separation

The rate of ionic separation with the CMV-AMV set was consistently greater than the rate of separation with the PCSK-PCSA stack, as shown in Figure 4.9. For removal

ratios less than 40%, the rate of separation with the CMV-AMV stack was approximately 36% greater for the 1.5 V/cell-pair application and approximately 26% greater for the 0.5 V/cell-pair application. However, the CMV-AMV stack was constructed with ten cell-pairs, whereas the PCSK-PCSA stack only contained nine cell-pairs. Thus, when normalized by the number of cell-pairs, the differences between stack separation rates were 22% and 13% for the 1.5 and 0.5 V/cell-pair experiments, respectively.

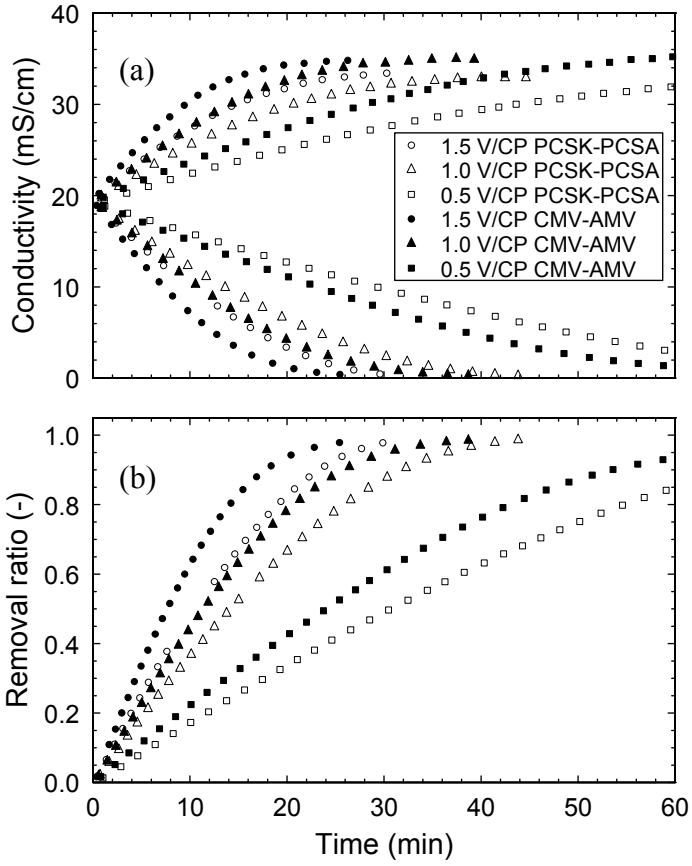

Figure 4.9 Effect of membrane type on separation efficiency

Ionic separation

Separation of individual components in these Texas/membrane experiments was very similar to separation from the Arizona/voltage experiments described previously.

Magnesium and sodium were separated at practically the same rate with the CMV-AMV and PCSK-PCSA stacks, as shown in Figure 4.10. As in the Arizona experiments, a significant variation in voltage caused only a slight variation (if any) in the rate of separation relative to the change in conductivity. Similar trends were observed in the separation of total carbonate (measured by alkalinity titrations) and sulfate. Again, the concavity of the removal of carbonate and sulfate is characteristic of a significant fraction of the total component concentration being fixed in neutral ion-pairs.

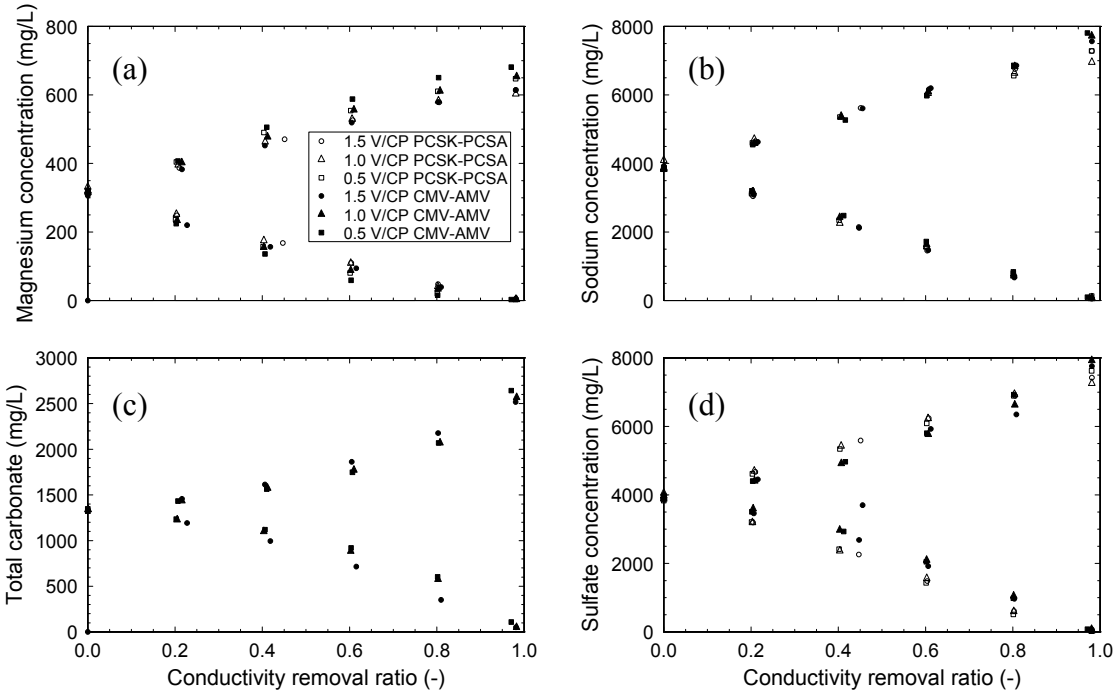

Figure 4.10 Effect of membrane type on removal of select ions

4.2.3 Electrical efficiency

The current density through the CMV-AMV stack was consistently 10-25% greater than the current density in the PCSK-PCSA stack, as shown in Figure 4.11.

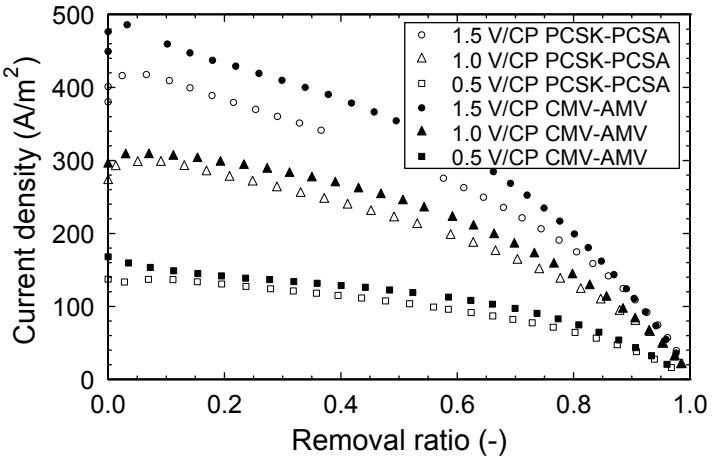

Figure 4.11 Effect of membrane type on current density

The better rate of separation in the experiments with the CMV-AMV stack was attributable to higher ion exchange capacities and thinner membrane thicknesses (as shown in Table 4.1), and therefore, lower membrane electrical resistances.

Table 4.1 Capacities and thicknesses of select ion exchange membranes

Membrane	Capacity (mEq/g)	Thickness (μm)
AMV	1.98	111
CMV	1.95	119
PCSA	1.5	193
PCSK	1.0	182

One might assume that the lower rate of separation in the PCSK-PCSK stack was due, in part, to lower membrane permselectivities, especially considering the lower ion exchange capacity of the membranes. However, the charge efficiency of the two systems was nearly identical (near 90%), as shown in Figure 4.12.

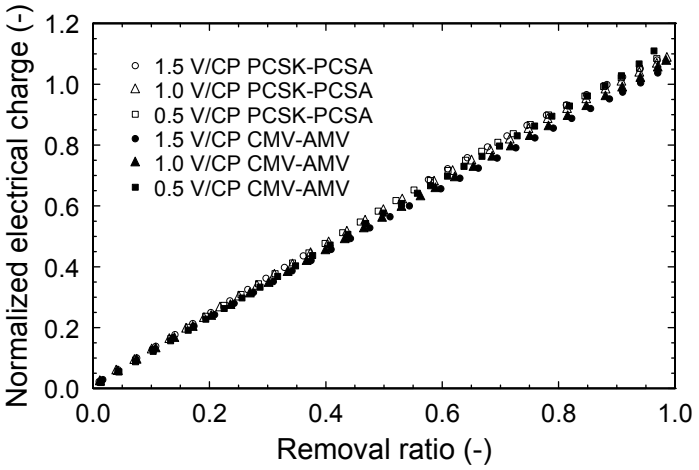

Figure 4.12 Effect of membrane type on charge efficiency

In spite of the difference in the rate of separation, the total specific energy invested in the treatment of the different stacks was largely independent of membrane type, as shown in Figure 4.13. The greater electrical resistance of the PCSK-PCSA stack compared to the CMV-AMV stack causes the specific energy to be proportionally higher with voltage applications (*e.g.*, approximately a 10% increase in specific energy at 1.5 V/cell-pair and only barely noticeable at 1.0 V/cell-pair).

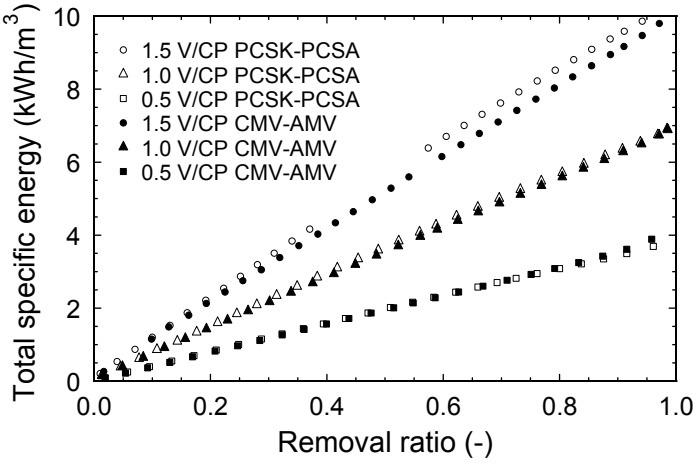

Figure 4.13 Effect of membrane type on specific energy

4.2.4 Hydraulic efficiency

Analysis of diluate mass change in the CMV-AMV stack with the synthetic Texas RO concentrate (not shown) revealed an electroosmotic flux of 9.1 mol/Eq transferred and an osmotic permeability of 0.70×10^{-10} kg·m/m^2·s·atm, which are slightly less than the respective values calculated in the Arizona/voltage experiments (see §4.1.4). Analysis of the diluate mass change in the PCSK-PCSA (shown in Figure 4.14) revealed an electroosmotic flux of 16.8 mol/Eq and an osmotic permeability of 2.1×10^{-10} kg·m/m^2·s·atm, which were significantly greater than the respective values calculated for the CMV-AMV stack. Thus, it is assumed that the greater ion exchange capacities of the AMV and CMV membranes (as compared to the PCSA and PCSK membranes) decrease the electroosmotic and osmotic fluxes. Considering electroosmotic and osmotic fluxes, the nominal recovery ratio of 50% in the PCSK-PCSA stack with synthetic Texas RO at 0.5 V/cell-pair was reduced to approximately 45% at a removal ratio of 98%.

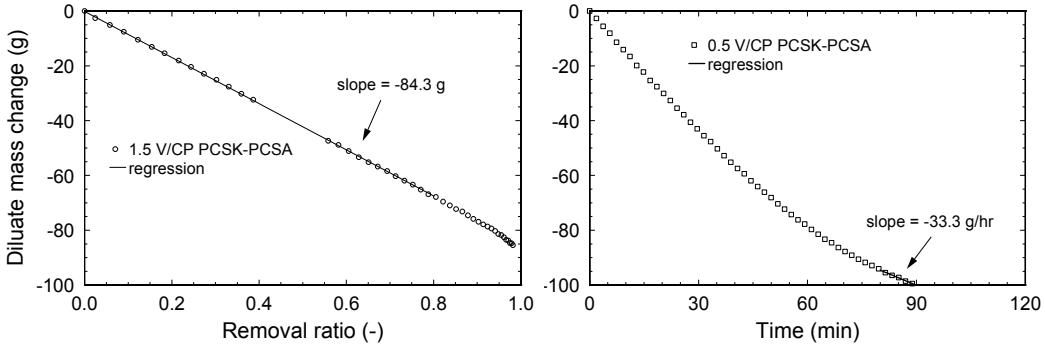

Figure 4.14 Rates of water flux by (a) electroosmosis at 1.5 V/cell-pair and (b) osmosis at 0.5 V/cell-pair

4.3 HYDRAULIC: EFFECTS OF SUPERFICIAL VELOCITY

4.3.1 Experimental conditions

Experiments were performed under similar conditions as those listed for the investigation of the effects of stack voltage, except that the stack voltage was 1.0 Volt/cell-pair for each experiment. Experiments were performed at three different superficial velocities (approximately 1.2, 2.4, and 4.8 cm/s), and the experimental solutions contained 5 mg/L of DQ2006 antiscalant. Synthetic Arizona RO concentrate was used as the initial concentrate and diluate solutions, and the initial solution volumes were each one liter, which corresponded to a nominal 50% single-stage electrodialysis recovery. The electrodialyzer was fitted with 11 CMV membranes and 10 AMV membranes to create ten cell-pairs.

4.3.2 Chemical efficiency

Bulk separation

While the applied voltage is the main process control of the rate of separation, the solution velocity controls the predominant rate limitation – the thickness of the diffusion boundary layer. Increasing the inter-membrane velocity increases the amount of mixing, which decreases the mass-transfer limitation at the membrane surfaces. This effect of superficial velocity on the technical efficiency of the separation is shown in Figure 4.15 and is consistent with Kabay *et al.* (2006b) . By quadrupling the superficial velocity from 1.2 to 4.8 cm/s, the rate of separation of the electrodialyzer was improved by approximately 30% for a removal ratio of 60%, and approximately 33% for a removal ratio of 80%.

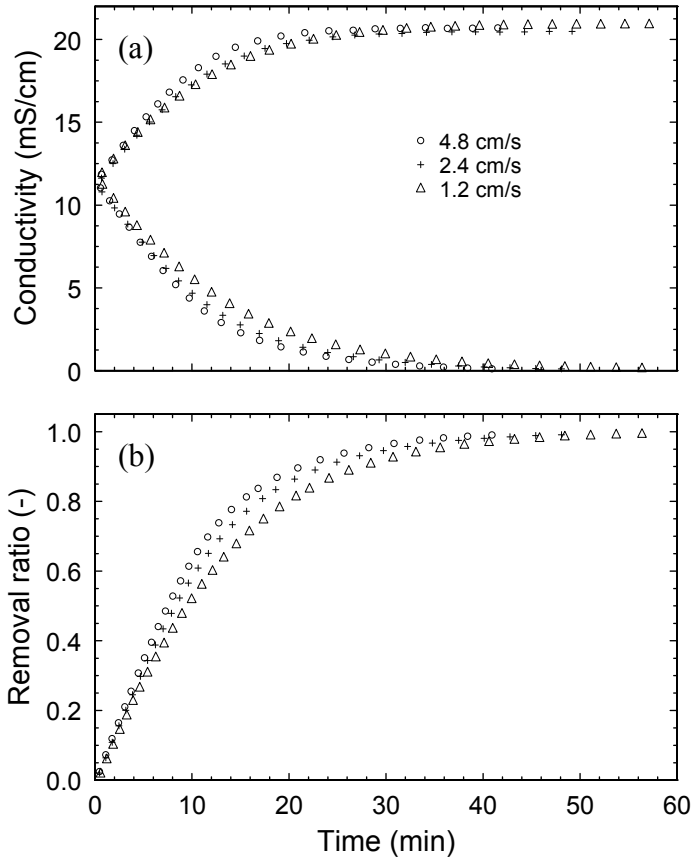

Figure 4.15 Effect of superficial velocity on separation efficiency

Note that in a full-scale system, the representative flow path length would be approximately proportional to the product of the abscissa value with the superficial velocity. A longer flow path requires a greater capital cost, and a higher velocity requires a greater hydraulic power (though hydraulic power is typically a small fraction of the total ED operating cost). Thus, for the conditions of this experimentation, these separation results indicate that the marginal improvement in the separate rate alone is not sufficient to justify the increase in capital and operating costs associated with the increase in superficial velocity. Therefore, the optimal superficial velocity (for a treatment system operating with similar conditions as these) is expected to be less than 1.2 cm/s.

Ionic separation

Not surprisingly, the dramatic variation in superficial velocity had little effect on the rate of separation of individual ions. The pH of each solution (not shown) was practically independent of variation in superficial velocity and was identical to the experiments with varying voltage in §4.1.2. Similarly, variation in superficial velocity had almost no effect on the removal of chloride and calcium, as shown in Figure 4.16.

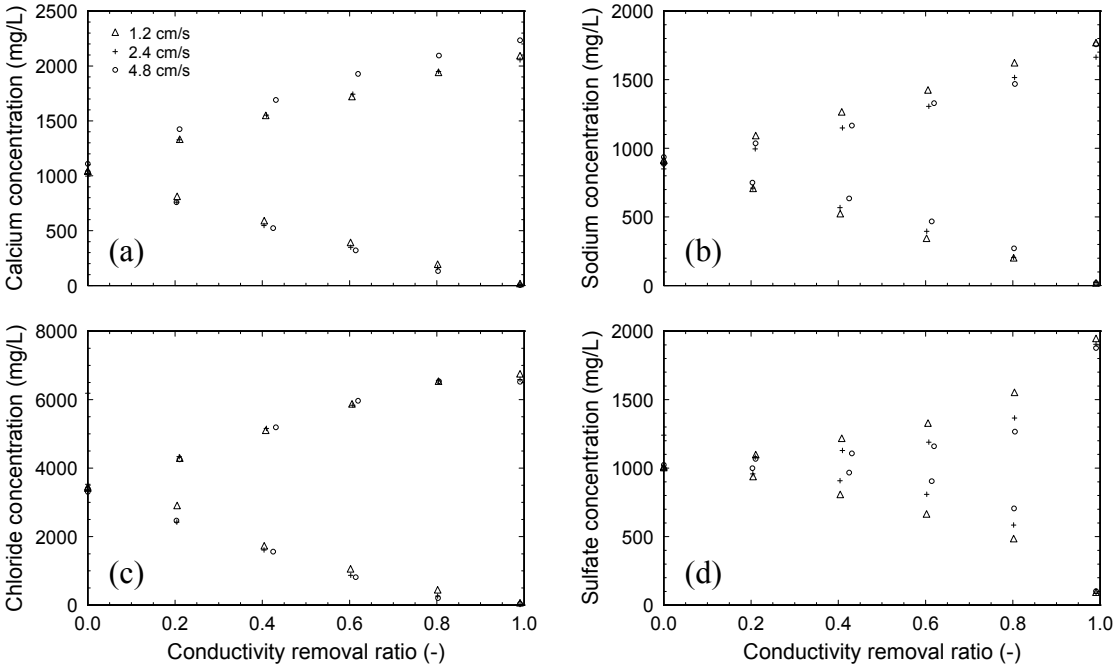

Figure 4.16 Effect of superficial velocity on removal of select ions

However, the separation of sulfate (and to some extent, sodium), showed a dramatic sensitivity to the variation in velocity in experiments with synthetic Arizona RO concentrate. The relative independence of the sulfate separation to applied voltage in these experiments was a consequence of solution composition, which is elucidated by comparing results from experiments with the synthetic Arizona RO concentrate in part (d) of Figure 4.3 and Figure 4.16 to results from experiments with the synthetic Texas

RO concentrate in part (d) of Figure 4.10. Analysis of the Arizona solution with Visual MINTEQ software revealed that free sulfate (SO_4^{2-}) only accounted for approximately 10% of the total anionic content, whereas in the Texas solution, free sulfate accounted for approximately 27% of the total anionic content.

4.3.3 Electrical efficiency

As the velocity increases, the thickness of the diffusion boundary layer decreases because of increased shear near the membrane surface. A thinner diffusion boundary layer results in a greater diluate concentration at the membrane surface and thus, a lower electrical resistance, which allows a higher current density, as shown in Figure 4.17.

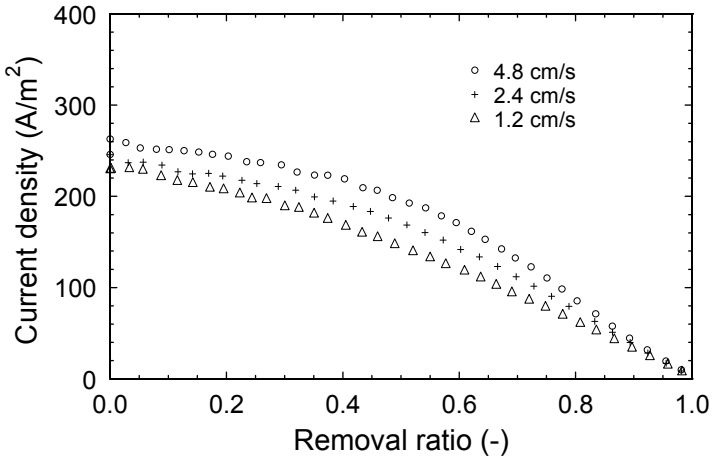

Figure 4.17 Effect of superficial velocity on current density

In spite of the increase in removal rate, the specific energy required to achieve a given removal ratio is practically independent of the velocity, as shown in Figure 4.18 and also by Kabay *et al.* (2006b) . Even in the case of the higher superficial velocity (4.8 cm/s), the hydraulic component only accounted for approximately 6% of the total specific energy.

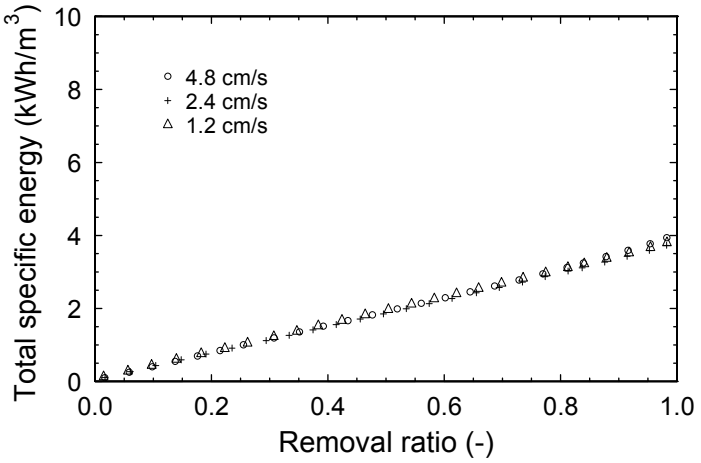

Figure 4.18 Effect of superficial velocity on specific energy

4.3.4 Hydraulic efficiency

As one might expect, the substantial variation in superficial velocity had very little effect on electroosmotic and osmotic fluxes, as shown in Figure 4.19. The very slight decrease in osmotic flux associated with thinner diffusion boundary layers is barely detectible in the experiment with the highest velocity.

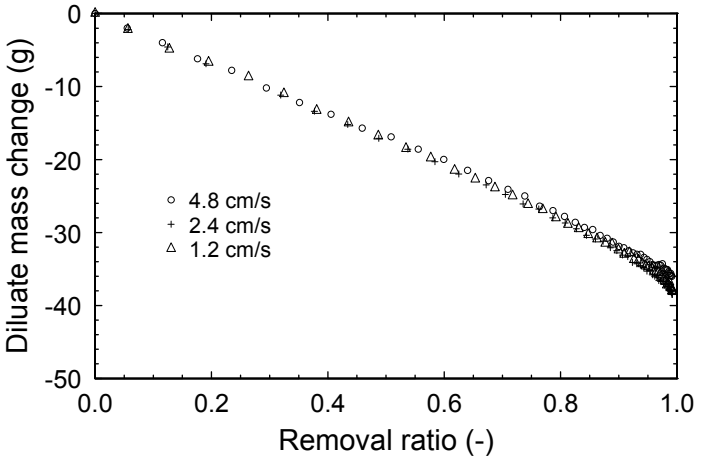

Figure 4.19 Effect of superficial velocity on mass transport

4.4 CHEMICAL: EFFECTS OF SOLUTION COMPOSITION

4.4.1 Experimental conditions

Experiments were performed on synthetic concentrates of various compositions to demonstrate the robustness of the electrodialysis system. Three experiments with synthetic Arizona concentrate and two experiments with the synthetic Florida concentrate were performed with a 1.0 Volt/cell-pair application on a 10 cell-pair CMV-AMV stack, and variations in solution composition are recorded in Table 4.2. The initial pH of the third Arizona experiment listed in Table 4.2 was raised by the addition of 0.1 M NaOH, which initiated precipitation at the beginning of the experiment. Precipitation continued throughout the experiment until the experiment was terminated at 95% removal due to elevated concentrate head loss. The concentration of the ED concentrate of the second Florida experiment listed in Table 4.2 was ten times the concentration of the Florida raw, which simulated a single-stage ED recovery of 70% (accomplished in full-scale systems by concentrate recycle).

Table 4.2 Variations in ED solution composition

RO cntrt. -	Concentrate Initial pH	Antiscalant Type	Antiscalant Conc. (mg/L)	ED Dilt. CF	ED cntrt. CF	ED Recovery
AZ	8.0	DQ 2006	5.0	5	5	50%
AZ	8.0	DQ 2066	5.0	5	5	50%
AZ	8.4	DQ 2006	5.0	5	5	50%
FL	7.7	DQ 2006	6.7	5	5	50%
FL	7.5	DQ 2066	8.8	5	10	70%

4.4.2 Chemical efficiency

The separation efficiencies of the five experiments listed above are shown in Figure 4.20, and several observations can be made. First, no significant difference was

observed between the removal rates of the two Arizona experiments started at pH 8 containing different antiscalants. Second, the rate of removal of the third Arizona concentrate was only 25% less than the two concentrates that did not precipitate. Third, the rate of separation of conductivity in the Florida concentrates was greater than that of the Arizona concentrates, though the relative rate of removal of the Florida concentrates was less than that of the Arizona. Fourth, the rate of removal of the second Florida concentrate was only slightly less than that of the first, in spite of the significant difference in concentrate concentration. These results demonstrate that the antiscalants are capable of preventing precipitation in the presence of the ED concentration polarization and that, in operations of higher recovery, the increase in voltage loss by concentration polarization is tempered by the decrease in voltage loss by electrical resistance in the concentrate.

Analysis of pH and concentrations of specific ions (not shown) revealed the same results shown previously. None of the individual ionic concentrations showed sensitivity to antiscalant type.

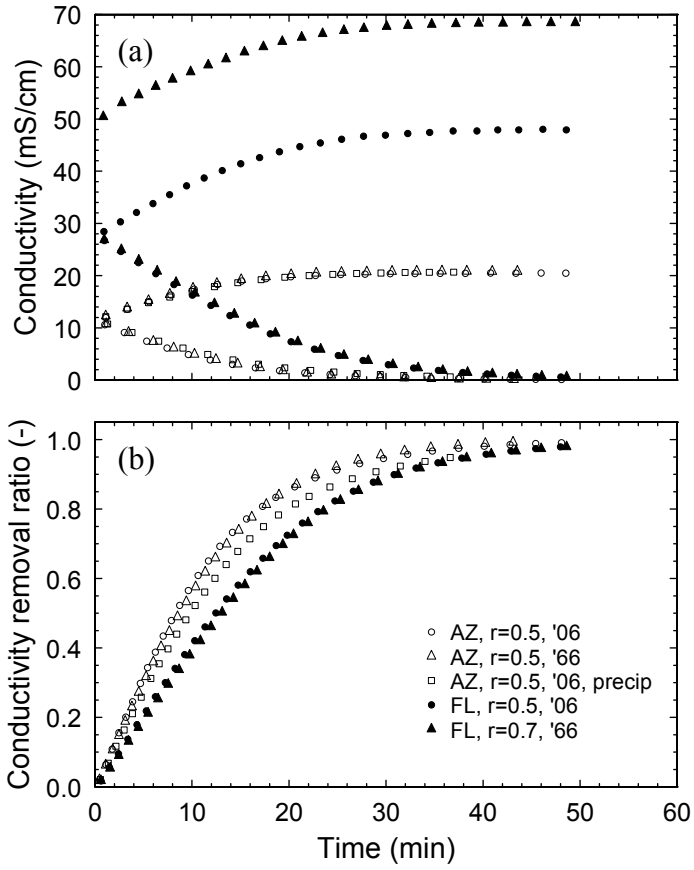

Figure 4.20 Effect of solution composition on separation efficiency

4.4.3 Electrical efficiency

The current density was greater in the treatment of the Florida concentrates than the Arizona concentrates, as shown in Figure 4.21. Due to the higher ionic content of the Florida concentrate, the lower electrical resistance of the ED concentrate and diluate cells in the Florida experiments allowed a higher current density for the same voltage application. However, higher current densities create a larger potential loss by membrane resistance and concentration polarization.

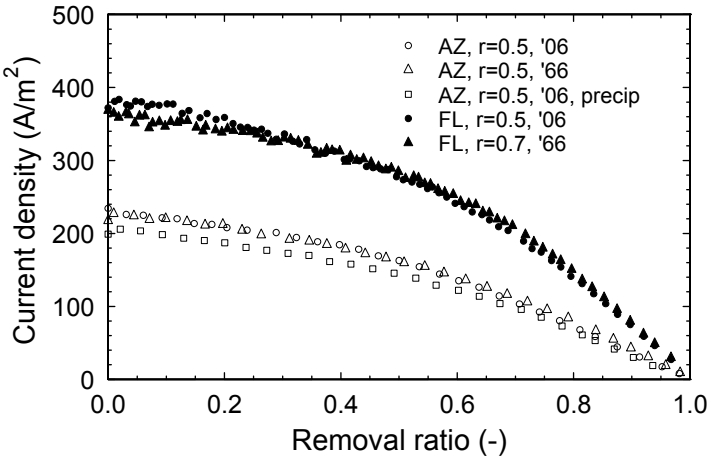

Figure 4.21 Effect of solution composition on current density

Consistent with previous experimentation, the specific energy consumption was proportional to the concentration of ions separated, as shown in Figure 4.22. The ratio of the ionic concentration (*e.g.*, equivalents per cubic meter) of Florida to Arizona concentrates is approximately 2.3, and the ratio of the slopes of the specific energy lines in Figure 4.22 is approximately 2.3.

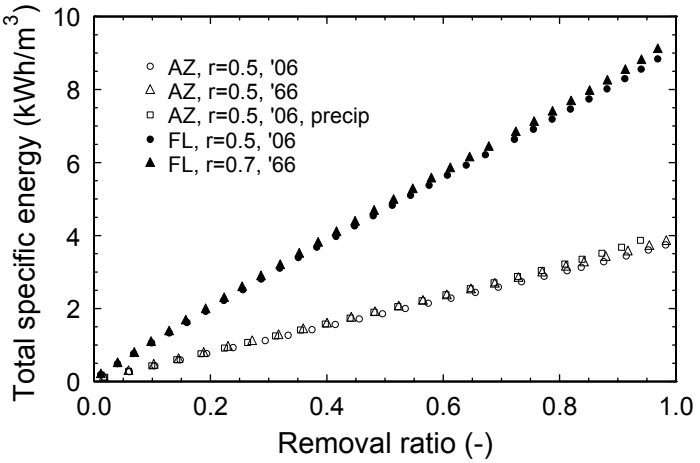

Figure 4.22 Effect of solution composition on specific energy

4.4.4 Hydraulic efficiency

In spite of the variations in antiscalant, concentrate concentration, and even active precipitation in the concentrate, the transport of water by electroosmosis was proportional to the transport of ionic content, as shown in Figure 4.23. Again, the transport of water by osmosis was proportional to the difference in concentration across the membranes.

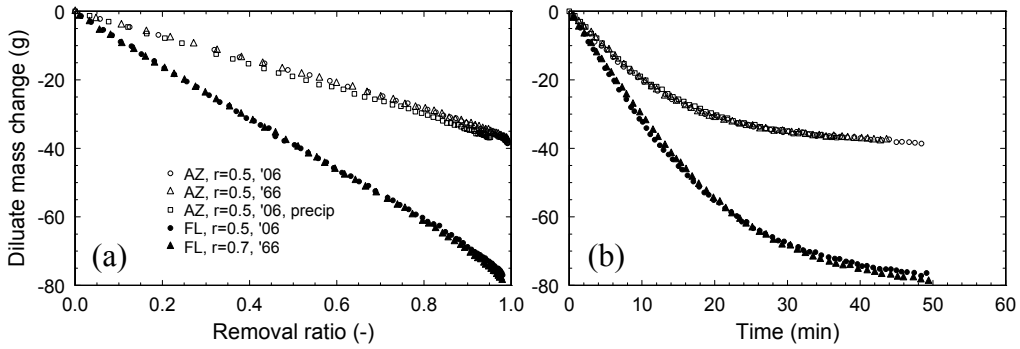

Figure 4.23 Effect of solution composition on mass transport by (a) removal ratio and (b) time

4.5 CHEMICAL: EFFECTS OF CONCENTRATE CONCENTRATION

4.5.1 Experimental conditions

In order to investigate the possibility to concentrate supersaturated RO concentrate with several successive stages of ED, successive batch recycle experiments were performed whereby the final ED concentrate from one experiment would be used as the initial concentrate and/or diluate solution for another experiment. These experiments were conducted with synthetic Texas RO concentrate as the initial solution, a 9 cell-pair stack of 10 PCSK and 9 PCSA membranes, an applied voltage of 1.5 Volts/cell-pair, an antiscalant dose of 12 mg/L of ATMP, and a superficial velocity of 4.8 cm/s. Each experiment (with initial and final conditions recorded in Table 4.3) was performed with

an initial concentrate and diluate volume of one liter, which simulated a nominal single-stage ED recovery of 50%. The actual single-stage recovery of each experiment was computed and used to determine the simulated overall system recovery. During the fourth experiment listed, visible precipitation began to occur in the concentrate stream near a removal ratio of approximately 40%, and the experiment was terminated due to elevated pressure in the concentrate stream.

Table 4.3 Variations in experimental ED solution concentrations and representative system recoveries

Initial Diluate Factor (-)	Initial Concentrate Factor (-)	Final Removal Ratio (-)	Final Concentrate Factor (-)	Final Concentrate Concentration (g/L)	Simulated System Recovery (-)
4.0	4.0	98%	7.4	27.2	86%
4.0	7.4	98%	10.5	38.8	90%
7.4	7.4	98%	13.0	48.2	92%
10.5	13.0	50%	16.6	61.4	94%

4.5.2 Chemical efficiency

Separation of conductivity for each experiment is shown in Figure 4.24. The rates of separation of the two experiments with initial diluate solutions of Texas RO concentrate were nearly identical, and the initial rate of conductivity removal was approximately the same for all experiments for removal ratios less than approximately 40%. These similar rates indicate that the rate limitation was not associated with the solution composition. Also, with respect to the concentration of concentrate, the nonlinearity of the conductivity with concentration is noticeable, as the concentration magnification of 3.25 (*i.e.*, from a concentration factor of 4.0 to 13.0) corresponded to a conductivity magnification of 2.8 (from 19.3 to 54.5 mS/cm).

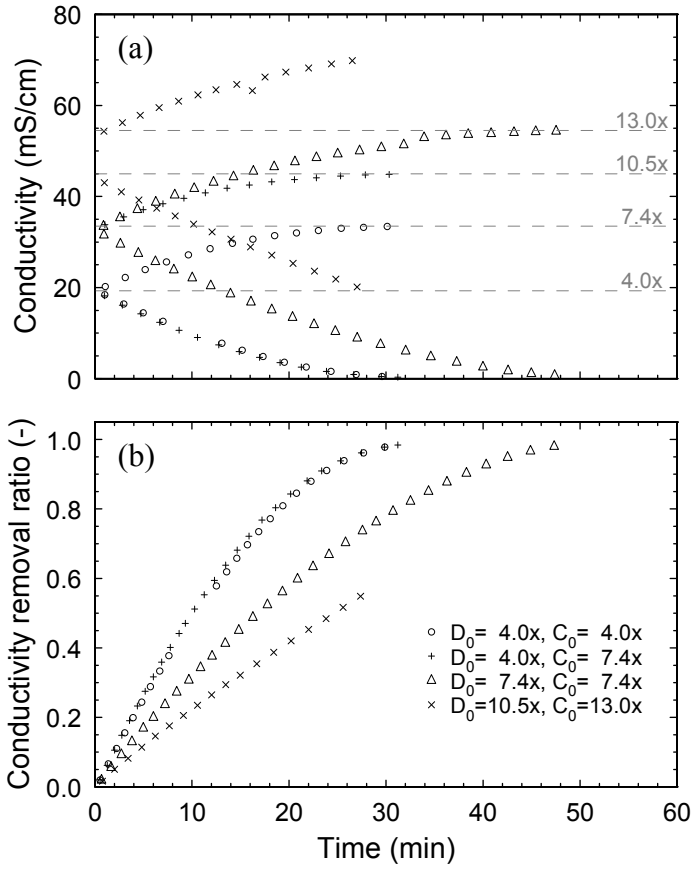

Figure 4.24 Effect of concentration on separation efficiency

The concentrations of individual components tracked the bulk concentration, as shown in Figure 4.25. Again, boron and silica concentrations were not separated, and the pH behaved similarly to previous experimentation. The curvature of the sulfate removal with conductivity removal became more pronounced with increasing concentration, as a larger fraction of sulfate was associated with divalent cations in the form of neutral ion pairs.

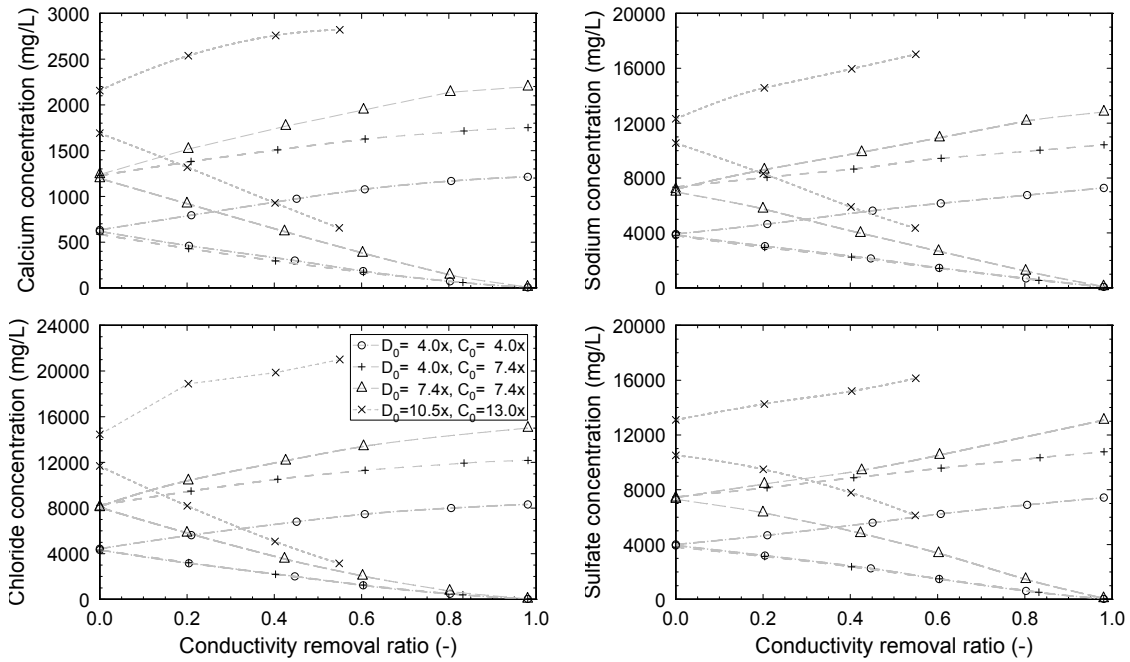

Figure 4.25 Effect of concentration on removal of select ions

Analysis of the final ED concentrate of the third experiment (concentration factor of 13) with Visual MINTEQ (ver. 3.0) revealed an actual ionic strength of approximately 0.66 mol/L (with a stoichiometric ionic strength of approximately 0.98 mol/L). Saturation ratios of most salts were magnified significantly, though not proportionally with the magnification in concentration factor (*i.e.*, from 4.0 to 13.0, a magnification of 3.25) because of decreasing activity coefficients with increasing ionic strength. The saturation ratios of the predominant sparingly soluble salts in the ED concentrate are shown in comparison to those of the RO concentrate, in Figure 4.26. The saturation ratios of calcite ($CaCO_3$) and dolomite ($CaMg(CO_3)_2$, ordered) were the greatest, followed by strontionite ($SrCO_3$) and magnesite ($MgCO_3$), indicating an opportunity for further concentrate treatment by precipitative softening via pH elevation.

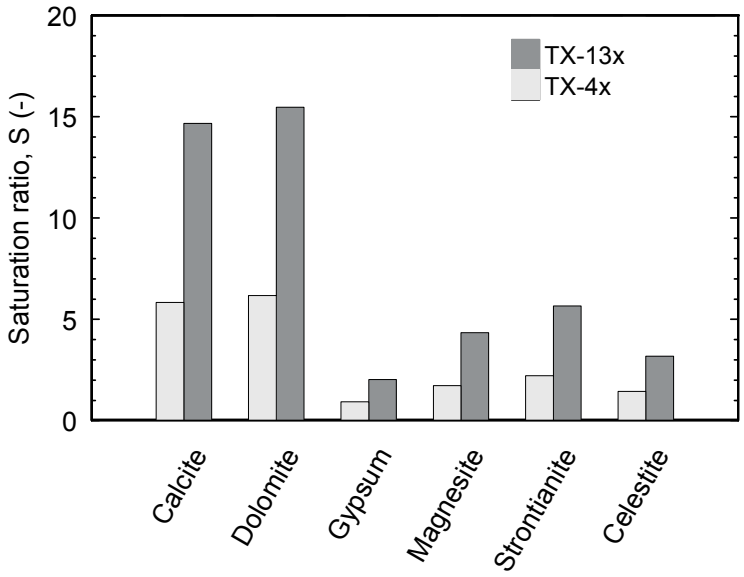

Figure 4.26 Comparison of saturation ratios for select salts in the Texas RO concentrate at concentration factors of 4.0 and 13.0

4.5.3 Electrical efficiency

Consistent with the similar rates of conductivity separation in Figure 4.24(a) and the experimental results of Banasiak *et al.* (2007), the current density through the stack was only slightly sensitive to the solution concentrations, and mainly for removal ratios less than 15%, as shown in Figure 4.27. Thus, it is assumed that the electrical resistance of the solutions was small compared to the electrical resistance of the membranes, which provided the predominant voltage loss in the stack. Thus, in the design of ED systems treating solutions of higher electrical conductivity (*e.g.*, greater than 10 mS/cm), the electrical resistance of the membranes should be heavily considered in performance optimization.

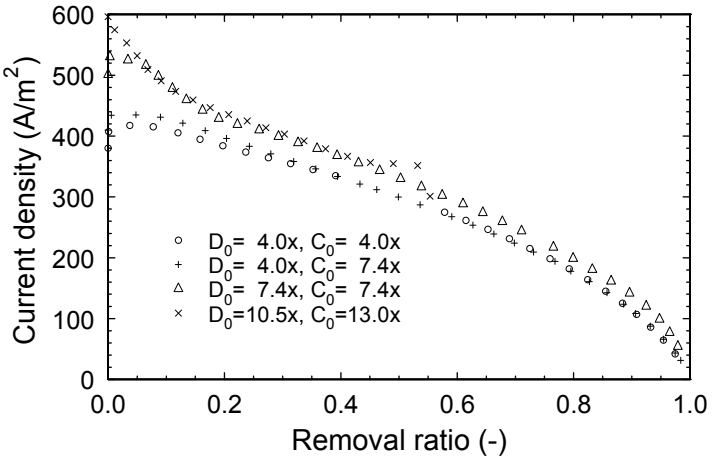

Figure 4.27 Effect of concentration on current density

Again, the specific energy consumption was proportional to the concentration of ionic content removed from the diluate, as shown in Figure 4.28. Recognizing that the specific energy is correlated with the financial cost of an ED system, it is important to note that, at some point, the energy required to concentrate a solution by ED would be greater than the energy required by a thermal process (which is practically insensitive to salinities in this range). Consideration of specific energy also provides another compelling argument for the use of low-resistance ED membranes in the treatment of solutions of higher salinities. Of course, a lower specific energy can also be achieved by operating at a lower voltage application.

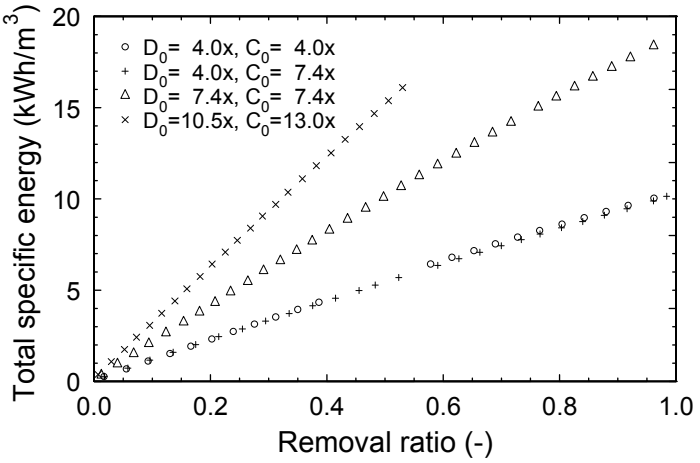

Figure 4.28 Effect of concentration on specific energy

4.5.4 Hydraulic efficiency

As expected, the transport of water by electroosmosis also increased with increasing salinity, as shown in Figure 4.29. In the third experiment shown (D_0 = 7.4x, C_0 = 7.4x), approximately 12% of the influent diluate water was transported to the concentrate by electroosmosis and osmosis, reducing the recovery from a nominal 50% to an actual 44%. Though perhaps not as apparent as the specific energy limitation, an inherent tradeoff exists in the recovery gained by ED treatment and the recovery lost by electroosmosis, and this effect is exacerbated in solutions of higher ionic strength. Admittedly, full scale ED systems are frequently designed to operate at significantly higher single-stage recovery ratios (*e.g.*, up to 70%) than those tested here.

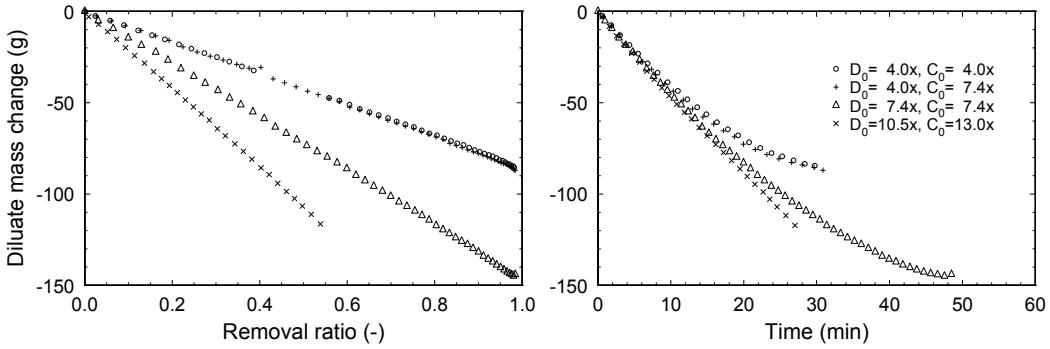

Figure 4.29 Effect of concentration on mass transport by (a) removal ratio and (b) time

4.6 SUMMARY AND DISCUSSION

Experiments with a laboratory-scale batch-recycle electrodialysis (ED) system were performed under a range of electrical, hydraulic, and chemical conditions. These experiments demonstrated that ED can be used effectively to treat reverse osmosis (RO) concentrate waste in order to further concentrate, and thereby, decrease the volume of costly disposal. The principal observations of electrical, hydraulic, and chemical behaviors are summarized here.

A very high degree of ionic separation can be achieved, even with the application of a very low stack voltage; removal ratios greater than 99% were realized with the application of 0.5 Volts/cell-pair. The rate of separation, however, is approximately proportional to applied voltage, since the ED stack behaves essentially ohmically. The charge efficiency is relatively high and stable (*i.e.*, approximately 90% or more of the electrical current is effectively utilized for separating ions, and this charge efficiency is stable up to removal ratios greater than 90%.) Also, the specific energy investment of electrodialysis is approximately proportional to the applied stack voltage.

An increase in superficial velocity can improve the performance of electrodialysis by minimizing the thickness of the process-limiting diffusion boundary layer, but this effect has diminishing returns. At lower voltage applications (*e.g.*, 0.5 V/cell-pair), the effects of concentration polarization are relatively small, so thinner diffusion boundaries do not significantly improve the performance of the system. However, at a higher voltage application (*e.g.*, 1.5 V/cell-pair), the concentration polarization is more significant, so the effect of the inter-membrane velocity is more significant. Even at the higher velocities tested in this experimentation, the hydraulic pumping power was a small contribution to (*e.g.*, less than 10% of) the total specific energy of the treatment process. Also, with respect to hydraulic losses, the electroosmotic water losses are proportional to the ionic concentration transferred, and the osmotic losses are more significant at very low voltage applications and very high removal ratios.

The specific energy requirement is approximately proportional to the ionic concentration separated since the charge efficiency is relatively high and stable. Analysis of the specific energy data in this experimentation revealed a consistent requirement of approximately 30 kWh/m^3 per Eq/L separated per Volt/cell-pair applied. Almost all ionic components are separated nearly proportionally to conductivity, with the exception of components with a large fraction complexed in the form of neutral species (*e.g.*, sulfate and sometimes carbonate). Neutral species such as boric and silicic acid are not propelled by the ED electric field and therefore are not separated under near-neutral pH conditions. The type (various phosphonic acids) and concentration of antiscalant used in this research did not noticeably influence the performance of ED. Successive stages of

ED treatment can be used effectively to further magnify the concentration of the RO concentrate to achieve recovery ratios greater than 90%. The potential for fouling and scaling of the ED system is assumed to be small since the typical reversal period in full-scale EDR systems is shorter than the duration of the batch-recycle experimentation performed here (*e.g.*, 20-30 minutes compared to 45-90 minutes, respectively). The high degree of supersaturation of carbonate salts suggests that further treatment of the ED concentrate could be accomplished by precipitative softening, yielding even higher system recoveries.

Chapter 5 – Modeling Methodology

Mathematical modeling of the experimental system was employed to more fully appreciate the interaction of the hydraulic, electrical, and chemical phenomena within electrodialysis. This modeling allowed the validation of understanding of the predominant controlling mechanisms by comparison to experimental results.

Two models were created; the first model simulated the steady-state plug-flow performance of an electrodialyzer, and the second model simulated the performance of the electrodialyzer within the batch-recycle system. That is, the first model simulated the hydraulic, electrical, and chemical characteristics as a function of flow path distance within the electrodialyzer, and the second model incorporated the results of the first model at a given "instant" to simulate the hydraulic, electrical, and chemical characteristics of the batch-recycle system as a function of time. Based on these performance results, a simple economic cost-benefit model was developed to simulate the cost of disposal of several typical concentrate disposals, as well as the capital and operating costs of an ED system.

5.1 Steady-state plug-flow electrodialyzer model: overview

The plug-flow ED model is a simplified steady-state simulation that is one-dimensional with respect to hydraulic and electrical characteristics (*i.e.*, the flow rate and current density only vary along the direction of bulk-fluid flow, the *y*-dimension), and two-dimensional with respect to chemical characteristics (*i.e.*, concentration profiles vary in the direction of flow, as well as perpendicular to the membranes – the *y*- and *x*-dimensions, respectively), as shown in Figure 5.1. Based on the model inputs of

electrodialyzer characterization, solution composition, flow rates, and stack voltage application, a series of subsequent chemical, hydraulic, and electrical calculations are made.

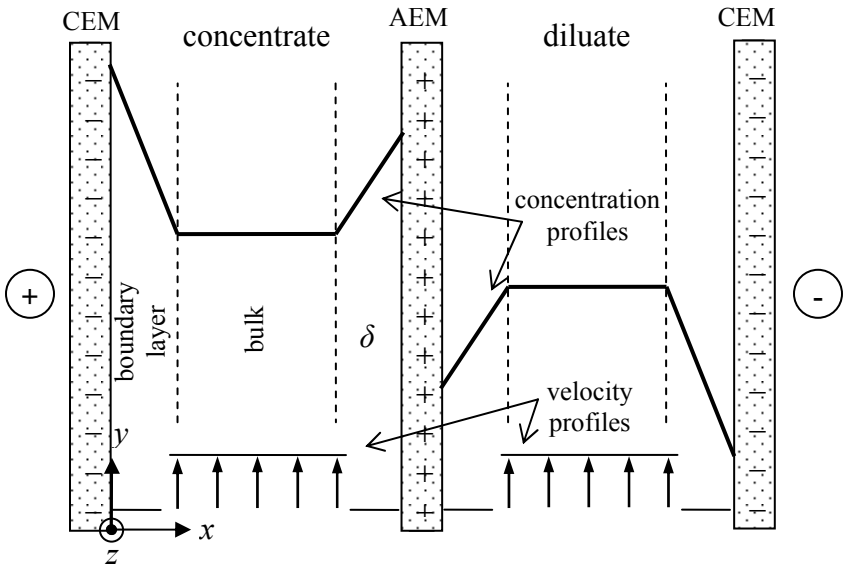

Figure 5.1 Model domain and simplified inter-membrane velocity and concentration profiles for a single cell-pair

In this model, the electrodialyzer is essentially assumed to be an ohmic device, while also accounting for several non-ohmic phenomena. At each discrete point along the flow path (in the *y*-dimension), the solution of the steady-state current density (at that point) is approached by iterative convergence as a function of the total restistive voltage loss of the stack and the total electrical resistance of the stack. The current density and concentration profiles are interdependent, that is, the concentration profile in the *x*-dimension is a function of the current density at that *y*-value, and the current density is a function of the concentration profile at that point. The bulk channel is assumed to be ideally plug-flow, so the bulk concentration at the next discreet point downstream is

calculated by mass-balance from the adjacent upstream conditions. An algorithmic summary of the model is as follows:

1. Initialize model variables.
2. Calculate solution properties based on chemical composition.
3. Guess a current density based on doubled bulk resistances.
4. Calculate transport numbers based on bulk concentrations and diffusivities.
5. Calculate the concentration gradients using the Nernst-Planck equation.
6. Calculate the concentration of each species at the membrane surface based on concentration gradient. (If necessary, adjust membrane transport number of individual species in the event of overlimiting current.)
7. Calculate liquid junction potentials, diffusion potentials, and total available resistive voltage loss.
8. Calculate the total resistance of the stack and an updated current density.
9. Iterate steps 3-9 until the current density converges.
10. Calculate the effective separation flux of each ion based on membrane transport numbers.
11. Calculate electro-osmosis and osmosis transport of water
12. Calculate new flow rates and concentrations
13. Advance to the next grid point in space

This steady-state plug-flow electrodialyzer model is a significant improvement over the less precise model presented by Lee *et al* (2002); the model developed here incorporates the following generalizations of simplifications (assumptions and approximations) made

by Lee *et al* (2002) that are (or can be) significant in the application to the treatment of RO concentrate waste:

Hydraulic:

- Concentrate and diluate cells are allowed to have different geometries and flow conditions instead of being identical.
- The diffusion boundary layer thickness is modeled as a simple function of solution velocity instead of being neglected entirely.
- Water transport through the membranes by electroosmosis is incorporated instead of being neglected.

Chemical:

- The electrical conductivity of the solution is a non-linear function of the multicomponent speciation instead of being a linear function of a single salt.
- Activity coefficients are modeled as a function of the multicomponent solution composition instead of approximated as unity.

Electrical:

- The liquid-junction potentials due to different concentrations in the diluate and concentrate cells are incorporated into the electrical calculations instead of assumed to be negligible.
- Changes in the ohmic resistance of the solutions in the boundary layer are incorporated into the electrical calculations.
- The membrane thickness is included in electrical calculations instead of being neglected.

5.2 STEADY-STATE PLUG-FLOW ELECTRODIALYZER MODEL: HYDRAULIC MODELING

5.2.1 Diffusion boundary layer thickness

In a parallel research project (Kim, 2010; Kim *et al.*, 2010) with the same electrodialysis system used here, the mean diffusion boundary layer thickness (δ) was determined to be a function of superficial velocity (v) through laboratory observation and extensive statistical modeling of transport numbers of cations used in this research. That study revealed a diffusion boundary layer thickness of approximately 40, 20, and 10 mm for superficial velocities of 1, 2, and 4 cm/s. A simplified empirical relationship between the diffusion boundary layer thickness and superficial velocity (assumed to be applicable for superficial velocities in the range of 1-5 cm/s) was developed for use in the current research model, as shown in the following expression:

$$\delta = \frac{(40\,\text{cm/s})}{v}\,\mu\text{m} \tag{5.1}$$

5.2.2 Solution density of multicomponent solutions of high ionic strength

For precise calculation of the conservation of mass (*i.e.*, in considering the transport of water, in addition to the transport of ions), it was necessary to develop an expression relating the mass- and volume-based concentrations. For 11 binary aqueous solutions ($BaCl_2$, $CaCl_2$, KCl, $MgCl_2$, NaCl, $SrCl_2$, $MgSO_4$, $NaNO_3$, KNO_3, KBr, and K_2CO_3), regression of the solution density and mass-fraction (up to mass fractions of 10%) revealed that the density of the solution (ρ) could be modeled as a function of the root-charge weighted solute-mass fraction (w′):

$$\rho = (0.7153w' + 0.9970)\frac{\text{g}}{\text{cm}^3} \tag{5.2}$$

which is accurate within 1% at a mass fraction of 10% and proportionally less for lower mass fractions. The root-charge weighted mass-fraction is given by:

$$w' = \frac{\sum_i \left(c_i \, MM_i \sqrt{|z_i|} \right)}{\rho} \tag{5.3}$$

where c is the molar concentration and MM is the molar mass. Substitution of Eq. 5.3 into Eq. 5.2 results in a quadratic expression with the following solution:

$$\rho = \frac{1}{2}\left(B + \sqrt{B^2 + 4AC} \right) \tag{5.4}$$

where A = 0.7153 g/cm^3, B = 0.9970 g/cm^3 (*i.e.*, the density of pure water at 25°C), and $C = \sum_i \left(c_i \, MM_i \sqrt{|z_i|} \right)$.

5.2.3 Electroosmosis

The flux of water through the membranes by electroosmosis was approximated as an aggregation of the waters of solvation transported with ionic species through the membranes. The electroosmosis numbers used in this model were taken from hydration numbers reported by Bockris and Reddy (1998) and Wright (2007) and are recorded in Table 5.1. For the sake of model simplicity, all of the carbonate system was modeled only as $HCO3^-$.

Table 5.1 Model values of ionic solvation numbers

Ion	Solvation	Ion	Solvation
Ba^{2+}	9	Br^-	4
Ca^{2+}	12.2	Cl^-	4
K^+	3	HCO_3^-	6
Mg^{2+}	14	NO_3^-	6
Na^+	5	SO_4^{2-}	6
Sr^{2+}	10.8	-	-

5.2.4 Osmosis

The molar flux of water through the membranes by osmosis ($J_{osmosis}$) was calculated according to the following expression:

$$J_{osmosis} = \frac{P_{mem}\,\Delta\Pi_{avg}}{h_{mem}} \tag{5.5}$$

where P_{mem} is the permeability of the membrane, h_{mem} is the thickness of the membrane (in the same direction as the flux), and $\Delta\Pi_{avg}$ is the average trans-membrane osmotic pressure difference over the discrete grid area. The computation of osmotic pressure is given in Eq. 4.1.

5.2.5 Conservation of mass

At each grid point from the inlet to the outlet of the electrodialyzer, accounting for transport of water and components was performed on a total mass basis (rather than a concentration basis) so that conservation of mass of each component was precisely maintained. At the n^{th} grid point, after the concentration profiles and current density solutions converged, the conservation equation was used to compute the effluent flow from the grid. For example, the flow of water leaving a diluate grid (*i.e.*, the flow of

water entering the adjacent downstream diluate grid, n+1) was computed according to the following:

$$N_{w,n+1} = N_{w,n} - J_{electroosmosis}\, w\, \Delta y \tag{5.6}$$

where $N_{w,n+1}$ is the molar flow rate of water entering the downstream diluate grid, $N_{w,n}$ is the molar flow rate entering the grid, w is the width of the grid in the z-dimension, and Δy is the length of the grid along the flow path. Of course, the n^{th} concentrate grid accumulates the water lost by the n^{th} diluate grid.

5.3 STEADY-STATE PLUG-FLOW ELECTRODIALYZER MODEL: CHEMICAL MODELING

5.3.1 Activity coefficients

Based on the comparison of the Debye-Hückel and Davies models to observed mean activity coefficients shown in Figure 2.9, the Debye-Hückel model is shown to have the advantage of distinguishing the behavior of ions of the same charge based on size, and for some salts. In fact, it is accurate within 10% up to ionic strengths near 0.5 M, even though the reported applicability is less than 0.1 M (Stumm and Morgan, 1995). The Debye-Hückel model better predicts the activity coefficients of carbonate and sulfate salts than the Davies model at higher ionic strengths. Thus, activity coefficients (γ_i) were calculated with the Debye-Hückel expression (Stumm and Morgan, 1995):

$$\gamma_i = \log^{-1}\left(- A \frac{z_i^{\,2} \sqrt{I}}{1 + B\mathring{a}_i \sqrt{I}} \right) \tag{5.7}$$

where A and B are constants (the values of which are given in §2.7.2), z_i is the charge of species i, I is the ionic strength of the solution, and $\mathring{a}_i$ is an empirical ion-specific size parameter (listed in Table 2.4).

While a more sophisticated model (such as the modified Debye-Hückel, SIT, or Pitzer) could have been used, the activity coefficient model only affects the calculation of the liquid-junction potentials, which generally account for a small fraction of the total voltage loss. Thus, the choice of activity model is not expected to significantly influence the performance of the model.

5.3.2 Electrical conductivity of multicomponent solutions

Within this mathematical model, it was necessary to calculate the electrical conductivity of multicomponent solutions as a function of composition. Considering the insufficiency of the binary and low ionic strength models listed in §2.7.2, a novel expression was required. Review of the more rigorous binary conductivity models (Horvath, 1985) revealed a common inclusion of the Debye-Hückel term in the form:

$$\frac{\Lambda}{\Lambda_0} = 1 - \frac{A z_i^2 \sqrt{I}}{1 + B \mathring{a}_i \sqrt{I}} \tag{5.8}$$

Recalling the Taylor Series approximation of the exponential function for small arguments,

$$e^{-x} \approx 1 - x \tag{5.9}$$

Eq. 5.7 was generalized to produce:

$$\lambda_i = \lambda_0 \log^{-1}\left(\frac{-0.32 z_i^{\,2} \sqrt{I}}{1 + B \mathring{a}_i \sqrt{I}}\right) \tag{5.10}$$

where λ_i is the ionic equivalent conductivity of species *i* within the solution, λ_0 is the ionic equivalent conductivity at infinite dilution (shown in Table 5.2), and the coefficient in the numerator (0.32) was determined empirically to fit the experimental BWRO

concentrates. This expression accurately predicts (within 1%) the conductivities of all of the experimental solutions in this research, up to 65-70 mS/cm.

Table 5.2 Ionic diffusivity and conductivity at infinite dilution (CRC, 2005a)

Ion	Ionic Diffusivity D_0 (10^{-5} cm^2 s^{-1})	Ionic Conductivity λ_0 (10^{-4} m^2 S Eq^{-1})
Ba^{2+}	0.847	63.6
Ca^{2+}	0.792	59.5
K^{+}	1.957	73.5
Mg^{2+}	0.706	53.0
Na^{+}	1.334	50.1
Sr^{2+}	0.791	59.4
Br^{-}	2.080	78.1
Cl^{-}	2.032	76.3
HCO_3^{-}	1.185	44.5
NO_3^{-}	1.902	71.5
SO_4^{2-}	1.065	80.0

With the equivalent ionic conductivities defined above, the conductivity of the multicomponent solution can be calculated by:

$$\kappa = \sum_i \lambda_i \, c_i \, |z_i| \tag{5.11}$$

where the variables are the same as defined above.

5.3.3 Transport numbers in the bulk

Since the bulk was assumed to be well-mixed and absent of concentration gradients, the transport number of each species (t_i) can be calculated as its contribution to the total conductivity (κ) of the solution:

$$t_i = \frac{\lambda_i c_i |z_i|}{\kappa} \tag{5.12}$$

5.3.4 Transport numbers in the membrane

Considering the generally high current densities in ED treatment of BWRO concentrate waste, it was assumed that the membrane transport numbers are proportional to the membrane permselectivity and the aqueous phase transport numbers at the interface of the membrane and the diffusion boundary layer. It was also assumed that the steady-state flux of a particular species through the membrane could be limited by the diffusion boundary layers. Thus, for each grid point, the value of the membrane transport number of each ion was initialized based on the aqueous concentrations at the membrane surface and then corrected (iteratively) in the event of limiting current.

5.3.5 Chemical flux

The transport of a particular ion (in the *x*-dimension) within the electrodialyzer was approximated by the Nernst-Planck Equation:

$$J_i = -D_i \frac{dc_i}{dx} - \frac{\lambda_i c_i}{F} \frac{d\phi}{dx} \tag{5.13}$$

where J is the molar flux of species i, D is the ionic diffusivity, c is the molar concentration of species i, F is the Faraday constant (which is the product of Avogadro's number, N_A, and the elementary charge, q_e), R_g is the molar gas constant, T is the solution temperature, z is the sign and magnitude of the charge of the ion, ϕ is the electric potential, and v is the bulk solution velocity (Bard and Faulkner, 2001). The summation of fluxes of charges yields the current density for the n^{th} grid point:

$$i_n = F \sum_i z_i J_{i,n} \tag{5.14}$$

Within the bulk regions, it is assumed that sufficient mixing eliminates any concentration gradients, which simplifies the flux expression,

$$J_{i,bulk} = -\frac{\lambda_i c_i}{F}\frac{d\phi}{dx} \tag{5.15}$$

where the gradient in electric potential is simply due to the electrical resistance of the solution:

$$\nabla\phi_{bulk} = -\frac{i}{\kappa} \tag{5.16}$$

Steady-state conservation of charge requires that the current density be constant in the *x*-dimension. By assuming that the concentration gradient of each ion is constant throughout the boundary layer, the concentration gradient can be calculated by:

$$\frac{dc_i}{dx} = -\frac{1}{D_i}\left(J_{i,bulk} + \frac{\lambda_i c_i}{F}\frac{d\phi}{dx}\right) \tag{5.17}$$

where the gradient in potential within the diffusion boundary layers is the summation of the resistive and diffusion potential gradients:

$$\nabla\phi_{DBL} = -\frac{i}{\kappa} + \nabla\phi_{diff} \tag{5.18}$$

By assuming that the diffusion boundary layer thickness is controlled by the hydrodynamic conditions according to Eq. 5.1, the concentration of each ion at the membrane surface can be calculated by:

$$c_{i,DBL-mem} = c_{i,bulk} + \frac{dc_i}{dx}\delta \tag{5.19}$$

Within the diluate diffusion boundary layers, the concentration gradient is such that the concentration decreases from the bulk to the membrane surface. Conversely, in the

concentrate diffusion boundary layers, the concentration gradient is such that the concentration increases from the bulk to the membrane surface, as drawn in Figure 5.1.

5.3.6 Conservation of mass

At the n^{th} grid point, after the concentration profiles and current density solutions converged, the conservation equation was used to compute the advective effluent from the grid. For example, the flow of species *i* leaving a diluate grid (*i.e.*, the flow of species *i* entering the adjacent downstream diluate grid, *n*+1) was calculated by:

$$N_{i,n+1} = N_{i,n} - J_{i,n}\, w\, \Delta y \tag{5.20}$$

where $N_{i,n+1}$ is the molar flow rate of species *i* entering the downstream diluate grid, $N_{i,n}$ is the molar flow rate entering the grid, *w* is the width of the grid in the *z*-dimension, and Δy is the length of the grid along the flow path. Of course, the n^{th} concentrate grid accumulates the mass of species *i* lost by the n^{th} diluate grid.

5.4 STEADY-STATE PLUG-FLOW ELECTRODIALYZER MODEL: ELECTRICAL MODELING

Considering the electrodialyzer as an electrically resistive device ("black box"), the electrical current density, *i*, passing through a point along the flow path within the electrodialyzer is given by:

$$i = \frac{\sum \Delta\phi_{res}}{\tilde{R}_{ed}} \tag{5.21}$$

where $\sum \Delta\phi_{res}$ is the effective electrical resistive potential loss (voltage drop) through the membrane and solution phases (*i.e.*, the stack), and $\tilde{R}_{ed}$ is the areal electrical resistance ($\Omega\ m^2$) of the electrodialyzer (Landau, 1994).

The voltage drop across the stack is a summation of resistive, thermodynamic, and kinetic voltage losses,

$$\Delta\phi_{stack} = \sum \Delta\phi_{res} + \sum \Delta\phi_{lj} + \sum \Delta\phi_{diff} \tag{5.22}$$

where $\Delta\phi_{res}$ is a resistive voltage drop across a membrane or solution phase, $\Delta\phi_{lj}$ is the liquid-junction potential across each ion exchange membrane, and $\Delta\phi_{diff}$ is the voltage drop from the diffusion potential in each diffusion boundary layer (two per ion exchange membrane).

5.4.1 Voltage loss from liquid junction potentials

A liquid junction potential across each ion exchange membrane arises from the difference in activity of ions across the membrane. The general expression for calculating a liquid junction potential is:

$$\Delta\phi_{lj} = \phi^{\beta} - \phi^{\alpha} = \frac{-R_g T}{F} \sum_i \int_{\alpha}^{\beta} \frac{t_i}{z_i} d \ln a_i \tag{5.23}$$

where α and β refer to the solution-membrane interface on each side of the ion exchange membrane (Bard and Faulkner, 2001). If the transport numbers are assumed to be constant across the membrane, then the expression can be simplified to:

$$\Delta\phi_{lj} = \frac{R_g T}{F} \sum_i \frac{t_i}{z_i} \ln \frac{a_i^{\alpha}}{a_i^{\beta}} \tag{5.24}$$

5.4.2 Voltage loss from diffusion potentials

The diffusion potential is a gradient in electric potential that is formed as a consequence of a gradient in salinity and differing diffusivities of the ions composing that salinity. As each ion diffuses according to its diffusivity and concentration gradient, a

gradient in potential occurs to "maintain" electroneutrality (or more precisely, conservation of charge) within each diffusion boundary layer (Newman and Thomas-Alyea, 2004). The diffusion potential ($\nabla\phi_{diff}$) at any point in the diffusion boundary layer can be calculated as:

$$\nabla\phi_{diff} = -\frac{R_g T}{F\kappa}\sum_i \lambda_i \nabla c_i \tag{5.25}$$

where ∇c_i is the gradient in concentration of species *i*.

5.4.3 Resistive potential loss

Considering the entire stack, the total resistive potential loss is the applied stack voltage, less the non-resistive potential losses:

$$\sum \Delta\phi_{res} = \Delta\phi_{stack} - \left(\sum \Delta\phi_{lj} + \sum \Delta\phi_{diff}\right) \tag{5.26}$$

5.4.4 Resistances within the stack

The resistance of a cell-pair, $\tilde{R}_{CP}$, at a point along the flow path is the series summation of the resistance of each of the eight resistive components of the cell-pair:

$$\tilde{R}_{CP} = \tilde{R}_{CEM} + \tilde{R}_{C,bl-c} + \tilde{R}_{C,bulk} + \tilde{R}_{C,bl-a} + \tilde{R}_{AEM} + \tilde{R}_{D,bl-a} + \tilde{R}_{D,bulk} + \tilde{R}_{D,bl-c} \tag{5.27}$$

where $\tilde{R}_{CEM}$ is the resistance of the cation exchange membranes (CEMs), $\tilde{R}_{C,BL\text{-}C}$ is the resistance of the concentrate diffusion boundary layers (DBLs) adjacent to CEMs, $\tilde{R}_{C,bulk}$ is the resistance of the concentrate bulk solutions, $\tilde{R}_{C,BL\text{-}A}$ is the resistance of the concentrate DBLs adjacent to anion exchange membranes (AEMs), $\tilde{R}_{D,BL\text{-}A}$ is the resistance of the diluate DBLs adjacent to the AEMs, $\tilde{R}_{D,bulk}$ is the resistance of the diluate bulk solutions, and $\tilde{R}_{D,BL\text{-}C}$ is the resistance of the diluate DBLs adjacent to CEMs.

The electrical resistance of the electrodialyzer, $\tilde{R}_{ed}$, is calculated by multiplying the cell-pair resistance ($\tilde{R}_{CP}$) by the number of cell-pairs, N_{CP}:

$$\tilde{R}_{ed} = N_{CP}\tilde{R}_{CP} \tag{5.28}$$

With all of the electrical properties characterized, the current density can be recalculated according to Eq. 5.21. Then, with an updated value of current density, all of the chemical parameters can be recalculated. This iteration continues until the current density converges within a relative error of 10^{-3}.

5.5 TIME-DEPENDENT BATCH-RECYCLE MODEL

The time-dependent batch-recycle model is a simulation of the hydraulic, electrical, and chemical characteristics of the experimental ED apparatus (*i.e.*, the electrodialyzer and concentrate and diluate reservoirs). The steady-state plug-flow ED model is a nested sub-routine incorporated within the material balance of the entire batch-recycle system.

The batch-recycle system is modeled as two coupled circulating streams, as shown in Figure 5.2. Each stream was modeled as four hydraulic control-volumes in series, each with ideal flow and forming a hydraulic loop: (1) the reservoir, modeled as a continuous-flow, stirred-tank reactor (CFSTR); (2) the tubing through which the solution is pumped to the influent of the electrodialyzer, modeled as plug-flow (3) the electrodialyzer, modeled as plug-flow; and (4) the tubing that returns the effluent of the electrodialyzer to the reservoir, modeled as plug-flow.

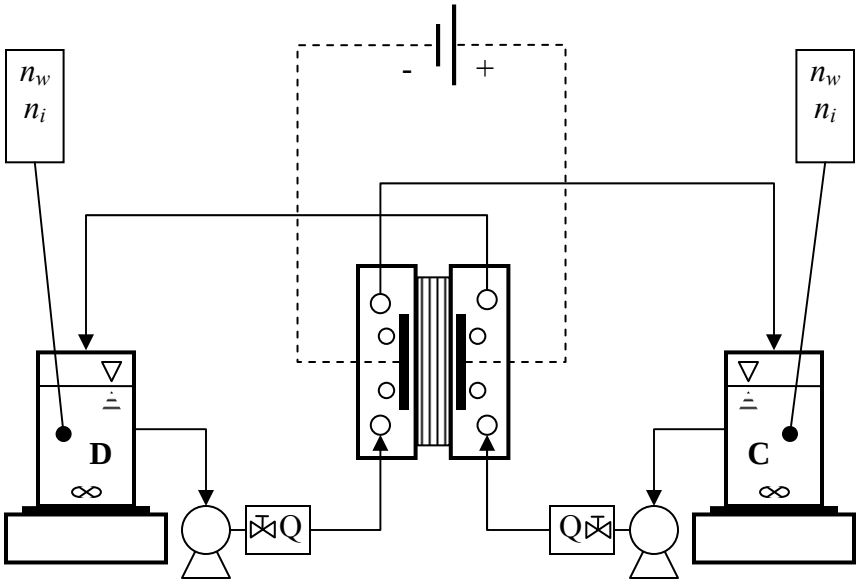

Figure 5.2 Batch-recycle experimental ED apparatus schematic

Flow through the system was assumed to be incompressible, and the volume of each plug-flow control volume was assumed to be constant. The solute and water storage in the CFSTRs, however, was allowed to vary with time. Thus, at each time step, the change in storage of water in the reservoir was calculated by:

$$n_{w,res,t+\Delta t} = n_{w,res,t} + \left(N_{w,res,in} - N_{w,res,out}\right)\Delta t \tag{5.29}$$

where $n_{w,res,t+\Delta t}$ is the number of moles of water in the reservoir at the following time-step (time $t+\Delta t$), $n_{w,res,t}$ is the number of moles of water in the reservoir at the current time step, $N_{w,in}$ is the molar flow rate of water into the reservoir (*i.e.*, the effluent from the electrodialyzer, delayed by the mean hydraulic residence time of the fourth control volume, τ_4), and $N_{w,in}$ is the molar flow rate of water being pumped out of the reservoir. Similarly, the conservation equation is applied to each solute species, as well:

$$n_{i,res,t+\Delta t} = n_{i,res,t} + \left(N_{i,res,in} - N_{i,res,out}\right)\Delta t \tag{5.30}$$

After the number of moles of water and solute have been calculated for each reservoir, the concentrations of solute and water, solution density, total mass, and total volume in each reservoir can be calculated.

At each time step, the space-average current density ($i_{avg,n}$) of the steady-state model was calculated by Simpson's rule:

$$i_{avg,n} = \frac{1}{6}\left(i_{in,n} + 4i_{mid,n} + i_{eff,n}\right) \tag{5.31}$$

where $i_{in,n}$ is the current density in y-grid at the influent of the stack, $i_{mid,n}$ is the current density in the grid at the mid-point between the influent and effluent of the stack, and $i_{eff,n}$ is the current density in the grid at the effluent of the stack. This space-average current density could be compared to the current density observed in laboratory experimentation.

5.6 ECONOMIC MODEL

The premise of this research project is that electrodialysis could be not only technically feasible, but also economically feasible for improving the recovery of RO in inland desalination systems because of the high cost of disposal of concentrate. While the salinity of the concentrate certainly impacts disposal options and permitting, the cost of disposal, by and large, is strongly correlated with the flow rate (volume) disposed. In addition to the following cost estimates, the product water recovered from concentrate was assumed to be saleable at \$1.00/kgal (\$0.26/m^3) (City of Austin, 2009).

5.6.1 Concentrate disposal costs

The cost of disposal of brackish water RO concentrate was modeled with several cost regressions from Mickley (2006). Three concentrate disposal options currently employed by larger facilities are deep-well injection, evaporation ponds, and zero-liquid

discharge (ZLD). Deep-well injection can be the least costly alternative for higher flow rates, assuming that an aquifer of very high salinity is conveniently located near the desalination facility. Evaporation ponds can be attractive for smaller facilities and especially where land is relatively inexpensive. Usually as a last resort, ZLD process are typically operated as a combination of thermal processes such as multi-effect evaporators, vapor compression, and crystallizers.

Three deep-well injection scenarios were considered – varying from a relatively shallow depth of 500 ft to a much deeper 10,000 ft. The total annual cost of disposal of 0.5, 1.0, and 2.0 million gallons per day (mgd) at these depths was estimated by Mickley (2006) and is shown in Figure 5.3. Linear regression of each data series revealed that the cost estimates are extremely sensitive to the depth of the disposal well, but the costs are quite insensitive to flow rate (*i.e.*, the marginal cost of disposal is small compared to the total price of disposal).

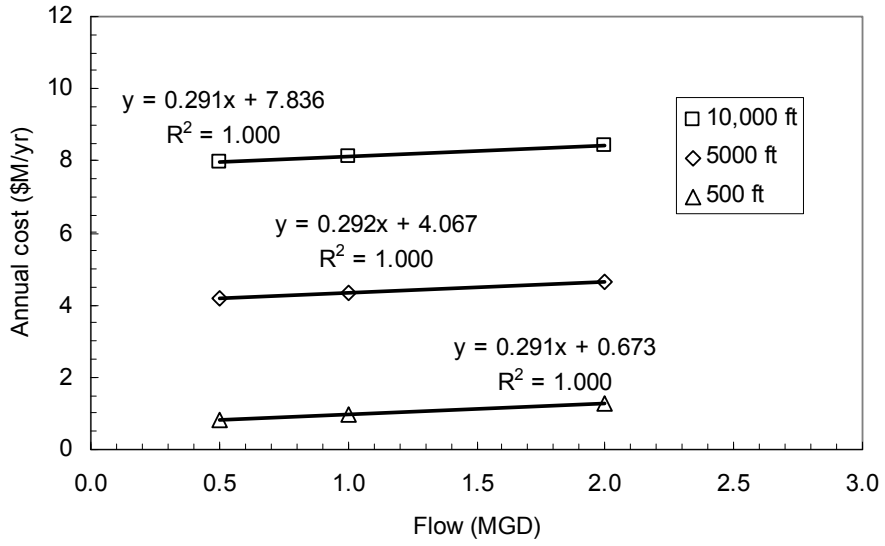

Figure 5.3 Annual cost estimates for concentrate disposal by deep-well injection

The annual cost associated with constructing and operating an evaporation pond was considered for two scenarios. The first scenario (Evap-1) uses cost parameters that result in a less costly scenario (8 ft/yr net evaporation, $1500/acre for land and clearing, 20 mil liner, and 8 ft dikes). The second scenario (Evap-2) used moderate values for the cost parameters (6 ft/yr net evaporation, $6000/acre for land and clearing, 60 mil liner, and 8 ft dikes). The estimated annual cost associated with these disposal options is shown in Figure 5.4. Regression of these cost estimates revealed a dramatic sensitivity to the flow rate, price of land, and required thickness of the liner.

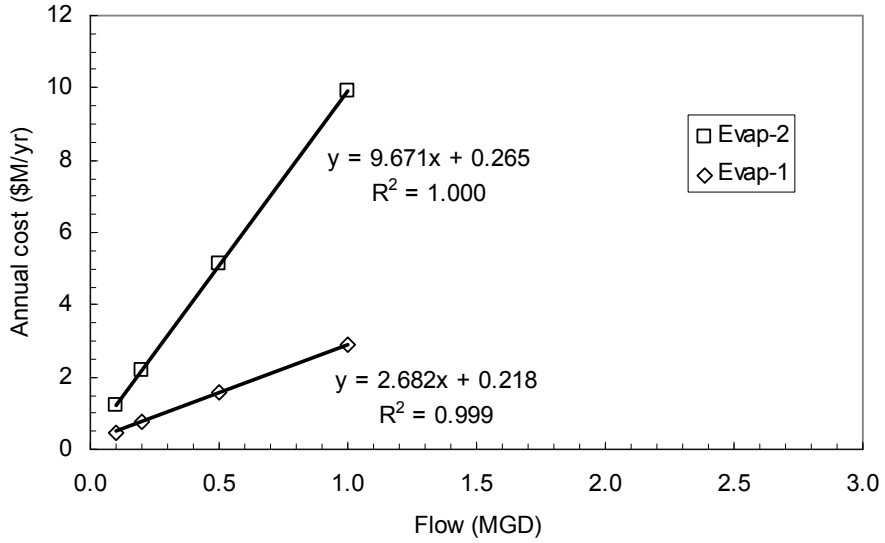

Figure 5.4 Annual cost estimates for concentrate disposal by evaporation ponds

Cost estimation for zero liquid discharge was performed for two scenarios of different energy costs and brine concentrator rejections, and these data are shown in Figure 5.5. Regression of these data reveals that the marginal cost of disposal is insensitive to a doubling of the energy price.

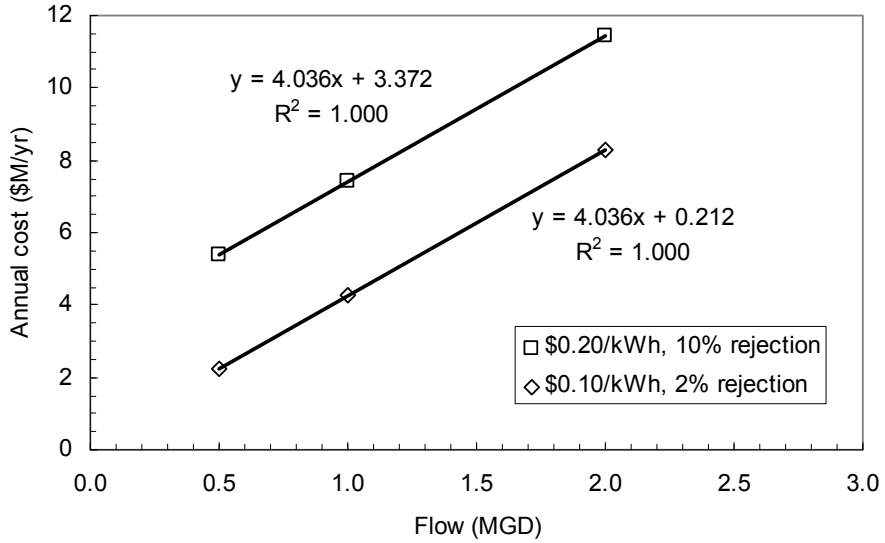

Figure 5.5 Annual cost estimates for for concentrate disposal by zero liquid discharge

Analysis of these seven concentrate disposal scenarios just described reveals four marginal costs, summarized in Table 5.3.

Table 5.3 Estimated marginal costs of concentrate disposal methods

Disposal Method	Estimated Marginal Cost		
	($M/yr-mgd)	($/kgal)	($/m^3)
deep-well injection	0.29	0.79	0.21
evaporation ponds – 1	2.68	7.34	1.94
evaporation ponds – 2	9.67	26.49	7.00
zero liquid discharge	4.04	11.07	2.92

5.6.2 Electrodialysis capital and operating costs

A cost analysis was performed for the treatment of RO concentrate with ED. Capital and non-electrical operating and maintenance (O&M) expenses for an ED system were estimated based on Badruzzaman (2009), Strathmann (2004), and Lee *et al*. (2002), as shown in Figure 5.6.

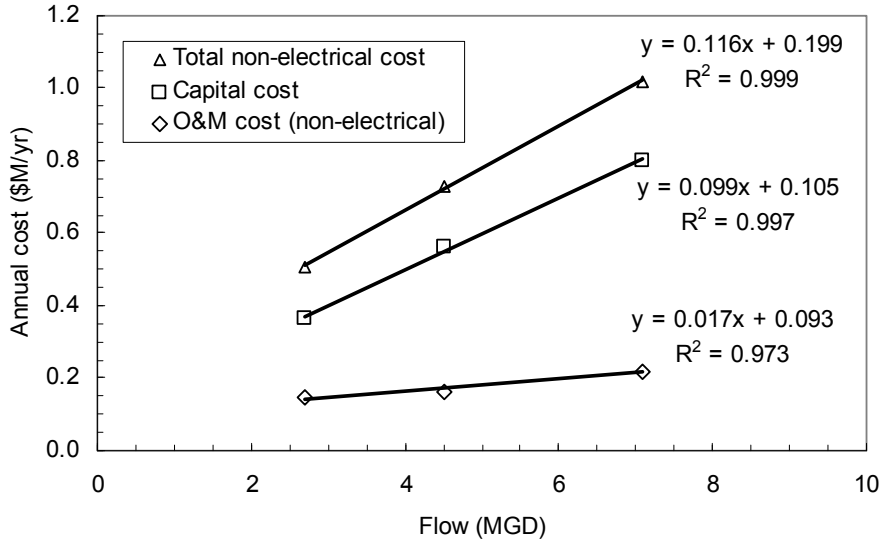

Figure 5.6 Capital and non-electrical O&M costs of an electrodialysis plant

The specific energy requirement determined experimentally in this research was approximately 30 kWh/m^3 per Eq/L separated per Volt/cell-pair applied. Two ED treatment scenarios were considered with this energy requirement: an energy cost of \$0.10/kWh with a stack voltage application of 1.0 V/cell-pair and an energy cost of \$0.15/kWh with a stack voltage application of 1.5 V/cell-pair. These assumptions yield specific removal costs of \$3/m^3 per Eq/L separated and \$6.75/m^3 per Eq/L separated, respectively.

Chapter 6 – Mathematical Modeling Results

6.1 BATCH-RECYCLE MODEL

The time-dependent batch-recycle model, which included the steady-state plug-flow electrodialyzer model, was executed to simulate the Arizona experiments shown in §4.1.

6.1.1 Chemical

In spite of their simplicities, the models were generally able to effectively simulate the ionic transport of the batch-recycle system. A comparison of the model and experimental results is shown for conductivity and removal ratio in Figure 6.1.

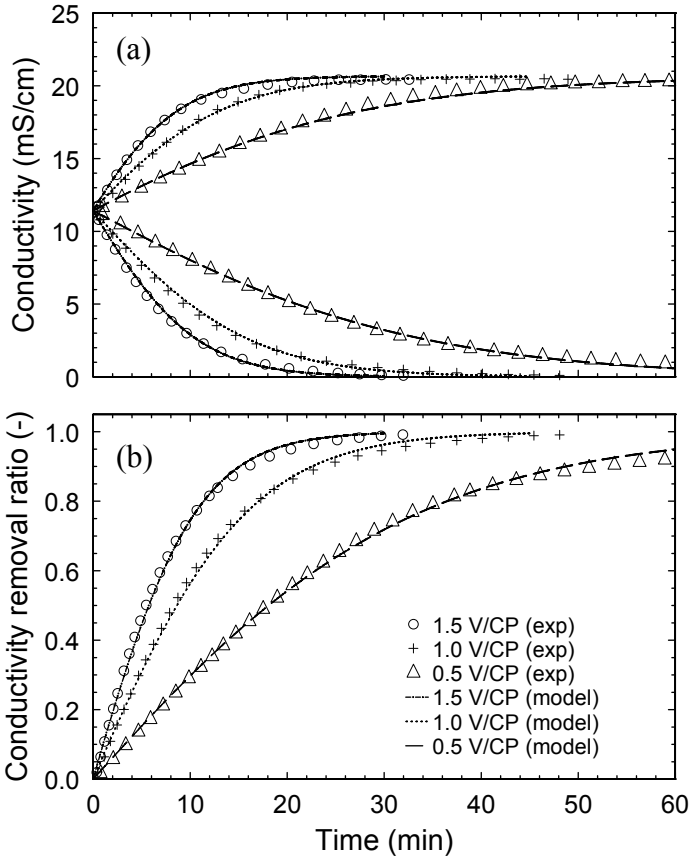

Figure 6.1 Model and experimental comparison for salinity removal

Figure 6.1 also illustrates the utility of the empirical model developed in this research for predicting electrical conductivity as a function of multicomponent concentrations (without consideration of complexation or speciation). The model converges to the infinite dilution values of conductivity at low concentration, but the model also accurately predicted (within 1%) the conductivities of the Texas and Florida waters up to conductivities of 60-70 mS/cm, which was the highest tested.

The batch-recycle model also predicted the general trends in removal of individual ions (shown in Figure 6.2), though not as well as the bulk conductivity. For example, the model did correctly predict the concavity of the sulfate removal, but not to the correct magnitude. The accuracy of the model prediction for individual removals could be improved with the incorporation of a speciation sub-routine to account for complexation, especially for sodium and sulfate. Nonetheless, the simplicity of this model emphasizes the ability to generally predict the performance of the electrodialyzer with fundamentals and well-established constitutive expressions for dilute and moderately dilute solutions.

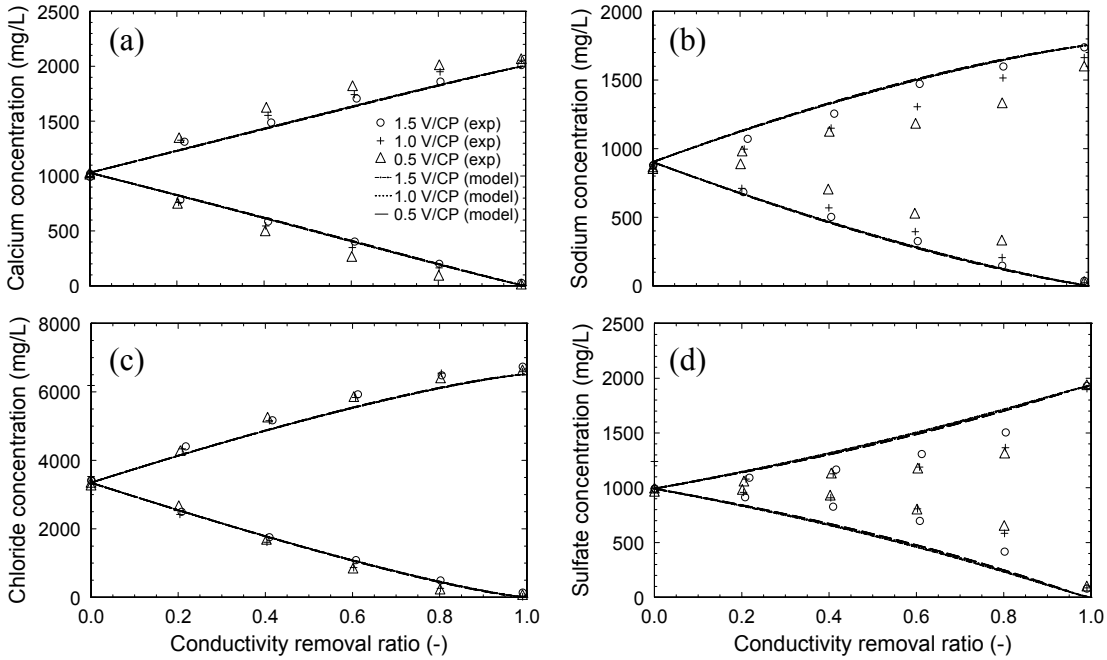

Figure 6.2 Model and experimental comparison for removal of select ions

6.1.2 Electrical

Not surprisingly, the prediction of the electrical current density through the stack was very close to that observed in experimentation, as shown in Figure 6.3.

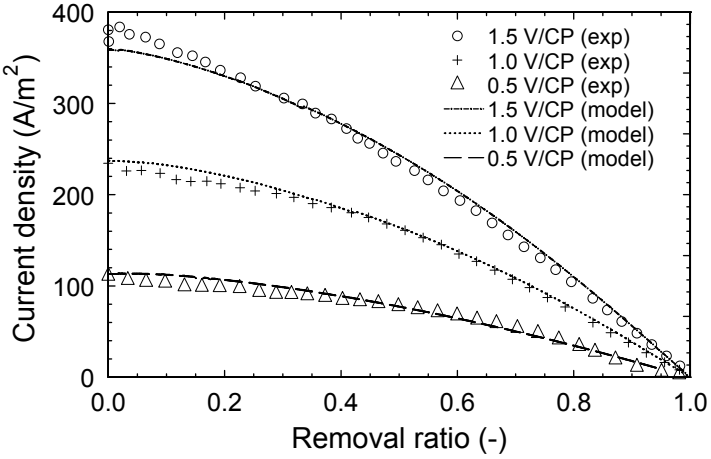

Figure 6.3 Model and experimental comparison for electrical current density

Analysis of the electrical potential losses at $t = 0$ for a stack voltage application of 0.5 V/cell-pair revealed that approximately 3.5% and 1.5% of the total stack voltage was lost to liquid junction and diffusion potentials, respectively. Approximately 15% of the remaining resistive voltage was lost within the membranes. Similar analysis of the treatment of the Florida RO concentrate with a voltage application of 0.5 V/cell-pair showed that approximately 2% and 0.8% of the total stack voltage was lost to liquid junction and diffusion potentials, and approximately 45% of the resistance was due to the membranes. This difference in the proportionality of the membrane voltage loss is consistent with the trend observed in Figure 4.24 where the rate of conductivity removal was essentially limited by the resistance of the membranes. Note that the AMV and CMV membranes used in this research are thin membranes with low electrical resistance compared to other commercial membranes (Strathmann, 2004).

6.1.3 Hydraulic

The change in mass within the diluate reservoir was also modeled in the batch-recycle model. In addition to solute removal, water transport by electroosmosis was modeled with theoretical ionic solvation numbers, which explains the linearity and reproducibility of the three model predictions shown in Figure 6.4. The model also simulates the curvature at higher removal ratios due to osmotic transport. By accounting for water flux by electroosmosis and osmosis, the precision of the final concentrate conductivity for all three voltages (Figure 6.1) is significantly improved over the model predictions of Ortiz *et al.* (2005), which neglected electroosmosis and osmosis.

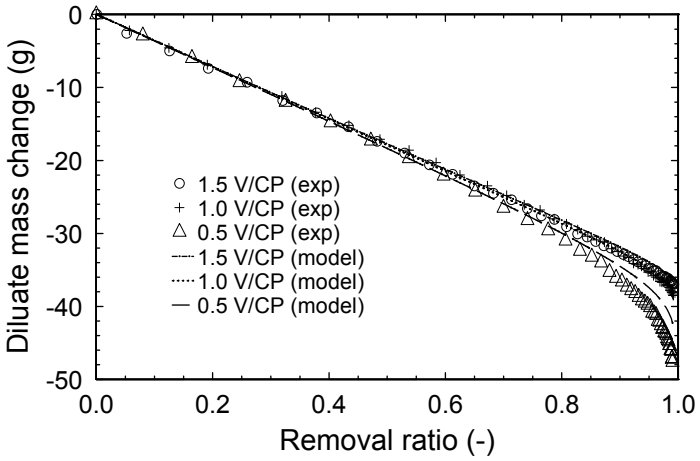

Figure 6.4 Model and experimental comparison for diluate reservoir mass transport

6.2 REVERSE OSMOSIS AND ELECTRODIALYSIS PROCESS INTEGRATION

6.2.1 Direct or indirect production

It is assumed that the diluate product of the electrodialytic treatment of BWRO concentrate could (1) directly augment the BWRO recovery by blending, (2) indirectly augment recovery via a subsequent RO treatment stage before blending, or (3) indirectly augment recovery by supplementing the BWRO feed. Schematics of these three cases are shown in Figure 6.5.

In Cases 1 and 2, the increase in overall system recovery is directly related to the recovery of the ED system by increasing the product flow. In Case 1, for example, if a BWRO operates at 80% recovery (represented by the first three RO stages), and the ED system operates at 80% recovery, then the overall system recovery would be 96%. This case could be implemented as long as the ED system was operated at a sufficient salinity removal ratio to allow blending with the RO product. Of course, Case 1 also requires that the RO feed water be devoid of electrically neutral microcontaminants. Considering the

three waters evaluated in the experimental portion of this research, Case 1 is a potential configuration for treating a source water like the Florida solution, which has a moderate concentration of silica (potable) but lacks boron (toxic).

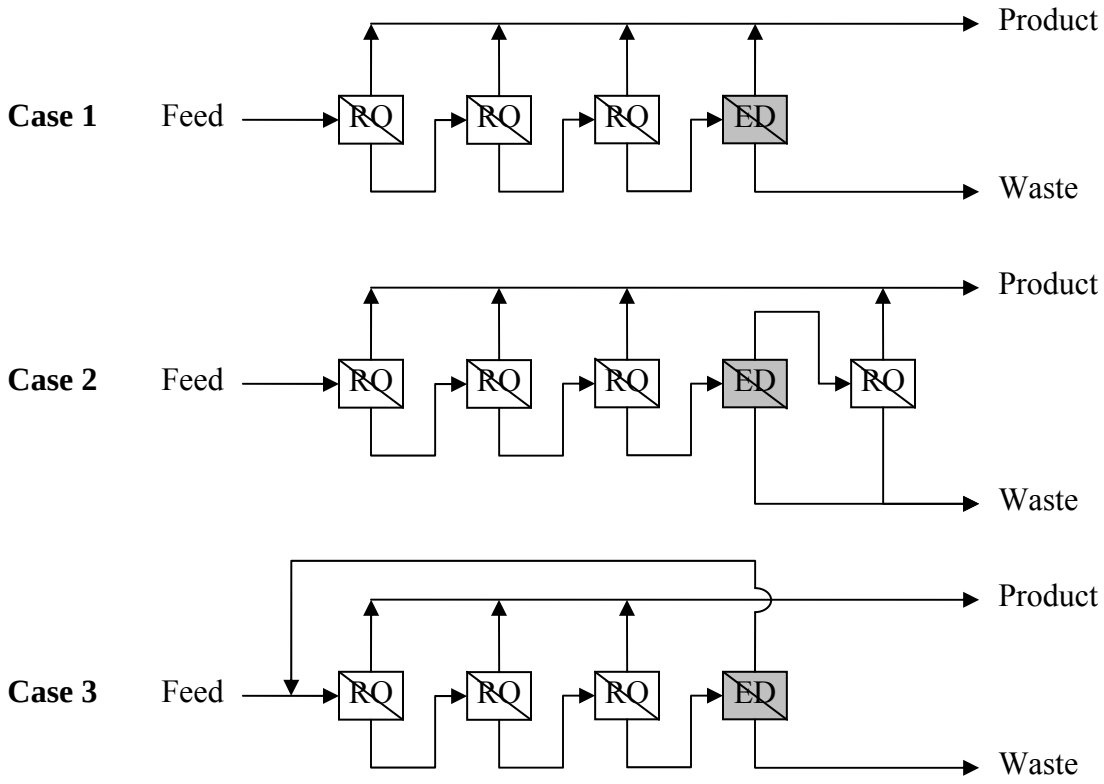

Figure 6.5 Schematics for electrodialytic improvement of BWRO recovery

Case 2 is a more realistic scenario, ensuring the integrity of the product water with a subsequent RO stage (or perhaps a nanofiltration system). However, the overall system recovery is limited by the recovery of the ED system as well as the recovery of the final RO stage. Assuming a maximum ED removal ratio of 85% (because of the rapid decrease in the rate of separation at higher removal ratios), the recovery of the final RO stage would be limited by scaling potential (saturation ratios) similar to the raw feed.

Thus, if the first three RO stages operated at a combined 80% recovery, operation of the ED and final RO stages at 80% and 60% recovery, respectively, would yield an overall system recovery of only 89.6%. However, Case 2 is a potential configuration for a source water like the Texas water studied in this research, which possesses moderate concentrations of boron, as well as silica.

Case 3 increases overall system recovery indirectly by supplementing the raw feed and, like Case 1, has the advantage of avoiding the repressurization of the final RO stage in Case 2. If the ED system operated at a recovery of 80%, the overall system recovery would be 95.2%. However, the concentration of those species not removed by ED will be magnified by the recycling loop. Thus, Case 3 would not be feasible for source waters like the Florida and Texas solutions because of the moderate concentrations of silica and boron, but it is a potential configuration for solutions like the Arizona water, which lacks silica and boron.

6.2.2 Electrodialysis in tandem with precipitation

In addition to implementing ED to improve the recovery of inland BWRO systems, controlled precipitation and solid-liquid separation can also be employed. Since a greater fraction of the precipitating ions is removed when the precipitation is initiated at a greater supersaturation ratio, the maximum symbiosis of these two treatment processes with respect to removal of sparingly soluble salts is achieved by implementing electrodialysis treatment followed by precipitation and separation. For example, precipitation and separation could be applied to the waste stream in any of the three cases in Figure 6.5, because the ED waste stream is more supersaturated than the waste from

the third RO stage. The supernatant from the separation process could be subsequently treated or recycled, as described above.

6.3 ECONOMIC FEASIBILITY

While the actual costs of inland BWRO facilities and concentrate disposal methods are highly site-specific, a proof-of-concept cost-benefit analysis was performed for ED treatment of RO concentrate waste, based on the three cases described in the previous section. A system feed flow rate of 5 mgd was assumed, and the cost-benefit was executed as a function of ED recovery in the range of 50-80%.

6.3.1 Case 1 with Florida source water

The RO system in Case 1 (shown in Figure 6.5) was assumed to achieve recovery and removal ratios of 80% and 97%, respectively, and the ED system was assumed to achieve a removal ratio of 85%. Based on the assumed flow rates, removal ratios, and Florida source water salinity, the estimated costs associated with the ED system are shown as a function of ED recovery ratio in Table 6.1. The estimated capital and non-electrical operating and maintenance costs are small compared to the low (1.0 V/cell-pair and $0.10/kWh) and high (1.5 V/cell-pair and $0.15/kWh) electrical costs.

Table 6.1 Estimated costs of ED treatment in Case 1 with Florida concentrate

System Recovery (-)	ED Recovery (-)	Waste Flow (mgd)	Non-Elec. Costs ($M/yr)	Electric Cost		Total Cost	
				Low ($M/yr)	High ($M/yr)	Low ($M/yr)	High ($M/yr)
80%	-	1.0	-	-	-	-	-
90%	50%	0.5	0.26	0.55	1.25	0.81	1.51
92%	60%	0.4	0.27	0.67	1.50	0.93	1.77
94%	70%	0.3	0.28	0.78	1.75	1.06	2.03
96%	80%	0.2	0.29	0.89	2.00	1.18	2.29

The economic benefits associated with improved recovery (*i.e.*, the disposal cost savings and sale of recovered water detailed in §5.6) were calculated and recorded in Table 6.2. A survey of these data reveals that the benefits associate with deep-well injection (DWI) and sale of recovered water are comparable to each other, but these benefits are dwarfed by the magnitudes of marginal cost savings of evaporation ponds (Evap-1 and Evap-2) and zero liquid discharge (ZLD).

Table 6.2 Estimated benefits of improved recovery: Case 1 with Florida BWRO concentrate

System Recovery (-)	Disposal cost savings				Water Sale ($M/yr)
	DWI ($M/yr)	Evap-1 ($M/yr)	Evap-2 ($M/yr)	ZLD ($M/yr)	
80%	-	-	-	-	-
90%	0.15	1.34	4.84	2.02	0.18
92%	0.17	1.61	5.80	2.42	0.22
94%	0.20	1.88	6.77	2.83	0.26
96%	0.23	2.14	7.74	3.23	0.29

Comparison of the costs (Table 6.1) and benefits (Table 6.2) associated with ED treatment of RO concentrate for the Case 1 configuration with the Florida source water yielded the net-benefits shown in Figure 6.6.

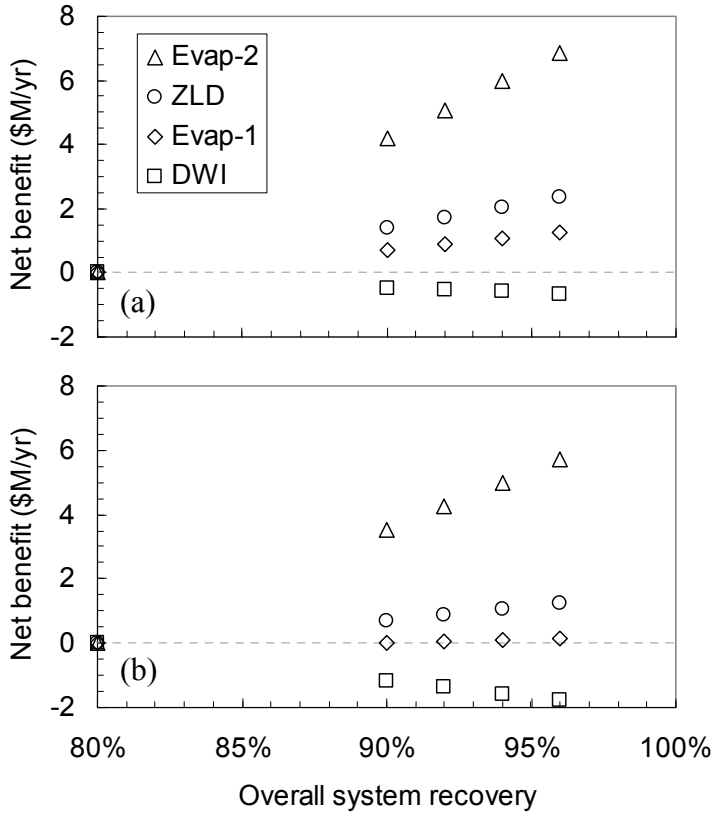

Figure 6.6 Estimated net-benefit of ED treatment: Case 1 with Florida BWRO concentrate for (a) low and (b) high electrical cost

In both the low and high electrical cost estimates, the ED concentrate treatment system was estimated to be economically feasible compared to the zero liquid discharge (ZLD) and the more expensive evaporation pond scenario (Evap-2), and the favorability increases with increasing recovery of the ED system. However, depending on the electrical cost, the ED system could be economically favorable or price-competitive when compared to the less expensive evaporation pond scenario (Evap-1). In both options, ED was estimated to be more costly than the benefits gained when compared to the low marginal cost of deep-well injection.

6.3.2 Case 2 with Texas source water

A similar analysis was performed for Case 2 (the second configuration shown in Figure 6.5), assuming a feed flow rate of 5 mgd of the Texas source water and a recovery ratio of 75% for the initial RO system. The final RO stage (after the ED system) was assumed to operate at 60% recovery and cost \$0.20/m^3, or approximately one third of the cost of a typical brackish water RO plant (Younos 2005). The estimated costs associated with the ED and final RO system are shown in Table 6.3, and benefits associated with the improved recovery are shown in Table 6.4.

Table 6.3 Estimated costs of final RO and ED treatment in Case 2 with Texas BWRO concentrate

System Recovery (-)	ED Recovery (-)	RO Cost (\$M/yr)	Non-Elec. Costs (\$M/yr)	Electric Cost		Total Cost	
				Low (\$M/yr)	High (\$M/yr)	Low (\$M/yr)	High (\$M/yr)
75%	-	-	-	-	-	-	-
83%	50%	0.10	0.27	0.51	0.88	1.14	1.51
84%	60%	0.12	0.29	0.61	1.02	1.37	1.78
86%	70%	0.15	0.30	0.71	1.15	1.60	2.04
87%	80%	0.17	0.32	0.81	1.29	1.82	2.30

Table 6.4 Estimated benefits of improved recovery: Case 2 with Texas BWRO concentrate

System Recovery (-)	Disposal cost savings				Water Sale (\$M/yr)
	DWI (\$M/yr)	Evap-1 (\$M/yr)	Evap-2 (\$M/yr)	ZLD (\$M/yr)	
75%	-	-	-	-	
83%	0.11	1.01	3.63	1.52	0.14
84%	0.13	1.21	4.35	1.82	0.16
86%	0.15	1.41	5.08	2.12	0.19
87%	0.17	1.61	5.80	2.42	0.22

The net-benefits of improving recovery in with the Case 2 configuration and the Texas source water are shown in Figure 6.7 for two ED electrical estimates.

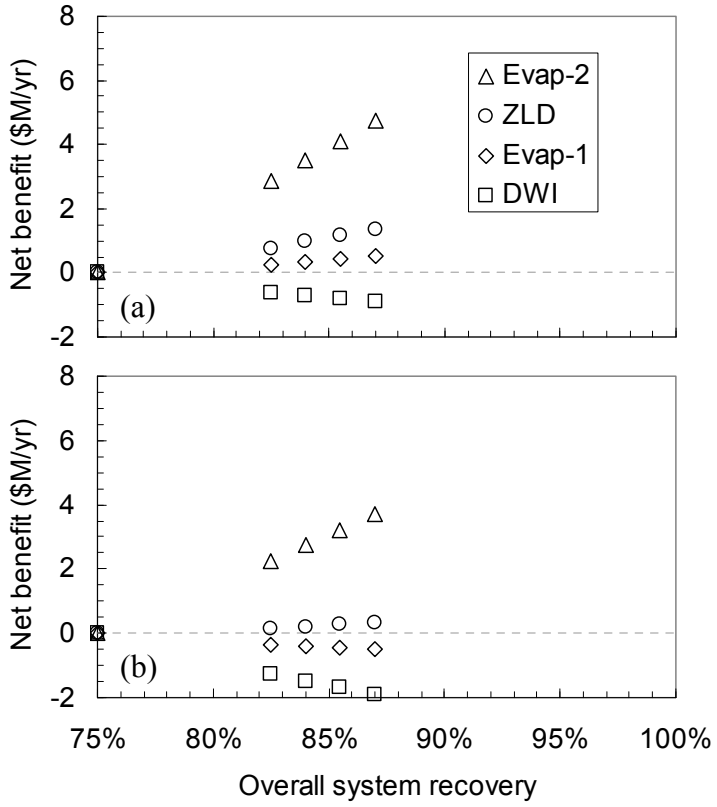

Figure 6.7 Estimated net-benefit of ED treatment: Case 2 with Texas BWRO concentrate for (a) low and (b) high electrical cost

With Case 2, improvement in overall system recovery is not as great as it is in Cases 1 and 3 with respect to the same ED recoveries, and the magnitude of the net-benefits are not as great as those in Cases 1 and 3. However, the feasibility of this configuration is very similar to that of Case 1. Assuming a lower energy investment and lower energy cost in the ED system (Figure 6.7 (a)), the Case 2 configuration is economically attractive for the zero liquid discharge and evaporation pond scenarios. For the higher ED cost estimate (Figure 6.7 (a)), the Case 2 configuration is economically attractive compared to the more expensive evaporation pond and zero liquid discharge scenarios, but slightly unfavorable compared to the less expensive evaporation pond

alternative. As with Case 1, the utility of Case 2 was not estimated to be economically feasible compared to the low marginal costs of deep-well injection.

6.3.3 Case 3 with Arizona source water

A third cost-benefit analysis was performed, similar to the previous two. A feed flow rate of 5 mgd of the Arizona source water was assumed, and consideration of costs and benefits were performed based on the Case 3 configuration shown in Figure 6.5. The estimated costs associated with the ED system are shown in Table 6.5, and benefits associated with the improved recovery are shown in Table 6.6 for several disposal options. The magnitude of the ED costs are significantly lower in this analysis because of the lower salinity of the Arizona feed water.

Table 6.5 Estimated costs of ED treatment in Case 3 with Arizona BWRO concentrate

System Recovery (-)	ED Recovery (-)	ED Eff. (mgd)	Non-Elec. Costs ($M/yr)	Electric Cost		Total Cost	
				Low ($M/yr)	High ($M/yr)	Low ($M/yr)	High ($M/yr)
80%	-	-	-	-	-	-	-
89%	50%	0.56	0.26	0.26	0.52	0.59	0.85
91%	60%	0.68	0.28	0.32	0.60	0.72	1.00
93%	70%	0.81	0.29	0.38	0.67	0.86	1.15
95%	80%	0.95	0.31	0.45	0.76	1.00	1.31

Table 6.6 Estimated benefits of improved recovery: Case 3 with Arizona BWRO concentrate

System Recovery (-)	Disposal cost savings				Water Sale ($M/yr)
	DWI ($M/yr)	Evap-1 ($M/yr)	Evap-2 ($M/yr)	ZLD ($M/yr)	
80%	-	-	-	-	
89%	0.13	1.19	4.30	1.80	0.20
91%	0.16	1.46	5.27	2.20	0.25
93%	0.19	1.75	6.30	2.63	0.30
95%	0.22	2.04	7.37	3.08	0.35

The net-benefit of recovery improvement with the Case 3 configuration is shown in Figure 6.8, in which similar trends are observed as Cases 1 and 2. Again, the implementation of an ED system to improve the recovery of an inland BWRO system is estimated to be economically feasible compared to the zero liquid discharge and more costly evaporation pond scenarios considered here. However, because of the lower salinity of the Arizona source water, the cost of the ED system was estimated to be cost-competitive with the deep-well injection scenario for low ED energy costs.

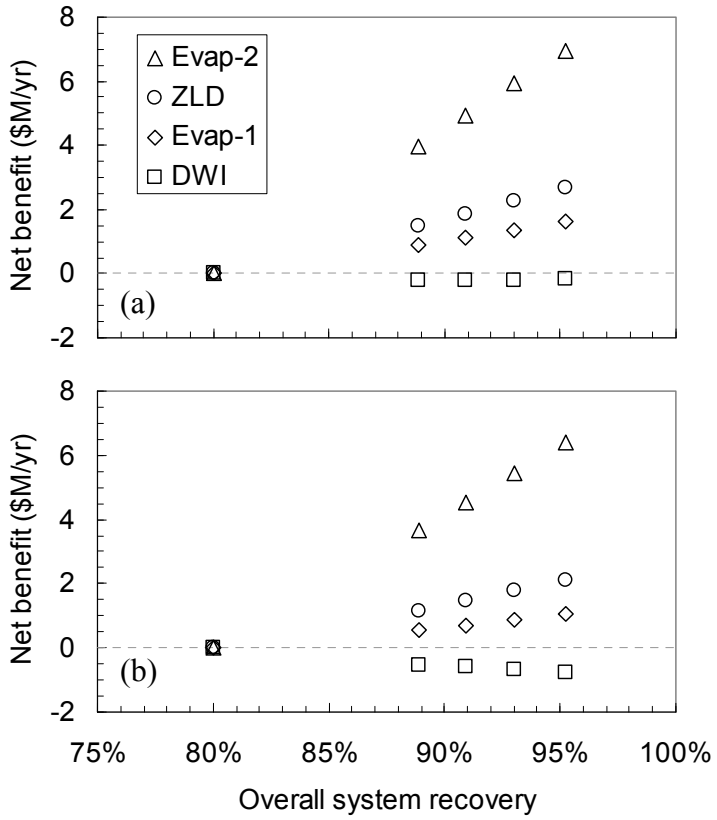

Figure 6.8 Estimated net-benefit of ED treatment: Case 3 with Arizona BWRO concentrate for (a) low and (b) high electrical cost

Chapter 7 – Conclusions

The hypothesis of this research was that the recovery of inland brackish water reverse osmosis (BWRO) systems could be improved by the integration of an electrodialysis (ED) system to treat the RO concentrate waste. The objectives of this research were to:

1. experimentally measure and quantify the efficacy and efficiency of electrodialysis separation of synthetic BWRO concentrates;
2. evaluate the performance sensitivities to hydraulic, electrical, and chemical design and operational variables;
3. develop a mathematical model to simulate batch-recycle electrodialysis performance on BWRO concentrates; and
4. perform a proof-of-concept economic cost-benefit analysis.

Objectives 1 and 2 were accomplished with a laboratory-scale batch-recycle ED system, the performance of which was investigated with respect to applied stack voltage, ion-exchange membrane type, stack superficial velocity, concentrate salinity, and concentration factor. Objectives 3 and 4 were accomplished through the development of three models which simulated (1) the steady-state plug-flow performance of the electrodialyzer, (2) the time-dependent operation of the batch-recycle system, and (3) the economic cost-benefit of implementing electrodialytic treatment of RO concentrate waste with respect to alternative concentrate disposal methods. The research accomplished in response to Objectives 1 and 2 is described predominantly in Chapters 3 and 4, and that of Objectives 3 and 4 is detailed in Chapters 5 and 6.

7.1 CONCLUSIONS FROM EXPERIMENTATION

Experiments performed with synthetic solutions representing BWRO concentrates from Arizona, Texas, and Florida demonstrated that electrodialysis can be effectively employed to further concentrate supersaturated BWRO wastes. Stack voltage applications in the range of 0.5-1.5 Volts/cell-pair and superficial velocities in the range of 1-5 cm/s effectively separated up to 99% of the diluate salinity to the concentrate at single-stage ED recoveries of 50-75%. Initial RO concentrate salinities in the range of 8-18 g/L were further concentrated by ED up to concentrations near 50 g/L, in which the phosphonate antiscalants used in this research were able to effectively prevent precipitation.

7.1.1 Electrical

The predominant process controlling parameter is the stack voltage application. The rate of separation is approximately proportional to the applied voltage and is relatively stable up to removal ratios near 60%, but the rate decreases more rapidly after approximately 80% removal. The length of flow path required to achieve a certain removal ratio is inversely proportional to the rate of separation, and the rate of separation at higher removal ratios is limited by the decreasing conductivity of the diluate. Thus, optimal design of the ED process may be to produce a product water salinity similar to the original RO feed, depending on solution conductivity.

The specific energy consumption is proportional to the applied voltage and the ionic concentration that is separated. That is, with the system used in this research, the specific energy consumption was observed to be approximately 30 kWh/m^3 per V/cell-

pair per Eq/L separated. For the treatment of solutions of moderate salinity (*e.g.*, less than 0.5 Eq/L) at low and moderate voltage applications (*e.g.*, 0.5-1.0 V/cell-pair), the specific energy consumption of ED is less than thermal desalination alternatives (*e.g.*, 15 kWh/m^3). The types of membranes tested here showed that thicker, more resistive membranes slightly increase the specific energy consumption and decrease the rate of separation.

7.1.2 Hydraulic

With the mesh spacers and superficial velocities tested here, a marginal increase in the rate of separation was observed with increasing stack superficial velocity, which decreases the thickness of the rate-limiting diffusion boundary layer. However, the increase in separation rate was approximately proportional to the square root of the velocity. While the hydraulic cost of pumping the solution at a higher velocity is not significant, the length of flow path required to achieve a certain removal ratio is proportional to the velocity, so a dramatic increase in velocity causes a dramatic increase in the capital cost to provide a longer flow path. Therefore, an implicit cost tradeoff exists between solution velocity and the capital cost.

The transport of water by electroosmosis and osmosis was observed, and electroosmosis was the predominant mechanism of water transport up to removal ratios near 80-90%. At higher removal ratios, osmotic transport of water became more significant, but the combined effect of electroosmosis and osmosis only decreased the nominal recovery ratio by a few percent.

7.1.3 Chemical

Individual ions were separated at approximately the same rate as bulk conductivity with the exception of sulfate, which was hindered by complexation with calcium and magnesium. Uncharged species such as boric acid and silicic acid are not influenced by an applied electric field, and thus were not separated. The presence of an RO antiscalant showed little impact on batch-recycle ED performance, aside from its essential purpose of preventing precipitation. Recognizing the significantly shorter hydraulic residence times of full-scale ED systems compared to the batch-recycle experiments performed in this work, it is possible that full-scale systems could operate at even greater recoveries than the 50-75% simulated in this experimentation. Experiments with insufficient antiscalant concentration or elevated concentrate pH resulted in precipitation within the electrodialyzer, but no irreversible damage to the membranes was observed.

7.2 CONCLUSIONS FROM MODELING

7.2.1 Technical

Even with simplified models, the experimental results were generally well simulated with respect to electrical, chemical, and hydraulic behavior. The steady-state plug-flow ED model was able to model the current density and chemical transport of the experimental electrodialyzer, and the batch-recycle model was able to simulate the conductivities of the experimental reservoir solutions.

The electrical conductivity of the solutions was modeled well with the novel formula developed in this research. The electrical current density was simulated by

treating it as an ohmic device after accounting for the non-resistive losses of liquid junction and diffusion potentials, which accounted for less than 5% of the total voltage loss at high flow rates and low voltage applications. The electrical resistance of the membranes was shown to be a significant source of voltage loss – up to 45% of the total electrical resistance of the system with solution conductivities near 25 mS/cm.

The general trends of separation of ionic species were captured, even though the steady-state model did not include the effects of speciation. The model overpredicted the rate of separation of sulfate, which could be improved by accounting for neutral and single-charge complexes. The transport of water by electroosmosis was modeled according to ionic solvation numbers, and together with the effects of osmosis, the total water and ionic mass flux from the diluate reservoir was simulated precisely.

7.2.2 Economic

The general feasibility of using electrodialysis to improve the recovery of inland BWRO systems through concentrate treatment was demonstrated. The capital and non-electrical operating and maintenance costs of electrodialysis treatment were estimated, along with a moderate and high energy expense. Concentrate disposal costs were estimated for three disposal methods: deep-well injection, evaporation ponds, and zero liquid discharge. Comparison of the ED system cost and benefits (disposal cost savings and recovered water sales) was performed for three desalination system configurations, one for each of the three source waters studied in this research.

In all three cases, the use of an ED system to improve the recovery of an inland BWRO system was estimated to be economically advantageous in disposal situations

involving zero liquid discharge or moderately priced evaporation ponds. In comparison to concentrate disposal by inexpensive evaporation ponds, the economic feasibility of an ED system for RO concentrate recovery is estimated to be dependant on the concentrate salinity, ED voltage application, and the price of electricity. However, due to the relatively low marginal cost of deep-well injection with respect to flow rate, the costs of the proposed ED treatment system were estimated to outweigh the benefits for the deep-well injection scenario considered here.

7.3 FUTURE WORK

Several logical extensions stem from this work. First, the steady-state plug-flow ED model could be expanded in several ways. Development of a sub-routine to account for speciation could greatly improve the simulation of fluxes of individual components, especially for sulfate. This addition would improve the model simulation at low voltage applications and very high removal ratios.

The steady-state model could also be extended to simulate full-scale ED systems so that it could be used for design optimization. Such a model could be used to quantify the electrical limitations in the tradeoff between operating and capital costs associated with voltage application. The model could also be used to consider the design optimization associated with the tradeoff between pumping power and capital costs associated with superficial velocity. Characterization of other spacer hydrodynamics could be incorporated to consider the tradeoff between liquid junction and diffusion potentials in systems with a different diffusion boundary layer behavior.

Considering the large fraction of electrical resistance that the ion-exchange membranes can contribute in ED systems treating RO concentrates of higher salinity, the development of thinner ion exchange membranes with higher ion-exchange capacity should be investigated. Also, the development of ion-exchange membranes with a high selectivity for divalent species would be extremely valuable in concentrate treatment.

A significant drawback of directly blending the ED product for potable use is that ED does not remove neutrally charged species such as boric acid. A laboratory study could be designed to consider the feasibility of elevating the pH of the ED product to ionize boric and silicic acid so that a subsequent ED stage could remove these species.

The type and concentration of natural organic matter (NOM) varies widely with source water, and while the electrodialysis technology is more robust than RO with respect to fouling by NOM, the effects of long-term exposure to hydrophilic, transphilic, and hydrophobic portions of NOM should be investigated.

Also, several topics of investigation would be more valuable if performed in pilot- or full-scale studies facilities involving real BWRO concentrates. Because of the proprietary nature of commercial antiscalants used in RO desalination, an optimization of type and concentration of antiscalants used/added in ED treatment of RO concentrate is predominantly empirical. The long-term effects of the use of antiscalants and the potential accumulation of those antiscalants within ion-exchange membranes should be evaluated. Also, the precipitation limitations associated with recycling ED concentrate for improved ED recovery should be evaluated to determine the upper limits of single-stage ED recovery.

Appendix A – Flow rate calibration procedure

1. prepare two liters of sample solution (*e.g.*, 0.1 M NaCl)

2. fill a one-liter beaker with the test solution to be used as a single-pass source beaker

3. fill another one-liter beaker with the test solution to be used as a circulating reservoir

4. evacuate the contents of each of the three streams by applying vacuum to each stream outlet

5. place all three stream inlets in the circulating reservoir

6. prime each of the three pumps by opening each valve and applying vacuum to each stream outlet for two seconds

7. place all three stream outlets in the circulating reservoir

8. open the custom LabVIEW™ software "Instrument Observation.vi"

9. turn on the pumps

10. set the flow rate through the meter to be calibrated near the desired flow rate (as indicated by the LabVIEW™ SCADA) by adjusting the needle valve

11. set the flow rate of the streams not being calibrated such that the concentrate/diluate trans-membrane head is less than five centimeters and the average head of the electrode rinse is equal to the average head of the concentrate or diluate

12. turn off the pumps

13. stop and close the custom LabVIEW™ software "Instrument Observation.vi"

14. place an empty one-liter beaker on the Mettler Toledo® XS6001S digital mass balance

15. remove the inlet of the stream to be calibrated from the circulation beaker and place the inlet in the single-pass source beaker

16. fix the stream outlet (of the stream to be calibrated) above the empty one-liter beaker on the mass balance so that the effluent will flow down the inside wall of the beaker

17. open the custom LabVIEW™ software “Calibration – Pumps.vi”

18. turn on the pumps

19. wait ten seconds for the flow rates and pressures to stabilize

20. run the custom LabVIEW™ software “Calibration – Pumps.vi”, enter the filename for the calibration, and confirm with [enter]

21. continue pumping until the desired volume pumped (or time limit) is reached

22. stop and close the custom LabVIEW™ software “Calibration – Pumps.vi”

23. turn off the pumps

24. recycle the effluent test solution from the beaker on the mass balance to the single-pass source beaker

25. place the inlets and outlets of all three streams in the circulation beaker

26. repeat steps 9-25 for each stream for each flow rate used in experimentation

27. use linear regression to determine the flow rate of each calibration sample (the slope of mass versus time is the mass rate

28. use linear regression of the results from step 27 to fit the flow rate of each stream to the following form $Q = m V + b$, where Q is the flow rate of the stream, m is a slope coefficient, V is the signal voltage of the flow meter, and b is an ordinate intercept coefficient

29. open the comma delimited file “analog_parameters.csv”

30. enter the newly determined slope and intercept parameters (from 28) in the slope and intercept fields

31. save and close the custom comma delimited file “analog_parameters.csv”

Appendix B – Pressure transducer calibration procedure

1. connect all transducers in hydraulic parallel with tubing to the wall manometer
2. fill the wall manometer with water
3. purge the tubing and manometer of air
4. open and run the custom LabVIEW™ software "Calibration – Pressure Transducers"
5. enter the filename for the calibration, and confirm with [enter]
6. fill the wall manometer to a level of 180 cm above the centerline of the pressure transducers
7. measure the manometer level to the nearest millimeter and enter the value in the "Manometer Reading" field in the custom LabVIEW™ software "Calibration – Pressure Transducers"
8. click the "READ" button
9. drain the manometer so that the level decreases approximately 20 cm
10. repeat steps 7 through 9 until a manometer level of 40 cm is recorded
11. click the "FINISH Calibration" button
12. stop and close the custom LabVIEW™ software "Calibration – Pressure Transducers"

Appendix C – Experimental solution preparation procedure

13. B/Si solution: In a 2 L volumetric flask,
    a. add 1.5 L of DI water
    b. add the amounts of silicic acid and boric acid for 4 L of diluate
    c. add 200 mL of 0.1 M NaOH (resulting pH ~ 12.0)
    d. dilute to 2.0 L with DI water, and mix until silica dissolves
    e. for 0.5 L, reduce pH by adding 20 mmol of concentrated HNO_3
    f. for 1.5 L, reduce pH by adding 20 mmol of concentrated HCl
14. Diluate: In a 2 L volumetric flask,
    a. add 1.0 L of Si/B+NaOH+HCl solution (from above)
    b. add antiscalant and 100 mL of multivalent-cation stock
    c. add 100 mL of multivalent-anion stock
    d. dilute to 2 L with DI water
15. Concentrate: In a 1 L volumetric flask,
    a. add 0.5 L of Si/B+NaOH+HCl solution
    b. add antiscalant and (100 mL)×CCF of multivalent-cation stock
    c. add (100 mL)×CCF of multivalent-anion stock
    d. dilute to 1 L with DI water
16. Electrode rinse: In a 1 L volumetric flask,
    a. add 0.5 L of Si/B+NaOH+HNO_3 water (from above)
    b. add antiscalant and 100 mL of electrode rinse stock
    c. dilute to 1 L with DI water

Appendix D – Experimental procedure

1. prepare an excess of the experimental concentrate and diluate solution(s), and prepare the experimental electrode rinse solution (salt and antiscalant)
2. turn on the water bath and the bath circulation pump
3. evacuate the contents of the concentrate, diluate, and electrode rinse streams
4. add the experimental electrode solution and the pre-rinse concentrate and diluate
5. prime each of the three pumps by applying vacuum to each stream outlet
6. turn on the ED pumps
7. adjust the pH of the electrode rinse solution by adding concentrated nitric acid
8. open the custom LabVIEW™ program “Instrument Observation.vi”, and click the yellow [SET VOLTAGE] button to set the power supply to three volts
9. click the green [ENGAGE] button to apply 3 V to the stack for five minutes
10. click the orange [DISENGAGE] button and rinse for five minutes
11. click the red [STOP] button to close the “Instrument Observation.vi” program, and turn off the ED pumps
12. evacuate the pre-rinse solutions from the concentrate and diluate streams
13. place the experimental concentrate and diluate solutions, and prime the pumps
14. insert the pH and conductivity/temperature probes into the respective beakers, and turn on the ED pumps
15. wait for the reservoirs to reach the desired temperature
16. open and run the custom LabVIEW™ software “ED Experiment SCADA.vi”
17. after completing the setup form, confirm the filename and location, and click [OK] to begin the experiment
18. stop the experiment by clicking the [STOP] button
19. close the “ED Experiment SCADA.vi” program, and turn off all pumps
20. remove, rinse, and store the pH and conductivity/temperature probes

Appendix E – Analytical sampling procedure

1. add 9.9 mL of distilled water to each ICP vial
2. before and during experimentation, periodically withdraw a 100 μL sample from each of the three reservoirs and inject into the respective ICP vials
3. cap the ICP vials, and mix thoroughly
4. add 2 mL of distilled water to each IC vial
5. with the 1000 μL electronic pipette, withdraw 2 mL of the 10 mL diluted solution and inject into the respective IC vials
6. cap the IC vials, and mix thoroughly
7. add 160 μL (2% v/v) of concentrated nitric acid to each ICP vial
8. add 40 μL of 1000 mg/L strontium reference standard stock to each ICP vial
9. cap the ICP vials, and mix thoroughly

Appendix F – Analysis procedure for the Metrohm IC

Startup

1. refill the IC beakers of sulfuric acid, distilled water, and carbonate eluent

2. lock the acid and water peristaltic tubing, and tighten to the mark

3. from the main menu, open your system file, and then from control menu in the system window, connect to workplace, and startup/measure baseline

4. double-click the separation center icon in the system window, and after five minutes of stable, near-zero conductivity, click the [step] button for the suppressor (repeat three times)

5. from the main menu, open your method file, and then from the method menu, update the calibration components, levels, and concentrations (save the method file and close)

6. double-click the autosampler icon in the system window, and then click the autosampler tab within the new window

7. type “22” into the field at the end of the “Move” row, and then click [start] so that you can refill the autosampler rinse bottles with distilled water

8. type “151” into the field at the end of the “Move” row, and then click [start] so that you can load the autosampler with your standard vials and sample vials

9. confirm that all vials are perfectly seated and that all caps are perfectly fit

10. from the system menu, create a new queue file, and edit it to match the autosampler positions and method file calibration levels

11. after five minutes since the previous suppressor [step], close the baseline window and start the queue

Shutdown

1. from the control menu in the system window, shutdown hardware, disconnect from workplace, and close the system file

2. loosen and unlock the peristaltic tubing

3. remove your standard and sample vials from the autosampler

Appendix G – Analysis procedure for the Varian 710-ES ICP-OES

Startup

1. turn on the exhaust fan and liquid cooling power supply
2. open the argon valve
3. lock the peristaltic tubing (autosampler rinse and ICP supply and waste)
4. place the autosampler rinse supply in the 2% nitric acid bottle
5. start the plasma
6. load the autosampler with your standard and sample vials
7. setup the software (method, sequence, analysis)
8. start the analysis

Shutdown

1. after the analysis is completed, and with the plasma on, set the autosampler to rinse with 2% nitric acid for five minutes
2. with the plasma on, place the autosampler rinse supply in the DI bottle, and rinse for five minutes
3. turn off the plasma
4. wait at least five minutes after the plasma has been turned off before turning off the exhaust fan and liquid cooling
5. park the autosampler probe
6. unlock and unstretch the peristaltic tubing
7. close the argon valve
8. remove your standard and sample vials from the autosampler

Appendix H – Speciation of BWRO concentrates

The following speciation distribution (Table H.1) was calculated for the Arizona BWRO concentrate (Table 3.4) at a pH of 8.0 using Visual MINTEQ (version 3.0) with the SIT activity coefficient model.

Table H.1 Species distribution for the Arizona BWRO concentrate

Component	Species	% of total	Component	Species name	% of total
Ba^{+2}	Ba^{+2}	87.2	CO_3^{-2}	CO_3^{-2}	0.9
	$BaCl^{+}$	2.4		HCO_3^{-}	80.8
	$BaCO_3$ (aq)	0.7		H_2CO_3* (aq)	1.4
	$BaHCO_3^{+}$	3.5		$MgCO_3$ (aq)	1.2
	$BaSO_4$ (aq)	6.3		$MgHCO_3^{+}$	4.4
Ca^{+2}	Ca^{+2}	83.1		$CaHCO_3^{+}$	7.0
	$CaCO_3$ (aq)	2.1		$CaCO_3$ (aq)	3.2
	$CaHCO_3^{+}$	4.5		$NaCO_3^{-}$	0.2
	$CaSO_4$ (aq)	10.3		$NaHCO_3$ (aq)	0.9
K^{+1}	K^{+1}	98.8		$Mg_2CO_3^{+2}$	0.1
	KSO_4^{-}	1.2	Cl^{-1}	Cl^{-1}	97.9
Mg^{+2}	Mg^{+2}	78.2		$MgCl^{+}$	2.1
	$Mg_2CO_3^{+2}$	0.2	NO_3^{-1}	NO_3^{-1}	99.4
	$MgCl^{+}$	9.4		$NaNO_3$ (aq)	0.6
	$MgCO_3$ (aq)	1.0	SO_4^{-2}	SO_4^{-2}	54.7
	$MgHCO_3^{+}$	3.4		$MgSO_4$ (aq)	16.0
	$MgOH^{+}$	0.0		$CaSO_4$ (aq)	25.7
	$MgSO_4$ (aq)	7.8		$NaSO_4^{-}$	3.5
Na^{+1}	Na^{+1}	98.6			
	$NaCO_3^{-}$	0.1			
	$NaHCO_3$ (aq)	0.4			
	$NaNO_3$ (aq)	0.0			
	$NaSO_4^{-}$	0.9			

Similarly, the speciation distribution (Table H.2) of the Texas BWRO concentrate (Table 3.5) was calculated for a pH of 7.8.

Table H.2 Species distribution for the Texas BWRO concentrate

Component	Species	% of total	Component	Species name	% of total
Ca^{+2}	Ca^{+2}	59.1	Br^{-1}	Br^{-1}	100
	$CaCl^{+}$	5.2	Cl^{-1}	Cl^{-1}	94.5
	$CaCO_3$ (aq)	1.1		$CaCl_{+}$	0.6
	$CaH_2BO_3^{+}$	0.2		$MgCl_{+}$	0.9
	$CaHCO_3^{+}$	4.3		KCl (aq)	0.0
	$CaSO_4$ (aq)	30.0		NaCl (aq)	3.9
	H_3SiO_4-	1.3	CO_3^{-2}	CO_3^{-2}	0.6
K^{+1}	K^{+1}	92.1		HCO_3^{-}	86.7
	KCl (aq)	2.8		H_2CO_3* (aq)	2.2
	KSO_4^{-}	5.1		$MgCO_3$ (aq)	0.4
Mg^{+2}	Mg^{+2}	61.9		$MgHCO_3^{+}$	2.2
	$Mg_2CO_3^{+2}$	0.1		$CaHCO_3^{+}$	3.0
	$MgCl^{+}$	8.7		$CaCO_3$ (aq)	0.8
	$MgCO_3$ (aq)	0.6		$SrHCO_3^{+}$	0.1
	$MgH_2BO_3^{+}$	0.1		$NaCO_3^{-}$	0.6
	$MgHCO_3^{+}$	3.6		$NaHCO_3$ (aq)	3.5
	$MgSO_4$ (aq)	25.0		$Mg_2CO_3^{+2}$	0.0
Na^{+1}	Na^{+1}	92.6	H_3BO_3	H_3BO_3	93.3
	NaCl (aq)	2.8		NaH_2BO_3 (aq)	0.6
	$NaCO_3^{-}$	0.1		$H_2BO_3^{-}$	4.9
	NaH_2BO_3 (aq)	0.0		$H_5(BO_3)_2^{-}$	0.0
	$NaHCO_3$ (aq)	0.5		$H_8(BO_3)_3^{-}$	0.0
	$NaSO_4^{-}$	4.0		$MgH_2BO_3^{+}$	0.4
Sr^{+2}	Sr^{+2}	62.5		$CaH_2BO_3^{+}$	0.8
	$SrCl^{+}$	3.4		$SrH_2BO_3^{+}$	0.0
	$SrCO_3$ (aq)	0.5	H_4SiO_4	H_4SiO_4	97.9
	$SrH_2BO_3^{+}$	0.1		$H_4SiO_4SO_4^{-2}$	0.8
	$SrHCO_3^{+}$	5.8	NO_3^{-1}	NO_3^{-1}	96.9
	$SrSO_4$ (aq)	27.6		$CaNO_3^{+}$	0.8
				$SrNO_3^{+}$	0.0
				KNO_3 (aq)	0.0
				$NaNO_3$ (aq)	2.2
			SO_4^{-2}	SO_4^{-2}	63.8
				$MgSO_4$ (aq)	8.1
				$CaSO_4$ (aq)	11.1
				$SrSO_4$ (aq)	0.2
				$NaSO_4^{-}$	16.5
				KSO4^{-}	0.2
				$H_4SiO_4SO_4^{-2}$	0.0

Similarly, the speciation distribution (Table H.3) of the Florida BWRO concentrate (Table 3.6) was calculated for a pH of 7.9.

Table H.3 Species distribution for the Florida BWRO concentrate

Component	Species	% of total	Component	Species name	% of total
Ba^{+2}	Ba^{+2}	85.6	CO_3^{-2}	CO_3^{-2}	0.9
	$BaCl^+$	5.1		HCO_3^-	80.7
	$BaCO_3$ (aq)	0.3		H_2CO_3* (aq)	1.6
	$BaHCO_3^+$	1.9		$MgCO_3$ (aq)	0.9
	$BaSO_4$ (aq)	7.1		$MgHCO_3^+$	4.1
Ca^{+2}	Ca^{+2}	84.1		$CaHCO_3^+$	4.8
	$CaCO_3$ (aq)	0.9		$CaCO_3$ (aq)	1.6
	$CaHCO_3^+$	2.6		$SrCO_3$ (aq)	0.0
	$CaSO_4$ (aq)	12.4		$SrHCO_3^+$	0.4
K^{+1}	K^{+1}	98.2		$NaCO_3^-$	0.8
	KSO_4^-	1.8		$NaHCO_3$ (aq)	4.1
Mg^{+2}	Mg^{+2}	70.1		$Mg_2CO_3^{+2}$	0.1
	$Mg_2CO_3^{+2}$	0.1	Cl^{-1}	Cl^{-1}	98.0
	$MgCl^+$	19.2		$SrCl^+$	0.0
	$MgCO_3$ (aq)	0.4		$MgCl^+$	2.0
	$MgHCO_3^+$	1.8	H_4SiO_4	H_4SiO_4	98.0
	$MgSO_4$ (aq)	8.4		$H_4SiO_4SO_4^{-2}$	0.3
Na^{+1}	Na^{+1}	98.3		H_3SiO_4-	1.7
	$NaCO_3^-$	0.0	NO_3^{-1}	NO_3^{-1}	97.2
	$NaHCO_3$ (aq)	0.2		$SrNO_3^+$	0.1
	$NaSO_4^-$	1.4		$NaNO_3$ (aq)	2.7
Sr^{+2}	Sr^{+2}	79.8	SO_4^{-2}	SO_4^{-2}	58.9
	$SrCl^+$	7.6		$MgSO_4$ (aq)	11.5
	$SrCO_3$ (aq)	0.3		$CaSO_4$ (aq)	13.8
	$SrHCO_3^+$	2.9		$SrSO_4$ (aq)	0.7
	$SrSO_4$ (aq)	9.4		$NaSO_4^-$	14.8
				KSO_4^-	0.3
				$H_4SiO_4SO_4^{-2}$	0.0

References

Adhikary, S. K., Gohil, J. M., and Ray, P. (2004). "Studies on the resistance developed at different stages in an electrodialysis stack operated in parallel-cum-series flow pattern." *Journal of Membrane Science*, 245(1-2), 131-136.

Anderko, A., and Lencka, M. M. (1997). "Computation of electrical conductivity of multicomponent aqueous systems in wide concentration and temperature ranges." *Industrial & Engineering Chemistry Research*, 36(5), 1932-1943.

Aseyev, G. G. (1998). *Electrolytes, interparticle interactions : Theory, calculation methods, and experimental data*, Begell House, New York.

Atkins, P. W., and De Paula, J. (2006). *Atkins' physical chemistry*, W.H. Freeman, New York.

AWWA. (1995). "M38 - electrodialysis and electrodialysis reversal." Manual of water supply practices, P. Murray, ed., American Water Works Association, Denver, CO.

Badruzzaman, M., DeCarolis, J. F., Subramani, A., Pearce, W., and Jacangelo, J. "Performance and cost effectiveness of reverse osmosis and electrodialysis reversal for desalination of brackish groundwater containing high silica." *AWWA and AMTA Membrane Technology Conference*, Memphis, TN.

Balster, J., Punt, I., Stamatialis, D. F., and Wessling, M. (2006). "Multi-layer spacer geometries with improved mass transport." *Journal of Membrane Science*, 282(1-2), 351-361.

Banasiak, L. J., Kruttschnitt, T. W., and Schafer, A. I. (2007). "Desalination using electrodialysis as a function of voltage and salt concentration." *Desalination*, 205(1-3), 38-46.

Bard, A. J., and Faulkner, L. R. (2001). *Electrochemical methods: Fundamentals and applications*, Wiley, New York.

Belfort, G., and Guter, G. A. (1972). "Experimental study of electrodialysis hydrodynamics." *Desalination*, 10(3), 221-262.

Berger, C., and Lurie, R. M. (1962). "Supersaturation of sulfates in electrodialysis." *Industrial & Engineering Chemistry Process Design and Development*, 1(3), 229-236.

Bernard, O., Kunz, W., Turq, P., and Blum, L. (1992). "Conductance in electrolyte solutions using the mean spherical approximation." *Journal of Physical Chemistry*, 96(9), 3833-3833.

Bird, R. B., Stewart, W. E., and Lightfoot, E. N. (2002). *Transport phenomena*, J. Wiley, New York.

Bird, R. B., Stewart, W. E., and Lightfoot, E. N. (2007). *Transport phenomena*, J. Wiley, New York.

Bockris, J. O. M., and Reddy, A. K. N. (1998). *Modern electrochemistry i: Ionics*, Plenum Press, New York.

Bonné, P. A. C., Hofman, J. A. M. H., and van der Hoek, J. P. (2000). "Scaling control of ro membranes and direct treatment of surface water." *Desalination*, 132(1-3), 109-119.

Burbano, A. A., Adham, S. S., and Pearce, W. R. (2007). "The state of full-scale ro/nf desalination - results from a worldwide survey." *Journal AWWA*, 99(4), 116-127.

Chandramowleeswaran, M., and Palanivelu, K. (2006). "Treatability studies on textile effluent for total dissolved solids reduction using electrodialysis." *Desalination*, 201(1-3), 164-174.

Choi, E.-Y., Choi, J.-H., and Moon, S.-H. (2003). "An electrodialysis model for determination of the optimal current density." *Desalination*, 153(1-3), 399-404.

City of Austin. (2009). "Current water service rates - retail customers, effective 11/1/2008." Austin, TX.

Cobb, M. (2009). "???," Masters, University of Texas at Austin, Austin, TX.

Cooley, H., Gleick, P. H., and Wolff, G. (2006). *Desalination, with a grain of salt: A california perspective*, Pacific Institute for Studies in Development, Environment, and Security, Oakland, CA.

CRC. (2005a). "Ionic conductivity and diffusion at infinite dilution." Handbook of chemistry and physics, P. Vany´sek, ed., CRC Press/Taylor and Francis, Cleveland, OH.

CRC. (2005b). "Mean activity coefficients of electrolytes as a function of concentration." Handbook of chemistry and physics, CRC Press/Taylor and Francis, Cleveland, OH.

Cussler, E. L. (1997). *Diffusion: Mass transfer in fluid systems*, Cambridge University Press, New York.

Davies, C. W. (1962). *Ion association*, Butterworths, Washington.

Deen, W. M. (1998). *Analysis of transport phenomena*, Oxford University Press, New York.

Demircioglu, M., Kabay, N., Ersöz, E., Kurucaovali, I., Safak, Ç., and Gizli, N. (2001). "Cost comparison and efficiency modeling in the electrodialysis of brine." *Desalination*, 136(1-3), 317-323.

Demircioglu, M., Kabay, N., Kurucaovali, I., and Ersoz, E. (2003). "Demineralization by electrodialysis (ed) - separation performance and cost comparison for monovalent salts." *Desalination*, 153(1-3), 329-333.

Eaton, A. D., Clesceri, L. S., Rice, E. W., Greenberg, A. E., and Franson, M. A. H. (2005). "Standard methods for the examination of water & wastewater." American Public Health Association, American Water Works Association, and Water Environment Federation, Washington, DC.

El Midaoui, A., Elhannouni, F., Taky, M., Chay, L., Menkouchi Sahli, M. A., Echihabi, L., and Hafsi, M. (2002). "Optimization of nitrate removal operation from ground water by electrodialysis." *Separation and Purification Technology*, 29(3), 235-244.

Elmidaoui, A., Elhannouni, F., Menkouchi Sahli, M. A., Chay, L., Elabbassi, H., Hafsi, M., and Largeteau, D. (2001). "Pollution of nitrate in moroccan ground water: Removal by electrodialysis." *Desalination*, 136(1-3), 325-332.

Firdaous, L., Maleriat, J. P., Schlumpf, J. P., and Quemeneur, F. (2007). "Transfer of monovalent and divalent cations in salt solutions by electrodialysis." *Separation Science and Technology*, 42(5), 931-948.

Franzini, J. B., and Finnemore, E. J. (1997). *Fluid mechanics with engineering applications*, McGraw-Hill, Boston, MA.

Fritzmann, C., Lowenberg, J., Wintgens, T., and Melin, T. (2007). "State-of-the-art of reverse osmosis desalination." *Desalination*, 216(1-3), 1-76.

Gleick, P. H., Cooley, H., Katz, D., Lee, E., Morrison, J., Palaniappan, M., Samulon, A., and Wolff, G. H. (2006). *The world's water 2006-2007: The biennial report on freshwater resources*, Island Press.

Greenlee, L. (2009). "Enhancing recovery of reverse osmosis desalination: Side-stream oxidation of antiscalants to precipitate salts," Dissertation, The University of Texas at Austin, Austin, TX.

Greenlee, L. F., Testa, F., Lawler, D. F., Freeman, B. D., and Moulin, P. (2010a). "The effect of antiscalant addition on calcium carbonate precipitation for a simplified synthetic brackish water reverse osmosis concentrate." *Water Research*, 44(9), 2957-2969.

Greenlee, L. F., Testa, F., Lawler, D. F., Freeman, B. D., and Moulin, P. (2010b). "Effect of antiscalants on precipitation of an ro concentrate: Metals precipitated and particle characteristics for several water compositions." *Water Research*, 44(8), 2672-2684.

Grigorchuk, O. V., Vasil'eva, V. I., and Shaposhnik, V. A. (2005). "Local characteristics of mass transfer under electrodialysis demineralization." *Desalination*, 184(1-3), 431-438.

Grossman, G., and Sonin, A. A. (1972). "Experimental study of the effects of hydrodynamics and membrane fouling in electrodialysis." *Desalination*, 10(2), 157-180.

Grossman, G., and Sonin, A. A. (1973). "Membrane fouling in electrodialysis: A model and experiments." *Desalination*, 12(1), 107-125.

Guggenheim, E. A., and Turgeon, J. C. (1954). "Specific interaction of ions." *Transactions of the Faraday Society*, 51, 747-761.

Gustafsson, J. P. (2010). "Visual minteq." KTH, Stockholm, Sweden, A free equilibrium speciation model.

Hekman, S. (2009). "Improved concentrate recovery for brackish water reverse osmosis," Masters, University of Texas at Austin, Austin, TX.

Helfferich, F. G. (1962). *Ion exchange*, Advanced chemistry series, McGraw-Hill, New York.

Hoffbuhr, J., Archuleta, E., Crook, J., Gritzuk, M., Lynch, G., Richardson, A., and Towry, J. V. (2004). "What's driving water reuse?" *Journal AWWA*, 96(4), 58-62.

Horvath, A. L. (1985). *Handbook of aqueous electrolyte solutions : Physical properties, estimation, and correlation methods*, Ellis Horwood Limited, Halsted Press, John Wiley & Sons, New York.

Jurenka, R. A., and Chapman-Wilbert, M. (1996). "Maricopa ground water treatment study: Water treatment technology program report no. 15." US Department of the Interior, Bureau of Reclamation, Denver, CO.

Kabay, N., Arda, M., Kurucaovali, I., Ersoz, E., Kahveci, H., Can, M., Dal, S., Kopuzlu, S., Haner, M., Demircioglu, M., and Yuksel, M. (2003). "Effect of feed characteristics on the separation performances of monovalent and divalent salts by electrodialysis." *Desalination*, 158(1-3), 95-100.

Kabay, N., Demircioglu, M., Ersoz, E., and Kurucaovali, I. (2002). "Removal of calcium and magnesium hardness by electrodialysis." *Desalination*, 149(1-3), 343.

Kabay, N., Ipek, O., Kahveci, H., and Yuksel, M. (2006a). "Effect of salt combination on separation of monovalent and divalent salts by electrodialysis." *Desalination*, 198(1-3), 84-91.

Kabay, N., Kahveci, H., Ipek, O., and Yuksel, M. (2006b). "Separation of monovalent and divalent ions from ternary mixtures by electrodialysis." *Desalination*, 198(1-3), 74-83.

Kim, Y. (2010). "Ionic separation in electrodialysis: Analyses of boundary layer, cationic partitioning, and overlimiting current," Dissertation, The University of Texas at Austin, Austin, Texas.

Kim, Y., Walker, W. S., and Lawler, D. F. (2010). "Effects of statistical parameters of boundary layer thickness on current density in electrodialysis." *Journal of Membrane Science*, (submitted).

Koprivnjak, J. F., Perdue, E. M., and Pfromm, P. H. (2006). "Coupling reverse osmosis with electrodialysis to isolate natural organic matter from fresh waters." *Water Research*, 40(18), 3385-3392.

Kortum, G. (1965). *Treatise on electrochemistry*, Elsevier Pub. Co., Amsterdam, New York,.

Kurup, A. S., Ho, T., and Hestekin, J. A. (2009). "Simulation and optimal design of electrodeionization process: Separation of multicomponent electrolyte solution." *Industrial & Engineering Chemistry Research*, 48(20), 9268-9277.

Landau, U. "Novel dimensionless parameters for the characterization of electrochemical cells." *Douglas N. Bennion Memorial Symposium: topics in electrochemical engineering*, San Francisco, CA, vii, 518 p.

Landolt, H., and Börnstein, R. (1960a). *Elektrische leitfähigkeit elektrochemischer systeme, 6. Auflage, ii. Band eigenschaften der materie in ihren aggregatzuständen, 2. Teil gleichgewichte außer schmelzgleichgewichten*, Zahlenwerte und funktionen aus physik, chemie, astronomie, geophysik und technik, Springer, Berlin.

Landolt, H., and Börnstein, R. (1960b). *Elektrische leitfähigkeit elektrochemischer systeme, 6. Auflage, ii. Band eigenschaften der materie in ihren aggregatzuständen, 7. Teil elektrische eigenschaften ii*, Zahlenwerte und funktionen aus physik, chemie, astronomie, geophysik und technik, Springer, Berlin.

Larchet, C., Auclair, B., and Nikonenko, V. (2004). "Approximate evaluation of water transport number in ion-exchange membranes." *Electrochimica Acta*, 49(11), 1711-1717.

Lee, H.-J., Hong, M.-K., Han, S.-D., Cho, S.-H., and Moon, S.-H. (2009). "Fouling of an anion exchange membrane in the electrodialysis desalination process in the presence of organic foulants." *Desalination*, 238(1-3), 60-69.

Lee, H.-J., Sarfert, F., Strathmann, H., and Moon, S.-H. (2002). "Designing of an electrodialysis desalination plant." *Desalination*, 142(3), 267-286.

Lobo, V. M. M. (1981). *Electrolyte solutions : Literature data on thermodynamic and transport properties*, The author, Coimbra, Portugal.

Lobo, V. M. M., and Quaresma, J. L. (1989). *Handbook of electrolyte solutions*, Elsevier, Amsterdam ; New York.

Mabrouk, A. A., Nafey, A. S., and Fath, H. E. S. (2007). "Thermoeconomic analysis of some existing desalination processes." *Desalination*, 205(1-3), 354-373.

Malewitz, T., Pintauro, P. N., and Rear, D. (2007). "Multicomponent absorption of anions in commercial anion-exchange membranes." *Journal of Membrane Science*, 301(1-2), 171-179.

Malmrose, P., Losier, J., Mickley, M., Reiss, R., Russell, J., Schaefer, J., Sethi, S., Manuszak, J., Bergman, R., and Atasi, K. Z. (2004). "Committee report: Current perspectives on residuals management for desalting membranes." *Journal AWWA*, 96(12), 73-87.

Mason, E. A., and Kirkham, T. A. (1959). "Design of electrodialysis equipment." Chemical engineering progress symposium series - adsorption, dialysis, and ion exchange, American Institute of Chemical Engineers, New York, NY, 173-189.

Meller, F. H. (1984). "Electrodialysis (ed) and electrodialysis reversal (edr) technology." Ionics, Inc., Watertown, MA.

Mickley, M. (2006). "Membrane concentrate disposal: Practices and regulation (second edition)." *123*, U.S. Department of the Interior, Bureau of Reclamation.

Mintz, M. S. (1963). "Electrodialysis - principles of process design." *Industrial and Engineering Chemistry*, 55(6), 18-28.

Moon, P., Sandí, G., Stevens, D., and Kizilel, R. (2004). "Computational modeling of ionic transport in continuous and batch electrodialysis." *Separation Science & Technology*, 39(11), 2531-2555.

Newman, J. S., and Thomas-Alyea, K. E. (2004). *Electrochemical systems*, J. Wiley, Hoboken, N.J.

Nicot, J.-P., and Chowdhury, A. H. (2005). "Disposal of brackish water concentrate into depleted oil and gas fields: A texas study." *Desalination*, 181(1-3), 61-74.

Nielsen, A. E. (1984). "Electrolyte crystal-growth mechanisms." *Journal of Crystal Growth*, 67(2), 289-310.

Noble, R. D., and Stern, S. A. (1995). *Membrane separations technology : Principles and applications*, Membrane science and technology series ; 2., Elsevier, Amsterdam ; New York.

Noyes, A. A. (1907). *The electrical conductivity of aqueous solutions*, Contributions from the research laboratory of physical chemistry of the massachusetts institute of technology, no. 19., Carnegie Institution of Washington, Washington, D.C.,.

Ortiz, J. M., Exposito, E., Gallud, F., Garcia-Garcia, V., Montiel, V., and Aldaz, A. (2007). "Electrodialysis of brackish water powered by photovoltaic energy without batteries: Direct connection behaviour." *Desalination*, 208(1-3), 89-100.

Ortiz, J. M., Expósito, E., Gallud, F., García-García, V., Montiel, V., and Aldaz, A. (2008). "Desalination of underground brackish waters using an electrodialysis system powered directly by photovoltaic energy." *Solar Energy Materials and Solar Cells*, 92(12), 1677-1688.

Ortiz, J. M., Sotoca, J. A., Expósito, E., Gallud, F., García-García, V., Montiel, V., and Aldaz, A. (2005). "Brackish water desalination by electrodialysis: Batch recirculation operation modeling." *Journal of Membrane Science*, 252(1-2), 65-75.

Parulekar, S. J. (1998). "Optimal current and voltage trajectories for minimum energy consumption in batch electrodialysis." *Journal of Membrane Science*, 148(1), 91-103.

Pawlowicz, R. (2008). "Calculating the conductivity of natural waters." *Limnology and Oceanography: Methods*, 6, 489-501.

Pawlowicz, R. (2010). "A model for predicting changes in the electrical conductivity, practical salinity, and absolute salinity of seawater due to variations in relative chemical composition." *Ocean Science*, 6, 361-378.

PCA. (2005). "Ion exchange membranes." PCA, GmbH, Heusweiler, Germany.

Pitzer, K. S. (1991). *Activity coefficients in electrolyte solutions*, CRC Press, Boca Raton, FL.

Prudich, M. E., Chen, H., Gu, T., Gupta, R. B., Johnston, K. P., Lutz, H., Ma, G., and Su, Z. (2008). "Section 20 - alternative separation processes." Perry's chemical engineers' handbook. , R. H. Perry and D. W. Green, eds., McGraw-Hill, New York.

Pytkowicz, R. M. (1983). *Equilibria, nonequilibria, and natural waters*, Wiley, New York.

Rajan, K. S., Boies, D. B., Casolo, A. J., and Bregman, J. I. (1968). "Electrodialytic demineralization of brackish waters by using inorganic ion-exchange membranes." *Desalination*, 5(3), 371-390.

Reahl, E. (2005). "Half a century of desalination with electrodialysis." GE.

Reahl, E. R. (1990). "Reclaiming reverse osmosis blowdown with electrodialysis reversal." *Desalination*, 78(1), 77-89.

Reedy, K. A., and Tadanier, C. J. (2008). "Controlling groundwater desalination costs: Facility and process planning (poster)." AWWA Annual Conference and Exposition (ACE), AWWA, Atlanta, GA.

Reynolds, O. (1883). "An experimental investigation of the circumstances which determine whether the motion of water shall be direct or sinuous, and of the law of resistance in parallel channels." *Philosophical Transactions of the Royal Society of London*, 174, 935-982.

Robinson, R. A., and Stokes, R. H. (1959). *Electrolyte solutions - the measurement and interpretation of conductance, chemical potential and diffusion in solutions of simple electrolytes*, Butterworths Scientific Publications, London.

Sadrzadeh, M., Kaviani, A., and Mohammadi, T. (2007). "Mathematical modeling of desalination by electrodialysis." *Desalination*, 206(1-3), 538-546.

Semiat, R. (2008). "Energy issues in desalination processes." *Environmental Science & Technology*, 42(22), 8193-8201.

Senik, Y., Andreeva, I., Pismenskaya, N., Nikonenko, V., and Pourcelly, G. (2006a). "Competitive ion transfer during electrodialysis of multicomponent solutions modeling natural waters." *Desalination*, 200(1-3), 429-431.

Senik, Y., Pismenskaya, N., Nikonenko, V., and Pourcelly, G. (2006b). "A model for calculating ion equilibria and electrical conductivity of natural water solutions." *Desalination*, 191(1-3), 232-235.

SFWMD. (2008). "Dbhydro." South Florida Water Management District.

Shahi, V. K., Thampy, S. K., and Rangarajan, R. (2001). "The effect of conducting spacers on transport properties of ion-exchange membranes in electrodriven separation." *Desalination*, 133(3), 245-258.

Shaposhnik, V., Vasil'eva, V., and Grigorchuk, O. (2006). "Diffusion boundary layers during electrodialysis." *Russian Journal of Electrochemistry*, 42(11), 1202-1207.

Shaposhnik, V. A., Kuzminykh, V. A., Grigorchuk, O. V., and Vasil'eva, V. I. (1997). "Analytical model of laminar flow electrodialysis with ion-exchange membranes." *Journal of Membrane Science*, 133(1), 27-37.

Shaposhnik, V. A., Vasil'eva, V. I., and Praslov, D. B. (1995). "Concentration fields of solutions under electrodialysis with ion-exchange membranes." *Journal of Membrane Science*, 101(1-2), 23-30.

Solan, A., and Winograd, Y. (1969). "Boundary-layer analysis of polarization in electrodialysis in a two-dimensional laminar flow." *Physics of Fluids*, 12(7), 1372-1377.

Solan, A., Winograd, Y., and Katz, U. (1971). "An analytical model for mass transfer in an electrodialysis cell with spacer of finite mesh." *Desalination*, 9(1), 89-95.

Sonin, A. A., and Probstein, R. F. (1968). "A hydrodynamic theory of desalination by electrodialysis." *Desalination*, 5(3), 293-329.

Spiegler, K. S., and El-Sayed, Y. M. (2001). "The energetics of desalination processes." *Desalination*, 134(1-3), 109-128.

Strathmann, H. (2004). *Ion-exchange membrane separation processes*, Membrane science and technology series, Elsevier, Boston.

Stumm, W., and Morgan, J. J. (1995). *Aquatic chemistry: Chemical equilibria and rates in natural waters*, Environmental science and technology., Wiley, New York.

Tanaka, Y. (2006). "Irreversible thermodynamics and overall mass transport in ion-exchange membrane electrodialysis." *Journal of Membrane Science*, 281(1/2), 517.

Tanaka, Y. (2007). *Ion exchange membranes: Fundamentals and applications*, Membrane science and technology series, Elsevier, Boston.

Tsiakis, P., and Papageorgiou, L. G. (2005). "Optimal design of an electrodialysis brackish water desalination plant." *Desalination*, 173(2), 173-186.

Tuan, L. X., Verbanck, M., Buess-Herman, C., and Hurwitz, H. D. (2006). "Properties of cmv cation exchange membranes in sulfuric acid media." *Journal of Membrane Science*, 284(1-2), 67-78.

Turek, M. (2003). "Cost effective electrodialytic seawater desalination." *Desalination*, 153(1-3), 371-376.

Turek, M. (2004). "Electrodialytic desalination and concentration of coal-mine brine." *Desalination*, 162, 355-359.

Turek, M., and Dydo, P. (2008). "Comprehensive utilization of brackish water in ed - thermal system." *Desalination*, 221(1-3), 455-461.

Van der Bruggen, B., Koninckx, A., and Vandecasteele, C. (2004). "Separation of monovalent and divalent ions from aqueous solution by electrodialysis and nanofiltration." *Water Research*, 38(5), 1347.

Varis, O. (2007). "Right to water: The millennium development goals and water in the mena region." 23(2), 243 - 266.

von Gottberg, A. "New high-performance spacers in electrodialysis reversal (edr) systems." *AWWA Annual Conference and Exposition (ACE)*, Dallas, TX, 215-229.

WIC. (2007). "Phosphonates scale & corrosion inhibitor." Water, wood, pulp treatment chemicals, Wanjie International Co., Limited (China).

Wiesner, A., Zacheis, A., Juby, G., Morquecho, R., and Mulvihill, T. "Pilot testing of zero liquid discharge technologies using brackish groundwater for inland desert communities." *24th WateReuse annual symposium*, Seattle, WA.

Wiesner, A. D., Katz, L. E., and Chen, C.-C. (2006). "The impact of ionic strength and background electrolyte on ph measurements in metal ion adsorption experiments." *Journal of Colloid and Interface Science*, 301(1), 329-332.

Winger, A. G., Bodamer, G. W., Kunin, R., Prizer, C. J., and Harmon, G. W. (1955). "Electrodialysis of water using a multiple membrane cell." 50-60.

World Health Organization. (2000). "Global water supply and sanitation assessment 2000 report."

World Health Organization. (2006). "Guidelines for drinking-water quality, 3rd ed."

Wright, M. R. (2007). *An introduction to aqueous electrolyte solutions*, John Wiley, Chichester, England ; Hoboken, NJ.

Xu, P., Drewes, J., Sethi, S., and Walker, S. "Assessment of a hybrid approach for desalination concentrate minimization." *AWWA Annual Conference and Exposition (ACE)*, Atlanta, GA.

Yang, J.-H., Yeon, K.-H., and Moon, S.-H. (2005). "Scale formation in the concentrate compartment of an electrodialysis stack during desalination of brackish water." *Memburein*, 15(2), 175-186.

Yang, Q., Lisitsin, D., Liu, Y., David, H., and Semiat, R. (2007). "Desupersaturation of ro concentrates by addition of coagulant and surfactant." *Journal of Chemical Engineering of Japan*, 40(9), 730-735.

Zhang, Y., Van der Bruggen, B., Pinoy, L., and Meesschaert, B. (2009). "Separation of nutrient ions and organic compounds from salts in ro concentrates by standard and monovalent selective ion-exchange membranes used in electrodialysis." *Journal of Membrane Science*, 332(1-2), 104-112.

Zhou, Y., and Tol, R. S. J. (2005). "Evaluating the costs of desalination and water transport." *Water Resources Research*, 41(3), 03003.

Vita

William Shane Walker attended Texas Tech University where he was involved in the student chapter of American Society of Engineers. He also served as President of Chi Epsilon, and Secretary of Tau Beta Pi. In addition, Shane served as a Teaching Assistant in Chemistry, Mathematics, and Civil Engineering. In May 2004, he received a B.S. degree in Civil Engineering with a minor in Mathematics; he graduated Summa Cum Laude and received awards of the Highest Ranking Graduate in the College of Engineering and Outstanding Senior in Civil Engineering. In the fall of 2004, Shane began graduate studies in the Environmental and Water Resources Engineering program at The University of Texas at Austin. There he served as a Graduate Research Assistant in the Center for Research in Water Resources (CRWR) with Dr. David R. Maidment. He received an M.S.E. degree in August 2006 (thesis: *Geodatabase Design for FEMA Flood Hazard Studies*). In the fall of 2006, Shane began working toward the doctoral degree under the supervision of Dr. Desmond F. Lawler. He was blessed to receive the Thrust 2000 - Hagedorn Endowed Graduate Fellowship through the Cockrell School of Engineering, as well as the Graduate Fellowship for Membrane Technology, co-sponsored by the National Water Research Institute and the American Membrane Technology Association. Upon graduation, Shane was pleased to accept an assistant professorship in Civil Engineering at The University of Texas at El Paso (UTEP) as a member of the Center for Inland Desalination Systems (CIDS) research group.

Permanent address: shanewalkertexas@gmail.com

This thesis was typed by the author.